CALCULATION OF ANGULAR SPECTRA OF THE SECONDARY PARTICLES (n,p,d,α) AFTER SPALLATION FOR $_{82}Pb^{206}$ AND $_{90}Th^{232}$ ELEMENTS

Bilal Othman HAMARASHID

MASTER THESIS

Department of PHYSICS

Supervisor: Prof. Dr. İskender DEMIRKOL

2017

REPUBLIC OF TURKEY
BİNGÖL UNIVERSITY
INSTITUTE OF SCIENCE

CALCULATION OF ANGULAR SPECTRA OF THE SECONDARY PARTICLES (n, p, d, α) AFTER SPALLATION FOR ${}_{82}Pb^{206}$ AND ${}_{90}Th^{232}$ ELEMENTS

MASTER'S THESIS

Bilal Othman HAMARASHID

Department : **PHYSICS**

Supervisor : **Prof. Dr. İskender Demirkol**

May 2017

PREFACE

To begin with, I thank (Allah) for his blessing who made me able to complete and perform this study with success. I would like to thank my supervisor, Prof. Dr. İskender DEMIRKOL for his patience and guidance throughout the project. I would like to acknowledge and thank the presidency of Bingol University, the Deanery of Faculty of physic Sciences and the giving me the chance and providing the available facilities to achieve this proposed project. And moral support I would like to extend my deepest appreciation and thanks to my friends in that university, for their encouragement, considerable assistance, and visited me in during the study period. I am also very much grateful to all my family for their love, assistance and encouragement especially my loyal mother Piroz and my Sisters and my Brothers Mr.Abubakr, Mr.Ali and Mr.Ahmad and my Lover to helped me during my study, also I thinks full to all of persons whose help me during my MSc study. I dedication to my mother, my brother and my sisters.

Bilal Othman HAMARASHID

Bingöl 2017

CONTENTS

LIST OF SYMBOL

ADS	:	Acceleratin Driven System
CEM	:	Cascade Exciton Model
INC	:	Intra-nuclear cascade
MeV	:	Megaelectron volt
KeV	:	kiloelectron volt
GeV	:	Gigaelectron volt
mb	:	Milibar
E	:	Energy
α	:	Alpha
n	:	Neutron
p	:	Proton
Z	:	Atomic number
A	:	Mass number
σ	:	Cross Section
θ	:	Angle
$^\circ$	:	Degree
Pb	:	Lead
Th	:	Thorium
He	:	Helium

LIST OF FIGURE

LIST OF TABLE

$_{82}Pb^{206}$ VE $_{90}Th^{232}$ ELEMENTLERİN SPALLASYON SONRASI OLUŞAN İKİNCİL PARÇACIKLARIN (p, n, d, α) AÇISAL SPEKTRASININ HESAPLANMASI

ÖZET

Bu çalışmada; p + $_{82}Pb^{206}$ ve p + $_{90}Th^{232}$ reaksiyonunda spallasyon sonrası oluşan (n, p, d,α) ikincil parçacıkların açısal spektrasının hesaplanması dengeöncesi etkiyi içine alan kaskat eksiton model ve intranükler kaskat model ile yapılmıştır. Proton ışınları 30-500 MeV enerji aralığına sahiptir. 35 ve 295 MeV enerjilerdeoluşan p+ $_{82}Pb^{206}$ reaksiyonu için CEM03 programı ile hesaplanan açısal dağılımın sonuçları deneysel değerler ile karşılaştırıldı. Ayrıca 65 ve 95 MeV enerjilerde oluşan p+$_{90}$ Th^{232} reaksiyonu için CEM03 programı ile hesaplanan açısal dağılımın sonuçları ile deneysel değerler karşılaştırıldı. Hesaplamalar CEM03 ve ALICE/ASH programları kullanılarak yapılmıştır. Hibrid, geometriye bağlıhybrid ve kaskad eksiton modele dayalı hesaplanan sonuçlar deneysel datalar ile karşılaştırılmıştır. Tüm reaksiyon boyunca dört safhada (Toplam, Kaskad, Bileşiköncesi ve Toplam Buharlaşma) üretilen nötron ve protonun (5°, 15°......... 175°) açılarında hesaplanması CEM03 programı ile yapılmıştır. Tüm reaksiyon boyunca (2.5°, 7.5°......... 177.5°) açılarında üretilen α parçacığının hesaplanması ALICE/ASH program ile yapılmıştır.

Anahtar kelimeler: Açısal spectra, Spallation, Kaskad, CEM03 ve ALICE/ASH.

CALCULATION OF ANGULAR SPECTRA OF THE SECONDARY PARTICLES (n, p, d, He) AFTER SPALLATION FOR $_{82}Pb^{206}$ AND $_{90}Th^{232}$ ELEMENTS

ABSTRACT

In this study calculation of angular spectra of the secondary particles (n, p, d, He) occurring after spallation in the reactions p + $_{82}Pb^{206}$ and p + $_{90}Th^{232}$ is performed using. Cascade Exciton Model including preequilibrium effect the intranuclear cascade model and the empirical parameterization. The proton beams have 30-500 MeV energy ranges. The results are compared with available experimental data (Angular distribution for p + $_{82}Pb^{206}$ reaction at 35 MeV and 295 MeV (compare between CEM03 and Experimental Data) and Angular distribution for p+ $_{90}Th^{232}$ reaction at 65 MeV and 95 MeV (compare between CEM03 and Experimental Data)). Calculations are made by using the CEM03.01 code and ALICE/ASH codes. Calculated results based on hybrid model, geometry-dependent hybrid model and cascade-exciton model are compared with the experimental data. As a result in CEM03 code for all reaction neutron emitted and produced has been made for four steps (Total, Cascade, Precompound, Total evaporation) at angle (5°, 15°......... 175°). As a result in ALICE/ASH code for all reaction α- particle emitted at these angles (2.5°, 7.5°......... 177.5).

Keyword: Angular spectra, Spallation, Energy, CEM03.01and ALICE/ASH.

1. INTRODUCTION

Spallation reactions are defined as collision between relativistic light projectiles, majority hadrons, and heavy target nuclei which are shattered into many small pies broken. In the relativistic energy area, the wave length related with the arriving projectile is such that the interaction can be describe as a chain of nucleon-nucleon collision referred to as intra-nuclear cascade (Benlliure 2006). Spallation compose is the two stage process. In the initial stage, the primary particle interactions with nucleons-neutrons and protons within the nucleus. The interactions that pursue produce an intranuclear cascade of high-energy (larger than 20 Mev) protons, neutrons, and pions inside the nucleus. In the intranuclear cascade, a few of these energetic hadrons getaway as secondary particles. Others place their kinetic energy in the nucleus exit it in an excited state. In the second stage (nuclear de-excitation), evaporation occure at once the excited nucleus unwind by emitting low-energy (smaller than 20 Mev) neutrons, protons, alpha particles, etc., with the mostly of the particles being neutrons. The low-energy neutrons created causes by nuclear de-excitation are significant in a Spallation source because they can be reduced to lower energies level for employ as research probes. After evaporation, the nucleus that leftovers perhaps radioactive and emit gamma rays. Secondary high-energy particles formed through the intranuclear cascade pass nearly in the same direction as that of the incident proton and be able to collide with other nuclei in the target (Russell 1990). Spallation process depends on the substance property, the kinetic energy of the projectile and the geometric arrangement of the target (Shetty 2013).

The Accelerator Driven System (ADS) is an modern nuclear reactor which has be study to create energy and transform radioactive waste, or as a starter to breed the necessary ^{233}U in a thorium based kind of fuel. The spallation process is a nuclear reaction wherever high energy particles beat target nuclei of heavy elements. The main aim of the spallation target in an ADS is to give the primary neutron flux for driving the fission process in the nearby subcritical core. The amount of spallation neutrons per incident proton depends on the beam energy and on the mass of the target nuclei. Caused by their high atomic number, heavy metals for example lead, uranium, tungsten or eutectics for example lead-bismuth are the majority apposite choice for the target material (Barros et al. 2010). An accelerator driven sub-critical reactor (ADS-R) ability, meant at nuclear squander handling and/or energy production, is constituted of four assemblage: a sub-critical reactor, a spallation target, a high power proton driver, and nuclear data (Meot et al. 2015). The efficiency of an ADS depends highly on the fluence and energy circulation of secondary particles (Manolopoulou et al. 2006).

Recently, spallation reactions have attracted substantial attention due to their significance intechnical applications. For example, they can be used for the synthesis of neutrons in a spallation neutron source, and they can take action an strong neutron source in accelerator driven subcritical reactors, able of incinerating nuclear waste and of construction energy (Demirkol 2006).

Generally inelastic interactions of energetic particles (nucleons or mesons) among nuclei can be separate into three stages: (1) the first fast stage of the reaction when a projectile start a cascade of collisions with nucleons of the target nucleus; (2) a preequilibrium process when quick particles go out a highly excited nuclear system; (3) a deexcitation procedure of an equilibrated nuclear remainder. It is assumed that at the final of the first stage after the runaway of all quick particles, the evolution of the residual nuclear system changes its character. Causes bye of intensive interaction between the nucleons, the remaining nucleus evolves to statistical equilibrium. As a result a heat compound nucleus is shaped, which afterward on undergoes deexcitation by evaporation, fission and multifragmentation (Malyshkin et al. 2012).

For heavy ion induced reactions deficient experimental data and intricacy of the reaction system involved produce it difficult to determine any generally trend in the angular distribution of neutron emissions from various target-projectile combinations. It is observed in small energy heavy ion reactions that roughly all normalized angular distributions are peaked inside the forward direction. In this energy state the anisotropy in angular distribution is big for high energy bombardment of light targets by heavy particles and little for low energy light ions event on heavier targets. Neutron emission from heavy ion reactions composes direct preequilibrium (PEQ) and composite nuclear evaporation processes. The direct component participate projectile break up transport reactions and emission of particles from the projectile and the target earlier than some interaction between the projectile and the target nucleons takes place. There are investigational evidences representing a important probability for the breakup of the heavy ion projectile with transport of the branch of the projectile to the target nucleus. Subsequent particle emission from the resulting excited nucleus which moves backwards in the centre-of-mass (c.m.) scheme results in a backward peaking in this frame (Maiti et al. 2006).

2. LITERATURE REVIEW

(Sandberg 1982) reported that employ of copper multireaction spallation detectors in a particle yield testing at CERN super proton synchrotron to compute the angular and energy distributions of secondary hadrons about a thick copper target bombarded with 225 GeV/c protons.

(Delalic 1988) reported that mass, charge, angular and energy distributions of the secondary particles are calculated. The results are described and compared with the similar distributions obtained on the base of 12656 4 (GeV/c)/u d + C interaction events produced by the Dubna intranuclear cascade model [DICM] calculation.

(Wlazło et al. 2000) this research was conducted Spallation residues created in 1 GeV per nucleon ^{208}Pb on proton reactions have been calculated using the Fragment Separator facility at GSI. The recoil kinetic energies of the created fragments were as well determined. The achieved cross sections agree with the majority of the little existing gamma spectroscopic data. The data are compared with dissimilar intranuclear-cascade and evaporation-fission models. Drastic deviations were determined for a standard code used in technical applications.

(Meulders et al. 2000) in this study three nuclides Fe, Pb and U have been selected which provide a adequately broad coverage of the periodic table and are delegate of the target, composition and core materials of the ADS. Hence, not just a few of the top-precedence materials are selected but more significantly, with detailed theoretical and experimental information of these particular elements, the nuclear models current in the foreseen Simulation codes of this job were fine-tuned. This was utilized to produce nuclear codes and data libraries for the materials that are requested by the ADS communit.

(Gupta et al. 2001) this research was conducted the assessment of breakup cross sections are done inside the grazing angle and the comprehensive α and t angular distributions are establish to have maxima at around 60°, but compared to ^{7}Li + ^{58}Ni scattering for which data were in use after grazing angle, the present angular distributions go down rather gradually. Both for the ^{58}Ni and ^{208}Pb targets the comprehensive α-cross sections are greater than the comprehensive t-cross sections, implying additional reaction channels for creation of α-particles than tritons and possibly larger absorption of tritons in the targets.

(Kumar et al. 2003) in this study they have presented assessment of neutron array, isotopic distribution of the created nuclei and heat donations of dissimilar nuclear and atomic processes in collision of proton beam with heavy targets of dissimilar materials, shapes and sizes using current version of Dubna Cascade Code-2001.

(Manolopoulou et al. 2006) In this research investigating experiments the thermal–epithermal neutron fluence, determined via the $^{nat}Cd(n,x)^{115}Cd$ routes and the secondary proton fluence determined via the $^{nat}Cd(p,x)^{111}In$ processes are obtainable.

(Maiti et al. 2006) in the current work their aim is to estimate the existing empirical relations with the help of available experimental data and then to found a easy expression for angular distribution of emitted neutrons from heavy ion induced reactions involving dissimilar targets and projectiles with energies up to about 10AMeV.

(Benlliure 2006) reported that highlighted several of the majority interesting and new investigations of the structure and dynamics of the atomic nucleus obtained by using spallation or fragmentation reactions in inverse kinematics. The true measurement of the isotopic composition and kinematic properties of remaining nuclei have been proven to be innovative and powerful observables.

(Demirkol 2006) in this investigation the production cross sections of heavy remaining nuclides in the ^{208}Pb (1GeV/nucleon) + p reaction were calculated. The calculations were prepared with the Cascade-Exciton Model counting the pre-equilibrium effect, the Intranuclear Cascade Model, the empirical, and the semi-empirical parameterisation.

The results of the cross sections achieve were compared with the usable experimental data, and the relative between them was examined.

(Ricciardi et al. 2006) reported that in the reaction $^{238}U + H$ at 1 A GeV, separately from spallation reactions, which create rather heavy fragments (at Z = 75), the majority part of the cross section of the middle mass residues results from fission reactions.

(Matsumura et al. 2007) in this research, in order to compare the investigational generation rates with the theoretical ones, we replicated the energy spectra of the particles that passed through the detectors and the spallation generation rates in the detectors by using the particle-transport Monte-Carlo reproduction code system MARS15. Thus, it was establish that the results calculated by MARS15 were in good accord with the investigational ones. Furthermore, we replicated the involvement ratios of neutrons, protons, p+ and p_ for each generate mass, and the details of the ^{197}Au spallation induced by the secondary particles became obvious.

(Gaitanos et al. 2008) they concluded that this research provides a suitable theoretical basis for study on fragmentation with a innovative perspective for hypernuclear physics.

(Zamani et al .2010) reported that a measurement of the inelastic cross sections of 1, 1.5 and 2 GeV protons in Pb targets was achieved. Neutron and proton distributions along the spallation source were performed by Solid State Nuclear Track Detectors (SSNTDs) and activation process. The inelastic cross sections were determined from neutron and proton spatial distributions along the target employing a fitting process.

(Hashemi et al. 2012) in this research present and talk about the detection of reaction generates in interaction of protons with dissimilar target materials using a mica detector. They was concentrated on three target materials: uranium, lead and gold, for which detailed investigational results are available in literature.

(Quanzhi et al. 2015) in this study the results illustrate that the decay heat generated via the spallation process is comparable to that generated via the neutron capture process in the majority of the front W plates. Calculations illustrate that the decay heat produced in the W–Ta target decreases approximately linearly as the thickness of the Ta claddings decreases from 0.5 to 0 mm. At present, 0.3 mm thick Ta claddings are considered to be mechanically possible for the CSNS target.

(Asquith et al. 2015) In this research, the ^{232}Th (n,c) and ^{232}Th(n,f) reaction rates were calculated in a graphite moderated spallation neutron field. The ^{232}Th (n,c) reaction rate was calculated in arrange to study the propagation efficiency of fissile ^{233}U in a thermal ADS.

(Quanzhi 2016) In this study, they are aim to compute the energy statement in Pb spallation target by using the PHITS code. The comparisons of the replicated results by PHITS code with the investigational data are performed. The detailed energy statement in a Pb spallation target is calculated, including total energy statement, energy statement caused by dissimilar particles, and energy statement caused by dissimilar proton beam profiles.

(Santos et al. 2016) reported that excitation energy of hot remaining cascade nucleus is discussed against the vary of the nucleon effectual mass, since nucleon–nucleon collision kine-matic for the duration of the cascade phase are straight affected by this vary. They evaluated this effect on the particle give way, spectra and angular distributions, and on the thermal relaxation of the middle compound nucleus shaped in the spallation reaction. They compare their consequences for neutron multiplicity with data in literature for the Pb nucleus in the energy range typically of accelerator driven reactors.

(Wang et al. 2016) reported that spallation cross sections have been calculated for the fission products ^{137}Cs and ^{90}Sr on proton and deuteron at 185 MeV/nucleon in inverse kinematic.

(Kalbach C 1988) The present investigation extends the range of applicability of the past Kalbach-Mann systematic to upper born barding energies and improves their performance at very small emission energies. This has been consummate without dramatically increasing the number of modifiable parameters, and at the same time several useful insights have been gained into the special details of complex particle induced reactions. The input to the success of this employment was the use of a simple exponential in cosL9 to explain the angular dependence from multistep direct processes

3. MATERIAL AND METHOD

3.1. Accelerator Driven System (ADS)

The Accelerator Driven System (ADS) is a new nuclear reactor which has been studied to generate energy and transmute radioactive wastes, or as a starter to type the required ^{233}U in a thorium based kind of fuel (Barros et al. 2010). The majority different point between ADS and conservative reactor is the existence of the accelerator beam line and the spallation target area. The spallation target design is one of the majority important design parameters, because ADS is regulated by neutrons produced in the spallation target. The change of the beam current essential for obtaining similar power in fuel area by moving the incident face location is examined.

The transformation of MA and the burnup reactivity swing are particularly important to approximation the performance of ADS. The proton beam power wanted to operate ADS is related to the multiplication factor of the scheme. Therefore the minimization of the burnup swing is a significant factor in operation of ADS. The scheme is optimized to maximize the MA transformation rate and to minimize the burnup swing.

The beginning plant design was performed based on the results of neutronic computation. It will be hard to realize the heavy piping scheme, although the loop kind reactor is used for sodium cooled ADS. So the pool sort reactor is chosen for lead-bismuth cooled ADS. The middle heat exchange system is feasible to be eliminated as a result of utilizing remarkable features of the lead-bismuth coolant that is lead-bismuth is chemically still. The core, the core support formation and the primary heat transfer system components are built in a reactor vessel. The primary heat exchanger consists of the steam producer and its helical coil tubes, and encircles the middle part of the reactor which includes the core and the proton beam line.

This sort of steam producer will be able to get the reactor vessel size the minimum.

The space between the outer shell of steam producer and the reactor vessel is the cold-leg flow path of principal coolant. The primary pumps are positioned at the cold area of the primary coolant flow path. The pumps are positioned above the helical coil steam producer from the viewpoint of conservation. The steam produce are suspended from the reactor upper flange by the similar reason (Tsujimoto et al. 2000).

3.1.1. History of Accelerators

The former history of accelerators be able to traced from three divide roots. Every root is based on an idea for a dissimilar acceleration system and every three originated in the twenties (Bryant 1994).

3.1.1.1. The Main History Line

The first root to be explained is usually taken as the principal history line, since it was the logical result of the vigorous physics investigate programme in development at the turn of the century. Indeed, particle physics research has usually been the driving force behind accelerator growth and it is however very natural to as well consider high-energy physics as the birth location.

The main accidents along this history line are planned in Table 1. The line is initiated at the end of the last century to demonstrate the natural progression during atomic physics to nuclear physics and the predictable need for higher intensity and higher energy atomic projectiles than those supplied by natural radioactive sources. In this background, the particle accelerator was a planned growth and it fulfilled its aim of performing the first man-controlled splitting of the atom. Ernest Rutherford reported that, in the early twenties, who realised this require but the electrostatic apparatus, then obtainable, were far from reaching the required voltage and for a few years there was no progress. Abruptly, the situation alternated in 1928, when Gurney and Gamov independently anticipated tunneling (Gurney et al. 1928) and it appeared that energy of 500 keV might only be sufficient to split the atom. This implied technologically possible to Rutherford and he directly encouraged Cockcroft and Walton to start scheming a 500 kV particle accelerator.

After four years in 1932, they divide the lithium atom with 400 keV protons. This was the first completely man-controlled splitting of the atom (Crockcroft et al. 1932) which acquired them the Nobel prize in 1951.

Table 3.1. Main History Line

In 1895 Lenard. Electron scattering on gases (Nobel Prize).	< 100 keV electrons. Wimshurst type apparatus.
In 1913 Hertz and Franck excited electron shells by electron bombardment.	
In 1906 Rutherford bombards mica sheet by natural alphas and advance the theory of atomic scattering.	Natural alpha particles of numerous MeV.
In 1911 Rutherford reported theory of atomic structure.	
In 1919 Rutherford activate a nuclear reaction by natural alphas.	
Rutherford believes he requirements a source of several MeV to continue investigate on the nucleus. This is far after the electrostatic machines then existing, but ...	
In 1928 Gamov predicts tunnelling and maybe 500 keV would be sufficient ...	
In 1928 Cockcroft and Walton start scheming an 800 kV producer encouraged by Rutherford.	
In 1932 producer reaches 700 kV and Cockcroft & Walton split lithium atom with just 400 keV protons. They accepted the Nobel Prize in 1951.	

3.1.1.2. The Second History Line

The direct voltage accelerators were the first to be taken advantage for nuclear physics investigate, but they were limited to the highest voltage that could be produced in the system (except for the smart double utilize of the practical voltage in the Tandem). This limitation was too confining for the requirements of high-energy physics and another was needed.

Actually, an alternative had previously been suggested in 1924 in Sweden by Ising (Ising 1924). He proposed to repeatedly apply the similar voltage to the particle using irregular fields and his creation was to become the fundamental principle of every of today's ultra-high-energy accelerators. This is recognized as resonant acceleration. The main proceedings along this history line, starting by Ising, are known in Table 2.

The alternative between the acceleration mechanisms of Walton, Ising and Cockcroft depend by whether the fields are static (i.e. conservative) or time-varying (i.e. nonconservative). The electric field can be articulated in a very universal form as the sum of two conditions, the initially being derived from a scalar potential and the finally from a vector potential,

$$E = -\nabla\phi - \partial/_{\partial t}\, A \tag{3.1}$$

Where

$$B = \nabla \times A \tag{3.2}$$

Table 3.2. The history line

In 1924	Ising suggests time-varying fields across drift tubes. This is resonant acceleration, which can reach energies above that given through the highest voltage in the system.
In 1928	Wideröe shows Ising's principle through a 1 MHz, 25 kV oscillator to create 50 keV potassium ions.
In 1929	Lawrence, excited through Wideröe and Ising, conceives the cyclotron.
In 1931	Livingston shows the cyclotron through accelerating hydrogen ions to 80 keV
In 1932	Lawrence's cyclotron generates 1.25 MeV protons and he as well splits the atom only a few weeks after Walton and Cockcroft (Lawrence conventional the Nobel prize in (1939)

The first phrase in equation (1) explained the static electric field of the Cockcroft-Walton and Van de Graaff equipment. When a particle movements from one point to another point in an electrostatic field, it gains energy consistent with the potential difference, but if it returns to the original spot, for example, by creation a full turn in a circular accelerator, it necessity return to its fundamental potential and will lose accurately the energy it has gained. Thus a gap by a DC voltage has no net accelerating effect in a circular instrument.

The second phrase in equation (1) explained the time-varying field. This is the term that creates every one the current-day high-energy accelerators function. The addition of equation (1) and equation (2) yields Faraday's law,

$$\nabla \times \vec{E} = -\partial/\partial t \, \vec{B},$$

which relates the electric field to the value of modify of the magnetic field. There are two fundamental geometries used to utilize Faraday's Law for acceleration. The first of which is the origin of Ising's consideration and the second history line, and the second is the origin of the third history line to be explain afterward (Bryant 1994).

3.1.1.3. The Third And Fainter History Line

In the earlier section, it was specified that there were two apparatus configurations for exploiting Faraday's Law used for acceleration. First, believe the application of Faraday's Law to the linac, which is made additional apparent by enclosing the gaps in cavities (Bryant 1994).

Table 3.3. The Third History Line

In 1923 Wideröe, a Norwegian student, draws in his laboratory notebook the plan of the betatron with the well-known 2-to-1 law. After two years he adds the situation for radial stability but does not publish.
In 1927 afterward in Aachen Wideröe makes a form betatron, but it does not work. Discouraged he alternative course and builds the linear accelerator explained in Table 2.
In 1940 Kerst re-invents the betatron and builds the first working apparatus for 2.2 MeV electrons.
In 1950 Kerst makes the world's biggest betatron of 300 MeV.
In 1923 Wideröe, a young Norwegian student, draws in his laboratory notebook the design of the betatron with the well-known 2-to-1 rule. Two years later he adds the condition for radial stability but does not publish.

3.1.2. The Main Development of Acceleration

In the 1940's three acceleration mechanisms had been exposed:- resonant acceleration, DC acceleration and the betatron mechanism. actually there were to be no innovative ideas for acceleration mechanisms until the middle-1960's, when cumulative acceleration (James 1966) was suggested in which heavy ions are accelerated in the potential strong of an electron ring and the 1980's when there were some workshops dedicated entirely to determining new acceleration techniques. However, the acceleration mechanism is not adequate by itself and other equally significant developments are required.

So as to accelerate particles to very high energies, it is also required to have focusing mechanisms in the crossways and longitudinal (energy) planes. This was not at all times valued. In the recently cyclotrons, for example, the field was made as homogeneous as feasible just to find that the beam was unstable. Livingston (Livingston 1969) who was Lawrence's student, he reported that how they shimmed the magnet for all small step in energy to keep the beam constant, thus ending up with a field form for transverse constancy that decreased with radius. Theory has later exposed that this reduce should be an inverse power rule of the radius between zero and unity.

The cyclotron is limited through relativistic special effects, which cause the particles to slow downward and los synchronism by the RF field. At initial glance it would show that one would just have to decrease the frequency in order to preserve synchronism, but this is a small too naïve since the propagate in revolution frequency with energy would rapidly utilize the natural energy propagate in the beam and scatter the particles away from the peak of the RF voltage. In this station a longitudinal focusing mechanism is required. This trouble was overcome with (McMillan 1945) and independently with (Veksler 1945) who exposed the principle of phase stability in 1944 and made-up the synchrotron. Phase stability is universal to all RF accelerators excluding the stable-frequency cyclotron. The effect is that a group of particles, with an energy propagate, can be reserved grouped during the acceleration cycle by simply injecting them at a possible phase of the RF cycle. This focusing effect was strong adequate that the frequency transition in the synchro-cyclotron did not must be especially tailored and was simply sinusoidal. Synchro-cyclotrons be able to accelerate protons to about 1 GeV, a large improvement on the simple cyclotron, but the repetition speed decrease the particle yield. In the synchrotron the direct field increases by particle energy, so as to maintain the orbit stationary as in the betatron, but acceleration is useful with an RF voltage by a cavity or gap. In 1946 Goward F and Barnes D. (Goward and Barnes 1946) were the first to create a synchrotron vocation, and in 1947 Oliphant M, Gooden J and Hyde G (Oliphant et al. 1947) suggested the initial proton synchrotron for 1 GeV in Birmingham, UK. nonetheless, the Brookhaven National Laboratory, USA, built their 3 GeV Cosmotron by 1952, only 1 year ahead of the Birmingham group.

Up to this time the just mechanism recognized for focusing in the crossways plane was called weak, or constant-gradient focusing. In this situation, the direct field reduce slightly with increasing radius and its gradient is constant every round the circumference of the machine. The tolerance on the gradient is hard and sets a limit to the volume of such an accelerator. The aperture required to contain the beam as well becomes very big and the magnet correspondingly bulky and expensive. In the recent fifties the limit was supposed to be around 10 GeV.

At the same year as the Cosmotron was ended (1952) Courant E, Livingston M and Snyder H (Courant et al. 1952) suggested strong focusing, furthermore known as alternating-gradient (AG) focusing. The idea had been proposed previous by Christofilos (Christofilos 1956) but it was not published. This innovative principle revolutionized synchrotron drawing, allowing smaller magnets to be used and greater energies to be anticipated. It is straight analogous to a well-known consequence in geometrical optics, which the combined focal length F of a pair of lenses of focal lengths f1 and f2 isolated by a distance d is known by

$$\frac{1}{F} = \frac{1}{f1} + \frac{1}{f2} - \frac{d}{f1f2}$$

If the lenses have equal and reverse focal lengths, f1 = -f2 and in general focal length F = $\frac{f^2}{d}$, which is forever positive. Actually, F left over's positive over quite a great range of values when f2 and f1 have unequal values but are still of reverse sign. Thus in certain limits a chain of irregular lenses will focus. Instinctively one shows that, although the beam perhaps defocused by one lens, it reach at the following lens additional from the axis and is so focused more powerfully. Structures based on this assumption are indicated to as AG structures.

The synchrotron rapidly overshadowed the betatron and the synchrocyclotron in the race for greater energies. The adoption of substitute gradient focusing for apparatus and transfer lines was even faster. CERN for illustration directly abandoned its already-approved project for a 10 GeV/c powerless focusing synchrotron in favour of a 25 GeV/c AG machine, which it evaluated could be built for the similar price.

The subsequently step was the storage ring collider**.** In physics investigation, the helpful energy for innovative particle construction is the energy that is emancipate in the centre-of-mass system. When an accelerator beam is used on a stable objective, just a fraction of the particle's energy arrive in the centre-of-mass system, while for two equal particles in a head-on collision, every of the particles' energy is obtainable. This fundamental defect of the fixed-target accelerator becomes more disciplinary as the energy increases. For illustration, it would have required a fixed target accelerator of over 1TeV to match the centre-of-mass energy obtainable in the CERN ISR (2 x 26 GeV proton colliding rings).

The storage-ring collider currently controls the high-energy physics field. Single-ring colliders, applying particles and antiparticles in the same magnetic channel, were the first sort of collider to be used at Frascati in the AdA (Annelli di Accumulazione) propose (1961). The initial double-ring proton collider was the Intersecting Storage Rings (CERN ISR), 1972-1983. The maximum-energy collisions achieved to date are 2 × 900 GeV in the Fermi lab, single-ring, proton-antiproton collider.

Colliders have been very winning as physics investigate instruments. The $\frac{J}{\psi}$ particle was exposed at SPEAR by Richter B, and at the same time by Ting at BNL – they public the 1976 Nobel Prize. The CERN proton-antiproton storage ring was therefore the source of a Nobel Prize for van der Meer S, and Rubbia C, in 1984, following the exploration of the Z and W particles. The proton-antiproton colliders were just made feasible by the invention of stochastic cooling via van der Meer S, for the buildup of the antiprotons (Van der Meer 1972).

The utilize of superconductivity in proton apparatus has made the very highest energies likely. There has besides been one more change taking place, which has been called the Exogeographical evolution (an expression coined by Professor Cabibbo N, at a Workshop held at Frascati in 1984). This refers to the preparations that have made it suitable to bury the very large machines for example HERA and LEP deep below property which does not go to the laboratory concerned. Not including such agreements, Europe could not have retained its leading location in the world accelerator league.

The microtron, sometimes recognized as the electron cyclotron, was an clever idea due to Veksler (1945). The electrons pursue circular orbits of increasing radius, but with a general tangent. An RF cavity located at the point of the general tangent supplies a constant energy increase on every passage. The relativistic mass increment gradually by slowly the revolution frequency of the electrons, but by a constant increase on all passage. If this increase is a multiple of the RF oscillator frequency, the electrons stay in stage, but on a dissimilar orbit. Microtrons labor at microwave frequencies and are limited to tens of MeV. The electron storage rings have given delivery to the synchrotron radiation sources, more generally indicated to as light sources. These machines are currently the fastest increasing community in the accelerator world and the initial commercially obtainable compact synchrotron light source for lithography has only come onto the market.

The linear accelerator was eclipsed throughout the thirties by circular machines. Nevertheless, the advances in ultra-high frequency technology throughout World War II (radar) opened up innovative Possibilities and converted interest in linac composition. Berkeley was initial, with a proton linear Accelerator of 32 MeV made by Alvarez in 1946. The Alvarez accelerator has become very admired as an injector for big proton and heavy-ion synchrotrons every over the world with energies in the range of 50–200 MeV, that is fundamentally non-relativistic particles. The biggest proton linear accelerator to date is the 800 MeV 'pion factory' (LAMPF) at Los Alamos.

The first electron linear accelerators were calculated at Stanford and at the Massachusetts Institute for Technology (MIT) in 1946. This sort of accelerator has also had a spectacular evolution, up to the biggest now in operation, the 50 GeV linear accelerator at the Stanford Linear Accelerator Centre (SLAC). Like betatrons they have become extremely popular in fields exterior nuclear physics, particularly for medicine (Bryant 1994)

3.2. Spallation

3.2.1. Spallation Reaction

Spallation reaction is a practice in which a light projectile (proton, neutron, or light nucleus) with the kinetic energy from some hundreds of MeV to several GeV interacts with a heavy nucleus and causes the emission of a big number of hadrons (mostly neutrons) or fragments. Spallation has two stages: intra-nuclear cascade and deexcitation (Krása and Rež 2010), Fig 3.1. Shows schematic view of spallation reaction.

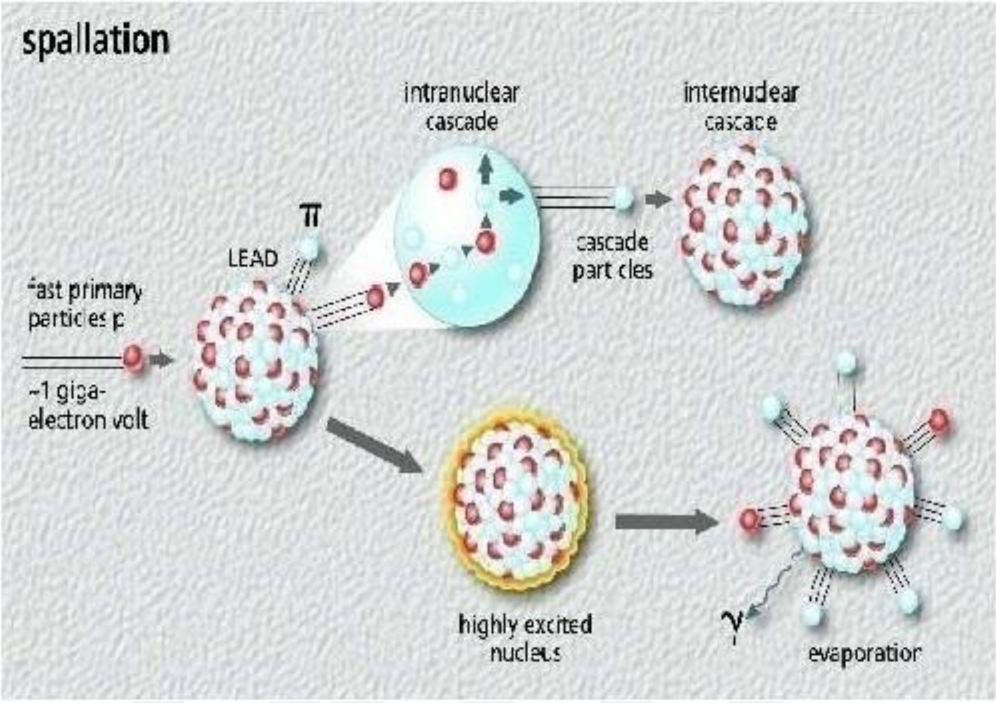

Fig 3.1. Proton induced spallation reactions in the energy range 0.1-10 GeV (Krása and Rež 2010)

3.2.1.1. The Intra-Nuclear Cascade (INC)

The intra-nuclear cascade (INC) is a quick direct stage (~10^{-22} s), Fig. 3.2. Shows warning principle of Intra-Nuclear Cascade. As the decreased de Broglie wavelength of the ~1 GeV proton is ~0.1 fm, it interacts with single nucleons in the target nucleus (instead of creating a compound nucleus). The missile shares its kinetic energy with target nucleons by elastic collisions and a cascade of nucleon-nucleon collisions proceeds (Krása and Rež 2010),

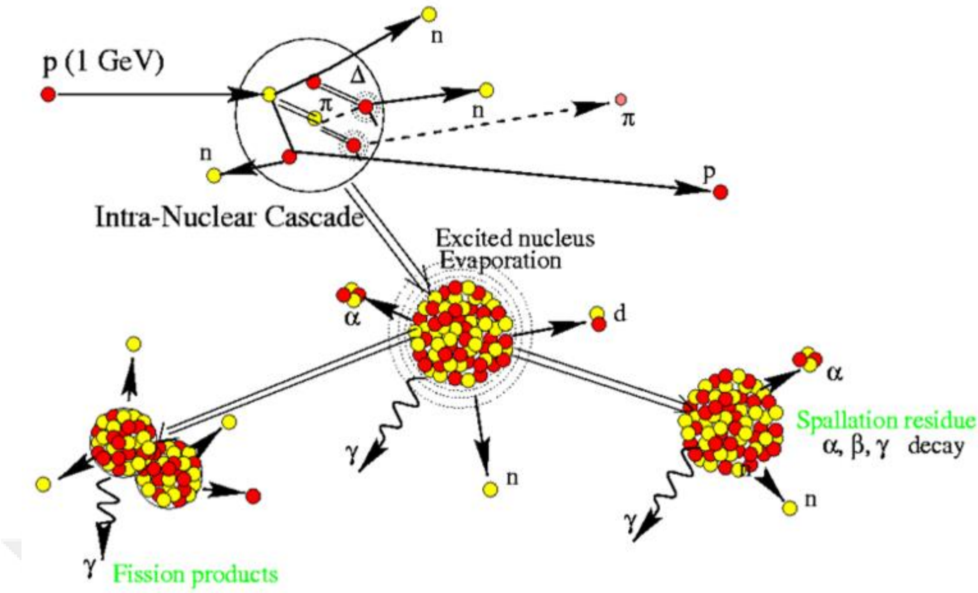

Fig 3.2. Intra-Nuclear Cascade (Krása and Rež 2010)

At low projectile energies (~100 MeV), every interactions occur only between nucleons and the process is called nucleon cascade (Cugnon 1993). Gradually, with development incident particle energy, the threshold energies for particle production in nucleon-nucleon collisions are being exceeded at first, pions come up (at energies of about hundreds of MeV), at larger energies (~2 – 10 GeV) heavier hadrons are being generated. They can furthermore participate in the intra-nuclear cascade and interact between all other, what is called hadron cascade (Cugnon 1993). Particles that get energy high adequate to escape from the nucleus are being emitted mostly in the direction of the incident particle. The rest of the energy is equally dispersed among nucleons in the nucleus which is left in a highly excited state.

The intra-nuclear cascade is not sharply isolated from the equilibrium decay. In a pre-compound stage, the pre-equilibrium emission can occur. In the course of this stage, quick particles or fragments perhaps emitted after every interaction between the incident or other cascade particle and a nucleon inside the nucleus. The energies of pre-equilibrium particles are larger than energies of particles emitted during the equilibrium decay (Krása and Rež 2010).

3.2.1.2. Deexcitation

Lastly, the equilibrium stage comes up (~10^{-16} s). Energy is equally dispersed throughout the nucleus that is in a highly excited state with small angular momentum. The nucleus loses its energy by evaporation of light charged fragments or neutrons (e.g., d, t, α) with energies up to $\approx$ 40 MeV (which is the nuclear potential well depth) (Adair 1954).

A competitive process to evaporation is fission (into two fragments alike in proton number). Fission products also undergo evaporation (depending on their excitation energy).

When the nucleus does not have energy adequate to emit neutrons (its excitation energy becomes lesser than the binding energy, typically about 8 MeV), it deexcites by γ-emission. Subsequent to the termination of de-excitation by γ -transitions, the resulting nucleus is generally β -radioactive and decay until the stable state (Krása and Rež 2010).

3.2.2. Spallation Target

Regarding target parameters, its material and volume are those which determine the neutron multiplicity. In principle, the heavier target nucleus the bigger amount of neutrons is being generated. The gain factor between light and heavy targets is around a factor of five (Armbruster and Benlliure 2001) however, the radiotoxicity convinced in the spallation target could be significantly decreased when using lighter targets (Ridikas and Mittig 1998). Neutron multiplicity can be heightened by using of a fissile material. In addition, significant parameters of target material are thermal conductivity, caloric receptivity, melting and boiling points (Wagner et al. 1996).

Some design concepts have been developed for the target system. One of the typical designs (Cho et al. 2008) is shown in Fig.3.3.

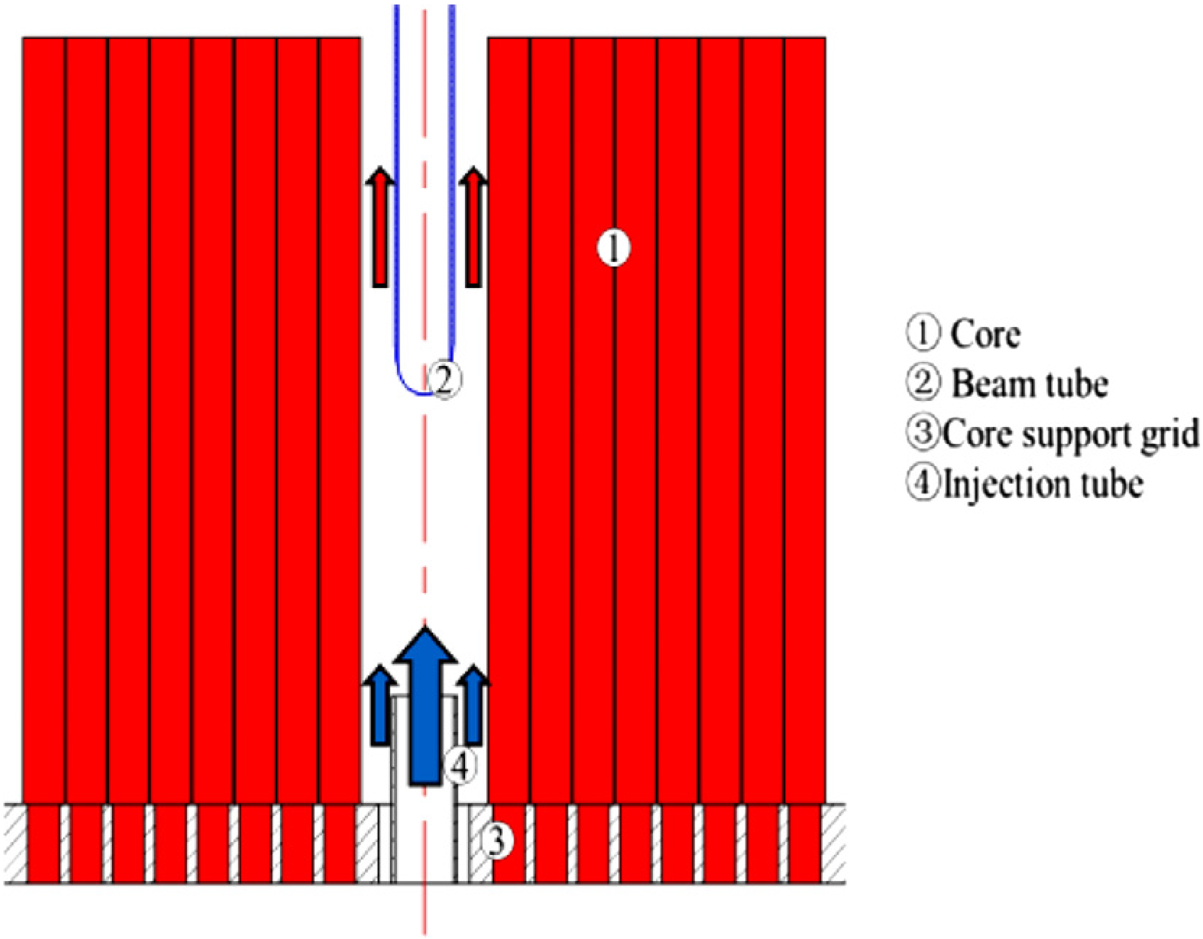

Fig 3.3. Schematic view of the typical target design (Cho et al. 2008)

In contrast to the suggested target, the target channel surrounded by assemblies which is almost cylinder. The target channel diameter is set at 260 mm. LBE at about 300 °C driven by the major primary pump from the flow distribution, rises in the space between the sleeve and the beam tube to eliminate the deposited heat. Then, the hot LBE is pumped from the hot pool, through the major heat exchange and down over pump to complete the LBE circuit. An injection tube is located at the inlet of the target channel and divides the inlet into two zones. The velocity in the central zones is bigger than that of the outer zones. The injection tube diameter and thickness are 168 mm and 10 mm, sequence. In the channel, the beam tube with a hemi-spherical window is adopted for the target. A thickness of the window about 2 mm is selected in this system, and the inner diameter is about 150 mm (He et al. 2016).

3.3. Nuclear Model

In nuclear physics, as in several areas of physics and chemistry, it has been suitable to treat questions dP reaction mechanisms by models that are at diametrically contrasting extremes in order to gain tractable results. On the other hand, models exist for "direct reactions" in which a particular interaction between a projectile and several or one nucleons of the target nucleus is treated. At the other intense, it is exposed that the projectile is captured by the target nucleus, and that the resulting "compound nucleus" attains statistical equilibrium without prior particle emission. The decay of the long-lived composite nucleus may then be treated by equilibrium statistical mechanics as was formulated for the instance of nuclear reactions by Weisskopf (Weisskopf 1937) nearly 40 years ago.

Several review articles perhaps found on both direct reaction models (Glendenning 1963) (Greider 1965) (Bethge, 1970) (Tamura 1969) and on the compound nucleus model (Thomas 1968) (Fleury and Alexander 1974) (Bodansky 1962), and these articles demonstrate that the dichotomy has been highly successful in several cases. However, in several spectra, continuous high energy structer were observed that neither were steady with predictions of the compound nucleus model nor with existing direct reaction models (Sidorov 1962) (Holbrow and Barschall 1963) (Wood et al. 1965). As isochronous cyclotrons came into wide usage in the 1960s and upper projectile energies became common for nuclear reaction investigation, these inexplicable spectral mechanism became ever clearer in a broad range of experimental results (Bertrand and Peelle 1973). In nearly years these phenomena have been treated by classical models that formulate the decay into the continuum of a scheme with an initial partition of projectile energy between relatively few (intrinsic) degrees of freedom, progressing through more complex configurations until an equilibrium distribution of energy is attained. A describe of these models, the assumptions implicit and explicit to them, and their degree of achievement in reproducing experimental results is obtainable herein (Blann 1975).

3.3.1. Preequilibrium Model

The later preequilibrium interaction stage of nuclear reactions is considered by the CEM in the framework of an extension of the modified Exciton Model (MEM) (Gudima). At the preequilibrium stage of a reaction we obtain into account every possible nuclear transitions changing the number of exciton n with $\Delta n= +2, -2$, and 0, as well as suitable multiple subsequent emission of n, p, d, t, ^3He, and ^4He .The CEM anticipate forward peaked (in the laboratory system) angular distributions for preequilibrium particles. This calculation system is easily realised by the Monte-Carlo technique. It provides good discussion of double differential spectra of preequilibrium nucleons and a not so good but yet statisfactory description of complex-particle spectra from different sorts of nuclear reaction at incident energies from tens of MeV to many GeV.

In this model nuclear states are characterized by the number of exited particles and holes (the exitons). INC collisions give rise to a gradually of states characterized by increasing exciton number, finally leading to a equilibrated nucleus. For practical achievement of the exciton model we employ level density parameters from (Ribansky et al. 1973) and the matrix elements from (Kalbach 1978).

In the exciton model the suitable selection rules for particle-hole configurations in the course of the cascade are: $\Delta p = 0,\pm1$ $\Delta h = 0,\pm1$ $-n = 0,\pm2$, where p is the number of particle, h is number of holes and n = p + h is the number of exitons. The cascade pre-equilibrium model employs target excitation data, and exciton configurations for neutron and proton to generate the non-equilibrium evaporation. The angular distribution is isotropic in the frame of rest of the exciton scheme. The parameterizations of the level density employed, are tabulated both with their Z and A including and dependence a high temperature behavior. The nuclear binding energy is employing a smooth liquid high energy formula (Heikkinen et al. 2003).

3.3.2. The Intranuclear Cascade Model (INC)

The intra-nuclear cascade model (INC) was first suggested by Serber in 1947 (Serber 1948). He noticed that, in particle-nuclear collisions the deBroglie wave-length of the incident particle is comparable to or shorter than the average intra-nucleon distance (Heikkinen et al. 2003).

The INC has been successfully utilized in the Monte Carlo simulations at intermediate energy state since Goldberger prepared first calculations by hand in 1947 (Goldberger

1948). First computer simulations were done via Metropolis et al. in 1958 (Metropolis et al. 1958). Standard methods in INC implementations were shaped when Bertini published his results in 1968 (Bertini et al. 1968). A significant addition was exciton model introduced by Griffin in 1966 (Griffin 1966).

The intranuclear cascade model in CEM03.01 is based on the standard (non-time dependent) version of the Dubna cascade model (Barashenkov 1972) .Every one the cascade calculations are carried out in a three dimensional geometry.

The momenta of the two nucleons involving in the absorption are selected randomly from the Fermi distribution, and the pion energy is distributed equally between these nucleons in the center of mass scheme of the three particles involving in the absorption.

In this version of the INC, the kinetic energy of the cascade particles is decreased or increased as they move from one of the seven potential regions (zones) for another, but their directions stay unchanged. That is, in our calculations, reflection or refraction of cascade nucleons at potential boundaries is ignored. CEM03.01 allows us to take into account reflections and refractions of cascade nucleons at potential boundaries, for this, one require to modify the value of the parameter irefrac from 0 to 1 in the subroutine initial (Stepan and Arnold 2012).

The basic steps of the INC model are summarized below:

1. The spatial position, where the incident particle enters, is chosen uniformly over the projected area of the nucleus.
2. Total, free particle-particle cross-sections and region-dependent nucleon densities are utilized to choose the path length for the projectile particle.
3. The momentum of a struck nucleon, the sort of reaction, and the four momentum of the reaction generates are determined.
4. The exciton model is updated as the cascade profits. If Pauli's exclusion principle allows and $E_{particle} > E_{cut\ off} = 2$ MeV, step (2) is performed to transfer the products.

After INC, the residual excitation energy of the resulting nucleus is utilized as input for a non-equilibrium model (Heikkinen et al. 2003).

3.3.3. The Coalescence Model

When the cascade stage of a reaction is finished, CEM03.01 utilizes the coalescence model (Gudima et al. 1975) to produce high-energy d, t,^{3}He, and ^{4}He by final-state interactions among emitted cascade nucleons, already exterior of the target nucleus.CEM03.01 assumes that all the cascade nucleons having differences in their momenta smaller than Pc and the accurate isotopic content form an appropriate composite particle (Stepan and Arnold 2012).

3.3.4. Evaporation Model

CEM03.01 utilizes an extension of the Generalize dE vaporation Model (GEM) code GEM2 by Furihata (Shiori Furihata 2003), complex particles, and light fragments heavier than ^{4}He (up to ^{28}Mg) from excited composite nuclei and to explain their fission,if the composite nuclei are heavy enough to fission ($Z \geq 65$). Furihata did not modify in the GEM the common algorithms utilized in LAHET to simulate evaporation and fission.

The decay widths of evaporated particles and fragments are appreciated using the classical Weisskopf-Ewing statistical model (Weisskopf and Ewing 1940). Note that when counting evaporation of up to 66 particles in GEM2, its running time increases importantly compared to the case when evaporating only 6 particles, up to ^{4}He. The main particles emitted from an excited nucleus are n, p, d, t, ^{3}He, and ^{4}He. For the majority cases, the overall emission probability of particles heavier than α is insignificant compared to those for the emission of light ejectiles (Stepan and Arnold 2012).

This model assumes complete energy equilibration before particle emission, and reequilibration of excitation energies between successive evaporation emissions. As a result, the angular distribution of emitted particles is isotropic (Heikkinen et al. 2003).

3.3.5. Fission Model

The fission model utilized in GEM2 is based on Atchison model (Atchison 1980) as achieved in LAHET (parel and Lichtenstein 1989), often indicated in the Rutherford Appleton laboratory (RAL) fission model, which is where Atchison developed it. In

GEM2 there are two option of parameters for the fission model: one of them is the unique parameter set by Atchison (Atchison 1980) as implemented in LAHET (parel and Lichtenstein 1989), and another is a parameter set developed by furihata (Furihata et al. 2001).

3.3.6. Fission Probability

The Atchison fission model is designed to explain only fission of nuclei with Z ≥ 70. It assumes that fission competes just with neutron emission, from the widths Γj of n, p, d, t, ^{3}He, and ^{4}He, the RAL code calculates the probability of evaporation of every particle. When a charged particle is chosen to be evaporated, no fission opposition is taken into account. When a neutron is chosen to be evaporated, the code does not really simulate its evaporation, as an alternative it considers that fission may perhaps compete, and selects either fission or evaporation of a neutron consistent with the fission probability P_f. This quantity is treated by the RAL code dissimilar for the elements above and below Z = 89. Mass distribution. The choice of the mass of the fission fragments depends on whether the fission is symmetric or asymmetric. For a pre-fission nucleus with $\frac{Z_i^2}{A_i} \leq 35$, just symmetric fission is acceptable. For $\frac{Z_i^2}{A_i} > 35$, both symmytric and asymmetric fission are acceptable, depending on the excitation energy of fissioning nucleus. No innovative parameters were determined for asymmetric fission in GEM2 (Stepan and Arnold 2012).

3.3.7. The Fermi Break-Up Model

Usually, after the fast INC stage of a nuclear reaction, a lot slower evaporation/fission stage follows, without or with taking into account an middle preequilibrium stage between the INC and the equilibrated evaporation/fission. Such an image is well grounded in cases of heavy nuclei, as both evaporation and fission models are based on statistical hypothesis, needing a large number of nucleons. Naturally, in the case of light nuclei with just a few nucleons, statistical models are less well necessary. Also, such light nuclei like carbon and oxygen show considerable alpha-particle clustering, not accounted for in evaporation/fission models. This is why in the case of light excited nuclei; their deexcitation is often calculated using the so called "Fermi break-up" model, suggested initially by Fermi (Fermi 1950).

It is impossible to measure all nuclear data needed for applications involving light target nuclei; therefore, Monte-Carlo transport codes are usually used to simulate fragmentation reactions. It is important that available transport codes predict such reactions as well as possible (Mashnik et al. 2016).

3.3.8. Total Reaction Cross Section (Normalization)

The total cross section σ_k for reactions between heavy ions has been extensively studied both theoretically and experimentally for a long time. The elastic-scattering cross sections of a large number of heavy-ion systems have been measured at several energies and the optical model has been found to be successful in extracting the total reaction cross section and the interaction radii. In addition there are some direct measurements of the total reaction cross section.

The determination of nuclear size is one of the most important problems in nuclear physics. Various experimental methods have been employed to determine the nuclear size; the measurement of total reaction cross section for heavy-ion collision is one of them. The radii of the proton and neutron distributions in nuclei have been determined with various experimental methods and compared with theoretical calculations (Shen et al. 1989).

3.3.9. Full Exciton Model

Nucleon-nucleus reactions in the medium-energy range $T_{\circ} \leq 100$ MeV are still attracting much attention because of the opportunity to investigate the preequilibrium particle emission. The mechanism of particle emission during the attainment of statistical equilibrium in an excited nuclear system is somewhat intermediate between direct reactions and decays through the states of a compound nucleus, and is not reduced to their simple combination. The development of the pre-equilibrium concept of the nuclear reactions has allowed one to understand the importance of this mechanism and its relation to the intermediate nuclear structure, and to explain a number of interesting physical effects. Among the available pre-equilibrium emission models similar in their physical assumptions, preference is given to those which, being internally self-consistent, describe the largest set of experimental data. The majority of the exciton models claim only to describe the shape of angle-integrated energy spectra of secondaries, mainly of nucleons. Some models are used to investigate the excitation functions and more rarely the angular distributions of particles.

Thus, the proposed cascade-exciton model (CEM) considers the nuclear reaction as proceeding through three stages - cascade, pre-equilibrium and equilibrium (or compound nucleus) - unlike the two-stage Serber mechanism.

The physical picture underlying our model is rather natural. A particle entering a nucleus can suffer one or several intranuclear collisions that give rise to the formation of an excited many-quasiparticle state like a “doorway state”. Due to residual interaction this state will evolve towards a more complicated one up to the formation of a compound nucleus. At each stage of this process a particle can be emitted. The behaviour of a primary particle and of those of the second and subsequent generations (if any) up to their capture or emergence from a nucleus is treated in the framework of the intranuclear cascade model. The number of captured nucleons and of “holes” produced due to the intranuclear collisions gives us the initial particle-hole configuration of the remaining excited nucleus, the excitation energy of which is defined by the conservation laws. A further destiny of the nucleus is traced in terms of the exciton model of pre-equilibrium decay which includes in a natural way the particle decay at the equilibrium stage too (Gudima et al. 1983).

3.3.10. Hybrid Model

The capability of the hybrid model of preequilibrium nuclear reactions to predict unknown excitation functions and to perform α priori calculations of nuclear reactions cross sections for a wide variety of reactions types is an outstanding feature of this model. However, there are distinct differences in the quality of such calculations depending on the type of bombarding particle and on the excitation energies of the reacting systems (Michel et al. 1985).

At the high energy end, one sees spectral transitions to discrete low lying states, which are not treated (unless in an averaged fashion) by the code ALICE. At low energies, we see the evaporation peaks which are treated in ALICE following preequilibrium decay (PE) (Blann 1991).

3.3.11. Geometry Dependent Hybrid Model

The nucleus has a density distribution which can affect PE decay in two ways. First, the nucleon mean free path is expected to be longer (on average about a factor of two) in the diffuse nuclear surface. Secondly, in a local density approximation, there is a limit to the hole depth, this will be expected to modify the Ericson state densities. These two changes were incorporated into the ‘geometry dependent hybrid model.

In order to provide a first order correction for the influence of nuclear density, the hybrid model may be reformulated as a sum of contributions, one term for each entrance channel impact parameter with parameters evaluated for the average local density of each impact parameter. In this way, the diffuse surface properties sampled By the higher impact parameters are crudely incorporated into the precompound decay formalism in the geometry dependent hybrid model (GDH)(Blann 1991).

4. RESULT AND DISCUSSION

4.1. Calculation Method

In this study, the reaction cross section and angular distribution of heavy elements were calculated using equilibrium and pre-equilibrium nuclear reaction models. In calculations; to examine pre-balance effects; Cascade Exciton, Hybrid and Geometry Additive Hybrid Model were used. ALICE / ASH codes are used for Cascade Exciton Model, CEM03 (Mashnik 1980) and Hybrid and Geometry additive Hybrid calculations.

${}_{90}Th^{232}$, ${}_{82}Pb^{206}$ Bombarding by the accelerated protons at different energies; Total reaction cross sections of the neutrons and protons that are formed in the calculation that are made with CEM03 and ALICE/ASH programs have been calculated.

The present paper describes new calculations on the angular distribution of p+${}_{82}Pb^{206}$ and p+${}_{90}Th^{232}$ reactions passed out in the 30–500 MeV proton incident energy range. In the calculations, the ALICE/ASH and CEM03 codes have been used. The pre-equilibrium calculations on the angular distribution were carried out with ALICE/ASH computer code for hybrid model and the geometry-dependent hybrid model, and CEM03 computer code for cascade exciton model. The ALICE/ASH code is an advanced and limited version of the ALICE-91 code. The ALICE/ASH code can be useful for the calculation of excitation functions, energy and angular distribution of secondary particles in nuclear reactions induced by nucleons and nuclei up to an energy range of 300 MeV. The general super fluid nuclear model has been applied for nuclear level density calculations in the ALICE/ASH code. We used the initial exciton number as $n_0 = 3$ (1 neutron,1 proton and 1 hole). New calculations have been made in the framework of cascade–exciton model (CEM) by making apply of CEM03 code with the level density parameter using the systematic of (Iljinov AS et al. 1992).

4.2. CEM03 Computer Program

CEM03.01 is the newest program in a series of codes including CEM2k+GEM2, CEM97, and CEM95. It is an extended and better version of the earlier codes, which use versions of the (CEM) Cascade-Exciton Model of nuclear reactions. CEM03.01 considers Intranuclear Cascade (INC), preequilibrium, evaporation, fission, and Fermi Break-up mechanisms of nuclear reactions as well as coalescence of complex particles up to ^{4}He from quick INC nucleons. CEM03.01 measures total reaction and fission cross-sections, nuclear facilities, excitation functions, nuclide distributions (yields) of every one generated isotopes separately in addition to their Z-and A- distributions, angular spectra and energy, mean multiplicities, double-differential cross-sections, i.e. the amount of ejectiles per inelastic interaction of the projectile by the target, ejectiles yields and their average energies for p, n, t, d, ^{3}He, ^{4}He, π^{+}, π^{-}, and π^{0}. By modifying an input changeable evaporation of as numerous as 60 isotopes heavier than ^{4}He (up to ^{28}Mg) may be also modeled. Also, CEM03.01 provides in its output individually the yields of Backward (B) and Forward (F) generated isotopes, their indicate kinetic energies, Z-and A- distributions of the represent emission angle, their parallel velocities, and the F/B ratio of every one products in the laboratory system, distributions of the indicate angle between two fission fragments, of momentum, of neutron multiplicity and angular momentum, of the excitation energy, and of mass and charge numbers of residual nuclei after the INC and preequilibrium stages of reactions, and for fissioning nuclei after and before fission. CEM03.01 measures reactions induced through nucleons, pions, bremsstrahlung and monochromatic photons on not too light targets at incident energies from ~10 MeV (~30 MeV, in the case of $\gamma + A$) up to some GeV (Mashnik et al. 2005).

4.3. ALICE / ASH Computer Program

The ALICE/ASH code is an highly developed and modified version of the ALICE code. The modifications concern the implementation in the code of models describing the pre-compound compound particle emission fast γ- emission different approaches for the nuclear level density estimate and the model for the fission fragment yield calculation. The ALICE/ASH code can be useful for the calculation of excitation functions, energy and angular distribution of secondary particles in nuclear reactions induced by nucleons and nuclei with the energy up to 300 MeV (Broeders CHM et al. 2006).

$$3Xp = 2\,\frac{\left(\frac{\sigma pn}{\sigma pp}\right)N+2Z}{2\left(\frac{\sigma pn}{\sigma pp}\right)N+2Z} \qquad \text{or} \quad 3Xn = 2\text{-}3Xp$$

Where (σpn, σpp) is the nucleon-nucleon interaction cross-section in the nucleus. Z and N are the proton and neutron numbers, respectively, of the target nuclei.

The ratio of nucleon-nucleon cross-sections calculated taking into account to Pauli principle and the nucleon motion is parameterized

$$\sigma\, pn / \sigma\, pp = \sigma\, np / \sigma\, nn = 1.375 \times 10^{-5}\, T^2 - 8.734 \times 10^{-3} T + 2.776$$

where T is the kinetic energy of the projectile outside the nucleus. The super-fluid model has been applied for nuclear level density calculations in the ALICE/ASH code.

4.4. Reactions

4.4.1. p + $_{90}Th^{232}$ Reaction

Thorium is a chemical element by indication Th and atomic number 90. A radioactive actinide metal, thorium is one of only two significantly radioactive elements that still occur naturally in large amount as a primeval element (the other being uranium). It was establish in 1829 by the Norwegian amateur mineralogist Morten Thrane Esmark (Krebs RE 2006) and determined by the Swedish chemist Jöns Jacob Berzelius, who named it following Thor, the norse god of thunder (https://en.wikipedia.org/wiki/Thorium).

Thorium's melting point of 1750 °C is greater than both that of protactinium (approximately 1560 °C) and that of actinium (1227 °C) (https://en.wikipedia.org/wiki/Thorium).

In the CEM03 Code, it is formed by p + $_{90}Th^{232}$ reaction at different energies; Angular spectra -induced angular distribution and the formation cross-sections of the elements with the same mass numbers (A) were calculated. The calculated principles and the experimentally measured values have been compared.

4.4.1.1. Neutron Angular Distribution for p + $_{90}Th^{232}$ Reaction at E_p=30 MeV

The CEM03 codes indicate asymmetrical angular distributions for secondary nucleons. This is because of high asymmetry of the cascade component. A convenient to have asymmetrical distributions for particles emitted throughout the pre-equilibrium interaction stage is connected to keeping several memory of the direction of a projectile.

Figure 4.1. and Table 4.1. Shows the evaluated results and angle-integrated emission spectra measurements at E_p= 30 MeV. Number of inelastic interactions is 10000, number of elastic interactions is 3686, reaction cross section is 1858.65 mb, and elastic cross section is 685.10 mb. The calculation obtained for neutron emitted has been made for four steps (Total, Cascade, Precompound, Total evaporation) at angle (5°, 15°......... 175°). As can be seen in Figure (4.1) cascade cross section and Precompound cross section are not change, and there is no change at total cross section and total evaporation cross section. The cross section of neutron produced in the total evaporation is higher than cascade and precompound cross section of neutron produced.

Table 4.1. Neutron scattered angular distributions (mb/sr) for p + $_{90}Th^{232}$ reaction, E_p= 30 MeV energy. Calculations have been made by CEM03 code program

$^{232}Th(p,n);E_p$=30 MeV CEM03 – Code				
Ang.n [deg.]	Total	Cascade	Precompound	Total Evaporation
	Cross Section (mb/sr)	Cross Section (mb/sr)	Cross Section (mb/sr)	Cross Section (mb/sr)
5	825.6	21.42	56.47	747.7
15	795.3	19.01	57.7	718.6
25	781	34.94	52.6	693.5
35	787.9	35.8	45.56	706.5
45	782.1	23.76	39.12	719.3
55	760.7	20.3	39.57	700.9
65	700.7	10.86	33.33	656.5
75	708.4	7.555	31.8	669
85	711.2	4.599	30.32	676.3
95	705.1	2.215	21.81	681.1
105	677.3	1.406	22.49	653.4
115	678.4	1.123	20.41	656.9
125	676.8	0	19.68	657.1
135	668.2	0.96	21.12	646.1
145	678.4	0	17.16	661.3
155	644.9	0	14.86	630
165	655	0	11.15	643.9
175	683.4	0	11.68	671.8

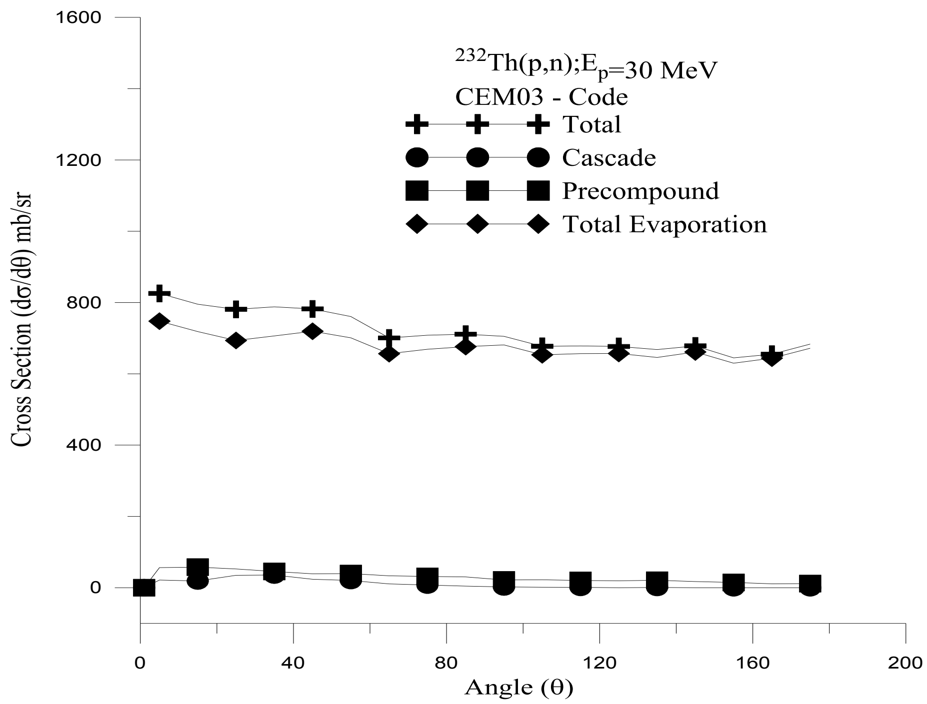

Figure 4.1. Angular Distributions (mb/sr) of the neutrons generated as a result of bombardment of element ${}_{90}Th^{232}$ with 30 MeV energetic protons

4.4.1.2. Neutron Angular Distribution for p + ${}_{90}Th^{232}$ Reaction at E_p=60 MeV

The CEM03 indicate asymmetrical angular distributions for secondary nucleons. This is because of high asymmetry of the cascade component. A convenient to have asymmetrical distributions for particles emitted throughout the pre-equilibrium interaction stage is connected to keeping several memory of the direction of a projectile.

Figure 4.2. and Table 4.2. Shows the evaluated results and angle-integrated emission Spectra measurements at E_p= 60 MeV. Number of inelastic interactions is 10000, number of elastic interactions is 4694, reaction cross section is 2080.11 mb, and elastic cross section is 976.40 mb. The calculation obtained for neutron emitted has been made for four steps (Total, Cascade, Precompound, Total evaporation) at angle (5°, 15°......... 175°). As can be seen in figure (4.2) cascade cross section is decreasing when angular distributions are increasing. Similarly, Precompound slightly decreases while angular distribution increases and there is no change at total cross section and total evaporation cross section. The cross section of neutron produced in the total evaporation is higher than cascade and precompound cross section of neutron produced.

Table 4.2. Neutron scattered angular distributions (mb/sr) for p + $_{90}Th^{232}$ reaction, E_p= 60 MeV energy. Calculations have been made by CEM03 code program

$^{232}Th(p,n)$; E_p=60 MeV CEM03 – Code				
Ang.n [deg.]	Total Cross Section (mb/sr)	Cascade Cross Section (mb/sr)	Precompound Cross Section (mb/sr)	Total Evaporation Cross Section (mb/sr)
5	1072	65.37	102.4	904.3
15	1148	126.2	109.3	912.9
25	1168	167.2	103.4	897.5
35	1167	160.6	87.42	918.9
45	1096	1 26.2	94.01	875.3
55	1053	86.71	62.37	903.8
65	1006	66.22	63.29	876.8
75	968.2	45.81	51.91	870.5
85	942	27.64	47.47	866.9
95	898.5	19.64	45.37	833.5
105	881.1	14.55	31.66	834.9
115	870.7	7.125	32.69	830.9
125	890.1	3.942	28.52	857.6
135	856.3	3.76	26.05	826.5
145	825.8	1.324	23.18	801.3
155	838.1	0	24.27	813.9
165	819.7	0	28.62	791
175	847.7	0	17.43	830.3

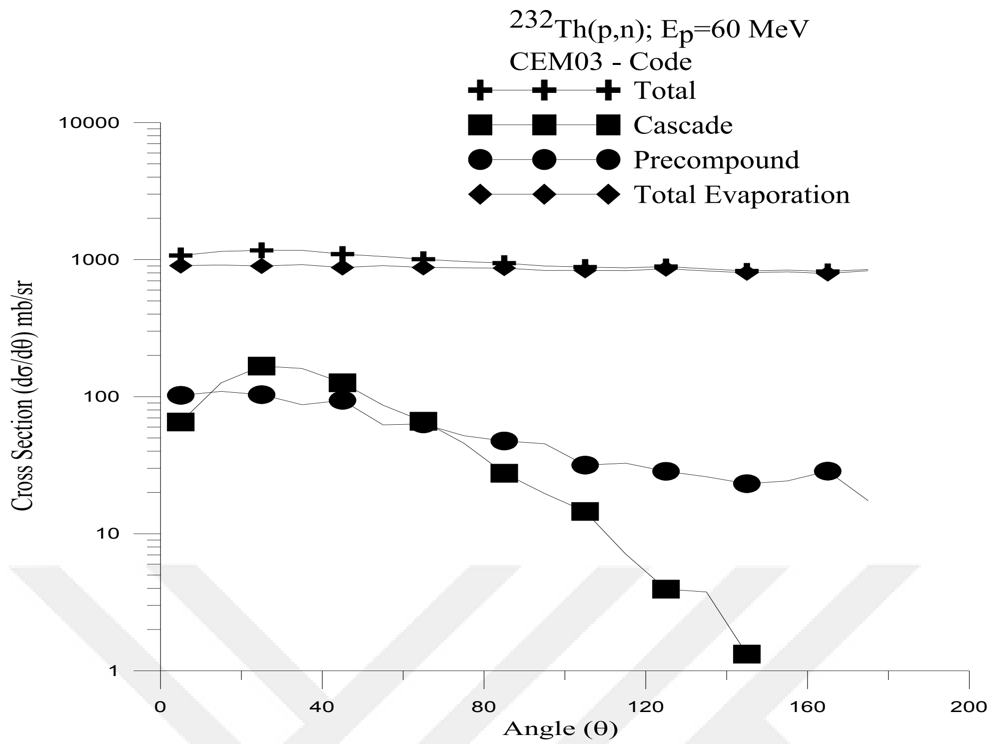

Figure 4.2. Angular Distributions (mb/sr) of the neutrons generated as a result of bombardment of element $_{90}Th^{232}$ with 60 MeV energetic protons

4.4.1.3. Neutron Angular Distribution for p + $_{90}Th^{232}$ Reaction at E_p = 90 MeV

The CEM03 indicate asymmetrical angular distributions for secondary nucleons. This is because of high asymmetry of the cascade component. A convenient to have asymmetrical distributions for particles emitted throughout the pre-equilibrium interaction stage is connected to keeping several memory of the direction of a projectile.

Figure 4.3. and Table 4.3. Shows the evaluated results and angle-integrated emission Spectra measurements at E_p= 90 MeV. Number of inelastic interactions is 10000, number of elastic interactions is 5153, reaction cross section is 2036.59 mb, and elastic cross section is 1049.45 mb. The calculation obtained for neutron emitted has been made for four steps (Total, Cascade, Precompound, Total evaporation) at angle (5°, 15°......... 175°). As can be seen in Figure (4.3) cascade cross section is decreasing when angular distributions are increasing. Similarly, Precompound slightly decreases while angular distribution increases and there is no change at total cross section and total evaporation

cross section. The cross section of neutron produced in the total evaporation is higher than cascade and precompound cross section of neutron produced.

Table 4.3. Neutron scattered angular distributions (mb/sr) for p + $_{90}Th^{232}$ reaction, E_p= 90 MeV energy. Calculations have been made by CEM03 code program

$^{232}Th(p,n);E_p$=90 MeV CEM03 – Code				
Ang.n [deg.]	Total Cross Section (mb/sr)	Cascade Cross Section (mb/sr)	Precompound Cross Section (mb/sr)	Total Evaporation Cross Section (mb/sr)
5	1387	142.9	196.3	1048
15	1401	216.3	165.2	1019
25	1404	253.9	128.5	1022
35	1377	207.2	129.4	1040
45	1273	161.2	98.88	1013
55	1250	150	103.1	996.5
65	1173	105.9	85.35	981.8
75	1126	72.77	65.84	987.6
85	1083	50.77	60.29	971.6
95	1051	37.15	54.88	958.7
105	1006	25.6	41	939.8
115	991.4	12.11	45.14	934.2
125	965.2	9.761	32.92	922.5
135	996.1	5.785	37.34	953
145	962.9	3.566	30.8	928.5
155	973.7	1.76	29.48	942.5
165	989.3	0	25.15	964.2
175	981.4	0	21.34	960.1

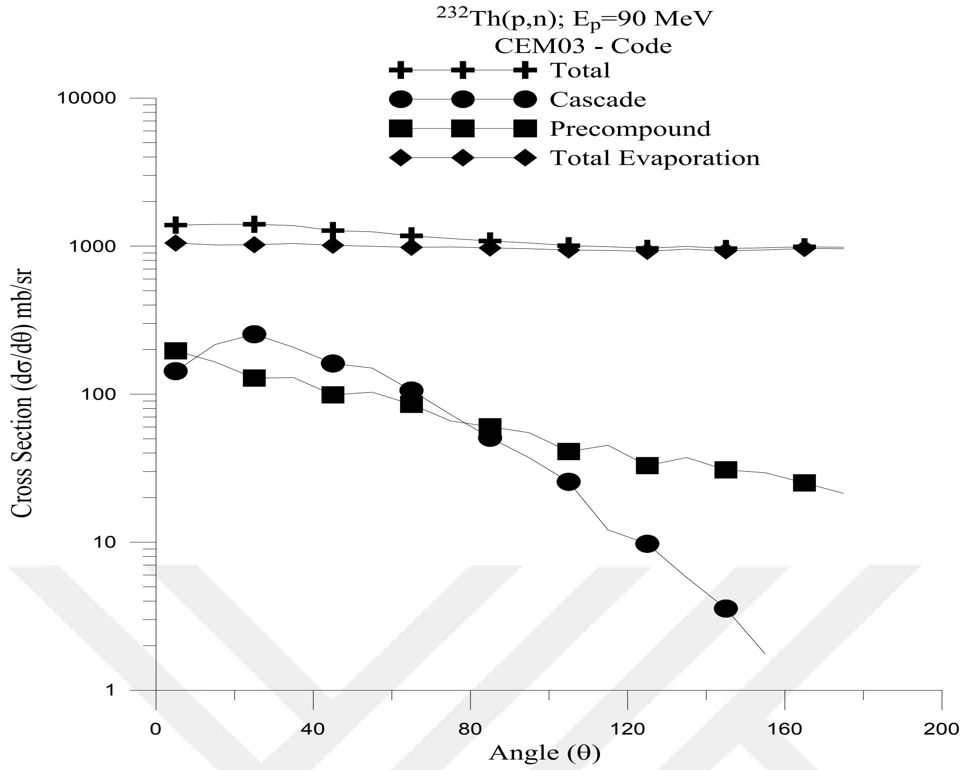

Figure 4.3. Angular Distributions (mb/sr) of the neutrons generated as a result of bombardment of element ${}_{90}Th^{232}$ with 90 MeV energetic protons

4.4.1.4. Proton Angular Distribution for p + ${}_{90}Th^{232}$ Reaction at E_p = 120 MeV

The CEM03 indicate asymmetrical angular distributions for secondary nucleons. This is because of high asymmetry of the cascade component. A convenient to have asymmetrical distributions for particles emitted throughout the pre-equilibrium interaction stage is connected to keeping several memory of the direction of a projectile.

Figure 4.4. and Table 4.4. Shows the evaluated results and angle-integrated emission Spectra measurements at (120 MeV). Number of inelastic interactions is 10000, number of elastic interactions is 5236, reaction cross section is 1961.86 mb, and elastic cross section is 1027.23 mb. The calculation obtained for proton emitted has been made for four steps (Total, Cascade, Precompound, Total evaporation) at angle (5°, 15°......... 175°). As can be seen in Figure (4.4) Precompound is decreasing when angular distributions are increasing. Similarly, cascade cross section slightly decreases while angular distribution increases. Similarly total cross section slightly decreases while angular distribution increases and there is no change at total evaporation cross section. The cross section of

proton produced in the cascade is higher than precompound and total evaporation cross section of proton produced.

Table 4.4. Proton scattered angular distributions (mb/sr) for p + $_{90}Th^{232}$ reaction, E_p= 120 MeV energy. Calculations have been made by CEM03 code program

$^{232}Th(p,p')$; E_p=120 MeV CEM03 – Code				
Ang.p [deg.]	Total Cross Section (mb/sr)	Cascade Cross Section (mb/sr)	Precompound Cross Section (mb/sr)	Total Evaporation Cross Section (mb/sr)
5	326.8	224	100.7	2.055
15	453.3	343.3	107.3	2.768
25	405.2	303.9	100.5	0.8477
35	331	246.4	84.01	0.6246
45	232.6	171.5	59.28	1.773
55	164.4	109.8	54.01	0.656
65	100.6	61.67	37.36	1.581
75	66.39	35.23	30.41	0.7418
85	49.27	17.62	30.39	1.259
95	26.79	7.732	17.98	1.079
105	22.44	6.12	15.02	1.298
115	19.57	2.569	15.81	1.186
125	13.34	0.8747	10.5	1.968
135	11.4	0.2533	10.64	0.5067
145	11.87	0.3123	9.057	2.498
155	5.51	0.4239	4.662	0.4239
165	8.305	0	6.229	2.076
175	12.33	0	12.33	0

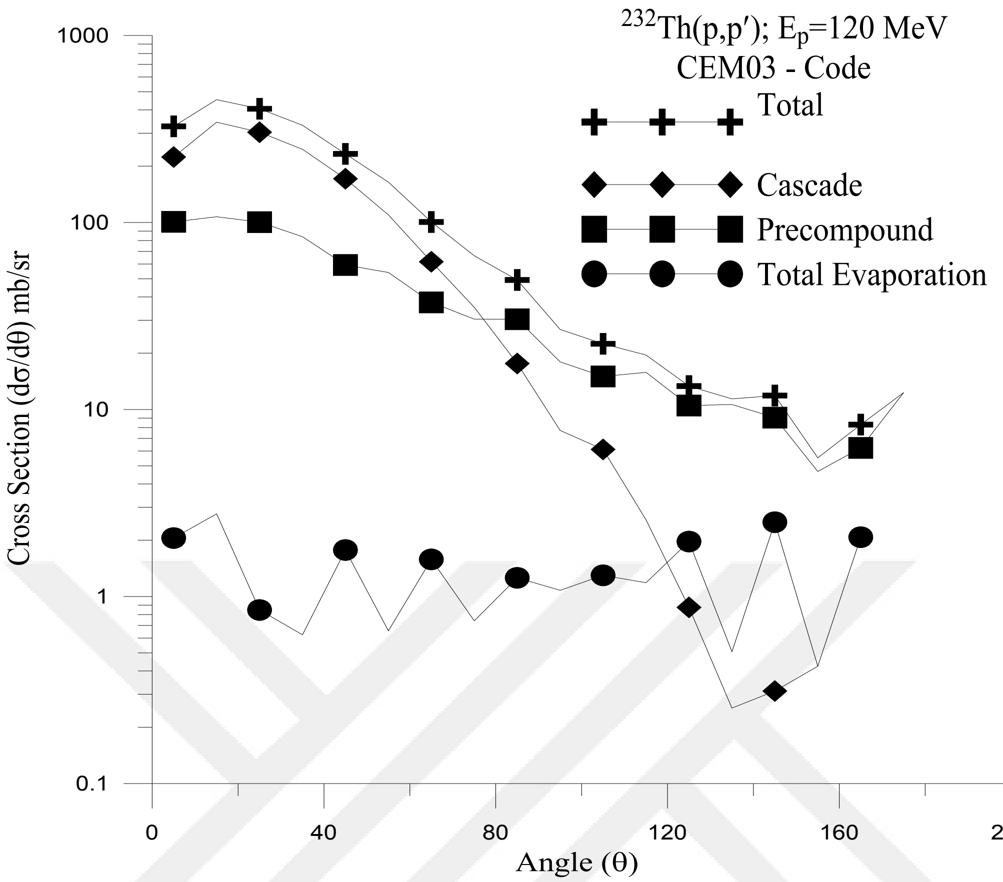

Figure 4.4. Angular Distributions (mb/sr) of the protons (p′) generated as a result of bombardment of element $_{90}Th^{232}$ with 120 MeV energetic protons

4.4.1.5. Neutron angular distribution for p +$_{90}$Th^{232} reaction at E_p = 150 MeV

The CEM03 indicate asymmetrical angular distributions for secondary nucleons. This is because of high asymmetry of the cascade component. A convenient to have asymmetrical distributions for particles emitted throughout the pre-equilibrium interaction stage is connected to keeping several memory of the direction of a projectile.

Figure 4.5. and Table 4.5. Shows the evaluated results and angle-integrated emission Spectra measurements at E_p= 150 MeV. Number of inelastic interactions is 10000, number of elastic interactions is 5675, reaction cross section is 1893.73 mb, and elastic cross section is 1074.69 mb. The calculation obtained for neutron emitted has been made for four steps (Total, Cascade, Precompound, Total evaporation) at angle (5°, 15°......... 175°). As can be seen in Figure (4.5) Precompound is decreasing when angular distributions are increasing. Similarly, cascade cross section slightly decreases while

angular distribution increases and there is no change at total cross section and total evaporation cross section. The cross section of neutron produced in the total evaporation is higher than cascade and precompound cross section of neutron produced.

Table 4.5. Neutron scattered angular distributions (mb/sr) for p + $_{90}Th^{232}$ reaction, E_p= 150 MeV energy. Calculations have been made by CEM03 code program

$^{232}Th(p,n)$; E_p=150 MeV CEM03 – Code				
Ang.n [deg.]	Total Cross Section (mb/sr)	Cascade Cross Section (mb/sr)	Precompound Cross Section (mb/sr)	Total Evaporation Cross Section (mb/sr)
5	1655	327.3	172.6	1155
15	1720	396.8	137.6	1186
25	1675	393.2	142.4	1140
35	1616	352.4	117.6	1146
45	1553	299.5	118.1	1135
55	1519	260.5	104.3	1154
65	1416	211.8	93.86	1110
75	1340	167	72.32	1101
85	1286	130.5	60.05	1096
95	1260	85.92	57.97	1116
105	1215	70.35	49.41	1096
115	1163	45.79	41.4	1075
125	1143	33.98	36.52	1072
135	1111	26.41	35.95	1049
145	1080	19.59	33.16	1027
155	1112	13.09	25.37	1073
165	1079	8.685	32.07	1038
175	1153	9.919	31.74	1111

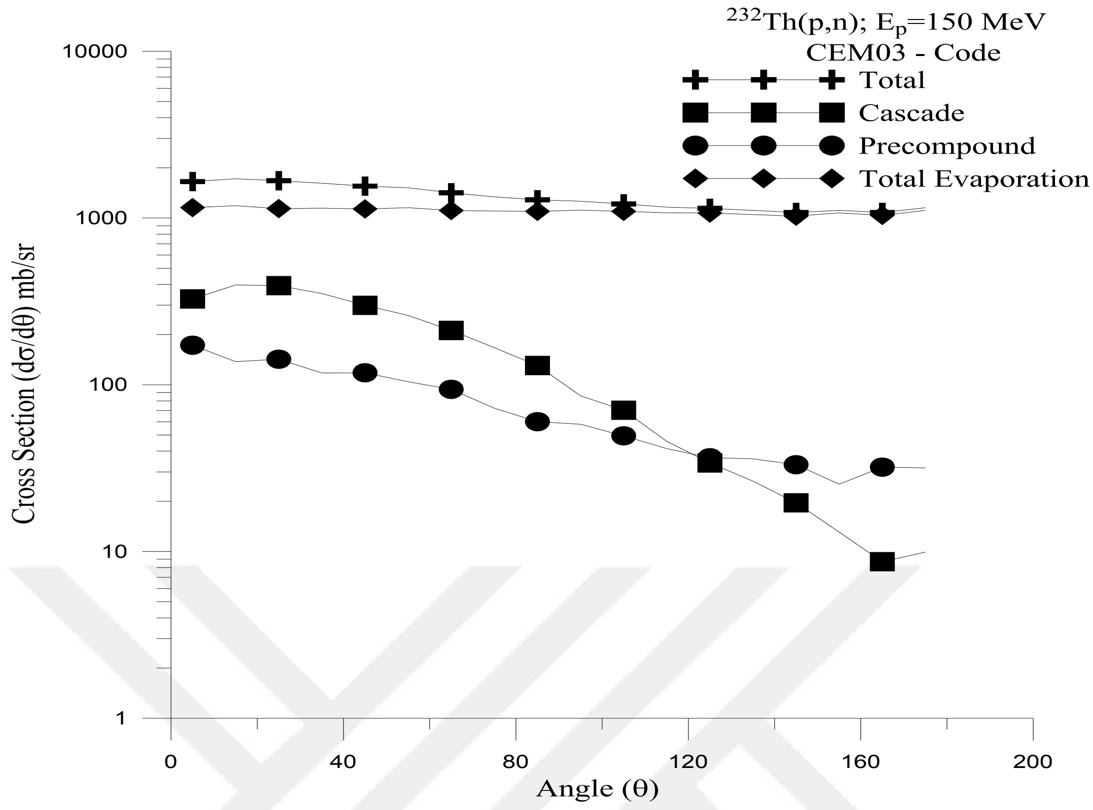

Figure 4.5. Angular Distributions (mb/sr) of the neutrons generated as a result of bombardment of element $_{90}Th^{232}$ with 150 MeV energetic protons

4.4.1.6. Proton Angular Distribution for p+$_{90}Th^{232}$ Reaction at E_p = 180 MeV

The CEM03 indicate asymmetrical angular distributions for secondary nucleons. This is because of high asymmetry of the cascade component. A convenient to have asymmetrical distributions for particles emitted throughout the pre-equilibrium interaction stage is connected to keeping several memory of the direction of a projectile.

Figure 4.6. and Table 4.6. Shows the evaluated results and angle-integrated emission Spectra measurements at E_p= 180 MeV. Number of inelastic interactions is 10000, number of elastic interactions is 5802, reaction cross section is 1839.32 mb, and elastic cross section is 1067.17 mb. The calculation obtained for proton emitted has been made for four steps (Total, Cascade, Precompound, Total evaporation) at angle (5°, 15°......... 175°). As can be seen in Figure (4.6) Precompound is decreasing when angular distributions are increasing. Similarly, cascade cross section and total cross section slightly decreases while angular distribution increases and there is no change at total

evaporation cross section. The cross section of proton produced in the cascade is higher than precompound and total evaporation cross section of neutron produced.

Table 4.6. Proton scattered angular distributions (mb/sr) for p + $_{90}Th^{232}$ reaction, E_p= 180 MeV energy. Calculations have been made by CEM03 code program

$^{232}Th(p,p')$; E_p=180 MeV CEM03 –Code				
Ang.p [deg.]	Total	Cascade	Precompound	Total Evaporation
	Cross section (mb/sr)	Cross section (mb/sr)	Cross section (mb/sr)	Cross section (mb/sr)
5	406.6	327.6	75.15	3.854
15	462	380.9	77.86	3.244
25	414.1	349.3	63.18	1.59
35	343.2	286.1	53.87	3.221
45	279.8	231.3	44.18	4.275
55	189.8	146	39.57	4.305
65	133.6	96.73	30.95	5.93
75	92.32	58.94	29.9	3.477
85	57.99	34.05	18.88	5.057
95	40.12	21.07	15	4.046
105	33.21	13.56	15.3	4.347
115	22.79	7.041	10.75	5.003
125	17.43	3.485	10.46	3.485
135	12.59	3.088	7.838	1.663
145	12.59	1.757	8.198	2.635
155	9.537	0.7948	6.755	1.987
165	9.733	1.298	4.542	3.893
175	11.56	0	3.854	7.708

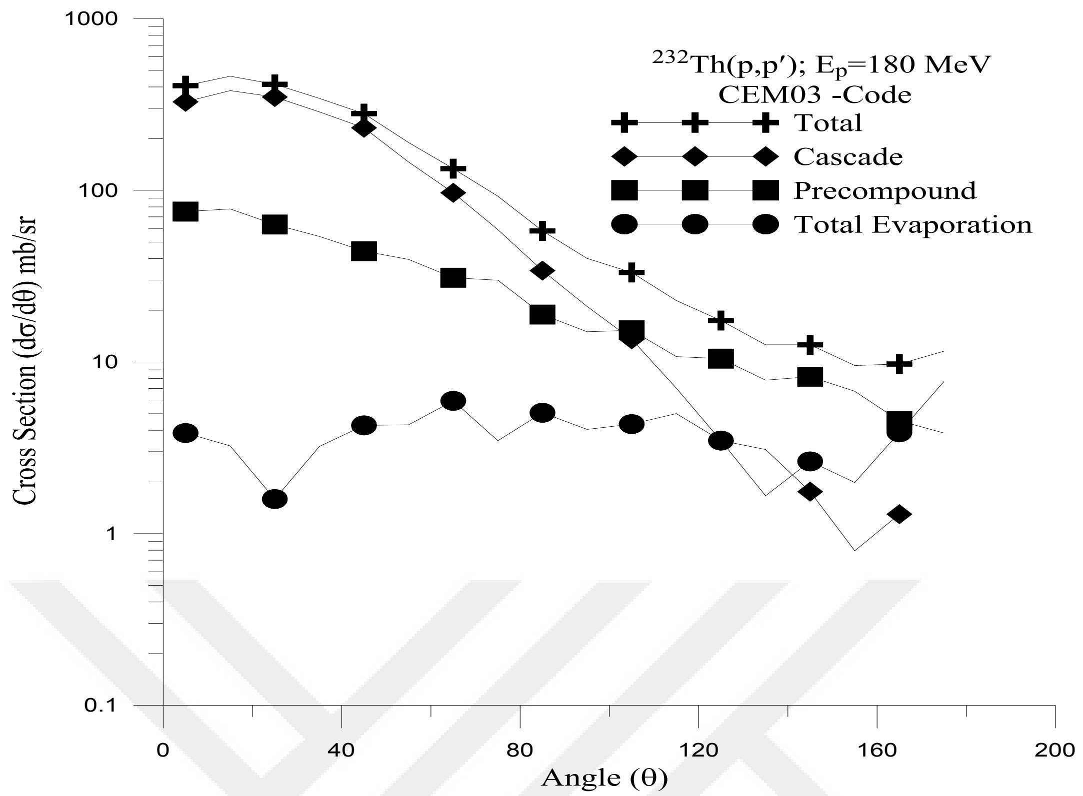

Figure 4.6. Angular Distributions (mb/sr) of the protons (p′) generated as a result of bombardment of element $_{90}Th^{232}$ with 180 MeV energetic protons

4.4.1.7. Proton Angular Distribution for p + $_{90}Th^{232}$ Reaction at E_p = 210 MeV

The CEM03 indicate asymmetrical angular distributions for secondary nucleons. This is because of high asymmetry of the cascade component. A convenient to have asymmetrical distributions for particles emitted throughout the pre-equilibrium interaction stage is connected to keeping several memory of the direction of a projectile.

Figure 4.7. and Table 4.7. Shows the evaluated results and angle-integrated emission Spectra measurements at E_p= 210 MeV. Number of inelastic interactions is 10000, number of elastic interactions is 5862, reaction cross section is 1798.55 mb, and elastic cross section is 1054.31 mb. The calculation obtained for proton emitted has been made for four steps (Total, Cascade, Precompound, Total evaporation) at angle (5°, 15°......... 175°). As can be seen in Figure (4.7) Precompound is decreasing when angular distributions are increasing. Similarly, cascade cross section and total cross section slightly decreases while angular distribution increases and there is no change at total

evaporation cross section. The cross section of proton produced in the cascade is higher than precompound and total evaporation cross section of proton produced.

Table 4.7. Proton scattered angular distributions (mb/sr) for p + $_{90}Th^{232}$ reaction, E_p= 210 MeV energy. Calculations have been made by CEM03 code program

$^{232}Th(p,p')$; E_p=210 MeV CEM03 – Code				
Ang.p [deg.]	Total Cross Section (mb/sr)	Cascade Cross Section (mb/sr)	Precompound Cross Section (mb/sr)	Total Evaporation Cross Section (mb/sr)
5	348.6	293.9	54.64	0
15	453	390.2	53.3	9.517
25	424.3	367.6	51.68	5.051
35	355.9	298.3	53.54	4.008
45	277.3	230.6	39.02	7.664
55	198.1	161.4	32.28	4.41
65	144	107.8	30.8	5.436
75	96.74	68.85	22.1	5.78
85	70.55	44.51	19.45	6.594
95	47.97	27.2	15.17	5.605
105	31.96	15.64	10.54	5.78
115	25.55	10.51	9.603	5.436
125	18.84	5.012	9.021	4.811
135	14.63	3.948	6.967	3.716
145	13.74	2.863	6.585	4.295
155	10.49	0.3886	5.051	5.051
165	12.69	1.269	5.71	5.71
175	3.768	0	1.884	1.884

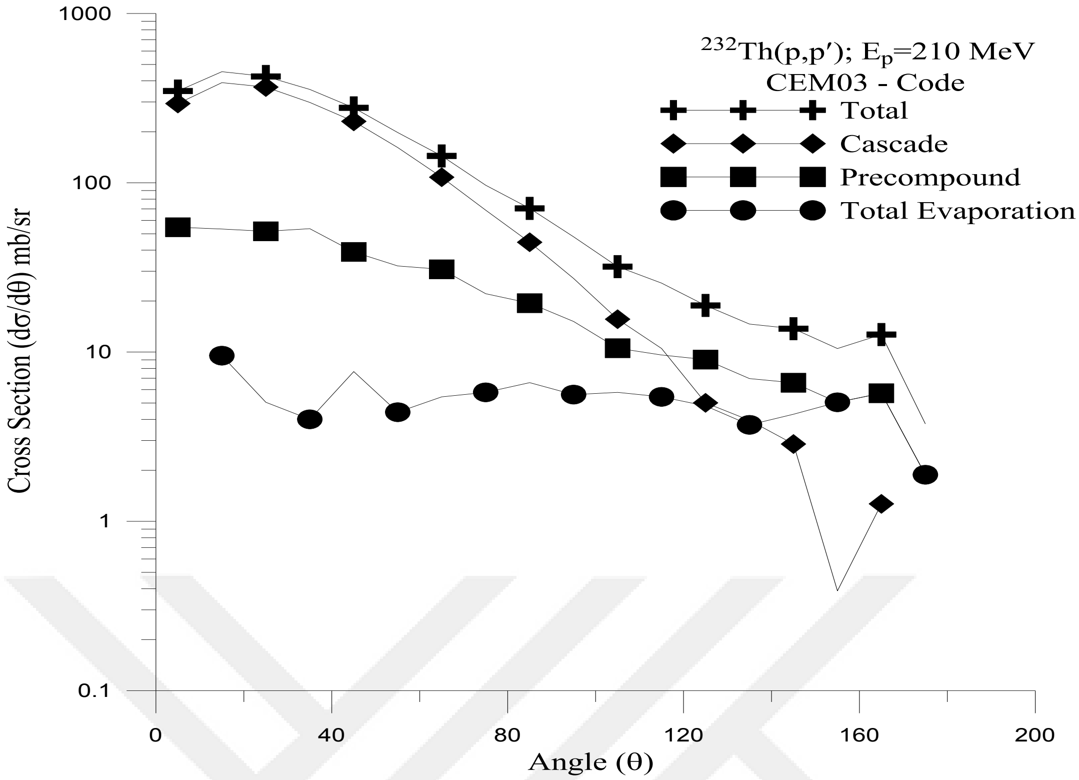

Figure 4.7. Angular Distributions (mb/sr) of the protons (p′) generated as a result of bombardment of element $_{90}Th^{232}$ with 210 MeV energetic protons

4.4.1.8. Proton Angular Distribution for p + $_{90}Th^{232}$ Reaction at E_p = 240 MeV

The CEM03 indicate asymmetrical angular distributions for secondary nucleons. This is because of high asymmetry of the cascade component. A convenient to have asymmetrical distributions for particles emitted throughout the pre-equilibrium interaction stage is connected to keeping several memory of the direction of a projectile.

Figure 4.8. and Table 4.8. Shows the evaluated results and angle-integrated emission Spectra measurements at E_p= 240 MeV. Number of inelastic interactions is 10000, number of elastic interactions is 5941, reaction cross section is 1769.50 mb, and elastic cross section is 1051.26 mb. The calculation obtained for proton emitted has been made for four steps (Total, Cascade, Precompound, Total evaporation) at angle (5°, 15°......... 175°). As can be seen in Figure (4.8) cascade cross section is decreasing when angular distributions are increasing. Similarly, total cross section slightly decreases while angular distribution increases and there is no change at Precompound and total evaporation cross

section. The cross section of proton produced in the cascade is higher than precompound and total evaporation cross section of proton produced.

Table 4.8. Proton scattered angular distributions (mb/sr) for p + $_{90}Th^{232}$ reaction, E_p= 240 MeV energy. Calculations have been made by CEM03 code program

$^{232}Th(p,p')$; E_p=240 MeV CEM03 –Code				
Ang.p [deg.]	Total Cross Section (mb/sr)	Cascade Cross Section (mb/sr)	Precompound Cross Section (mb/sr)	Total Evaporation Cross Section (mb/sr)
5	368.9	337.4	22.24	9.269
15	472.5	425.7	36.21	10.61
25	403.3	368.1	27.53	7.646
35	358.9	313.5	35.49	9.859
45	283.8	244.9	32.9	5.941
55	207.5	174	26.43	7.1
65	152.8	120.3	24.96	7.487
75	107.6	75.6	22.75	9.199
85	80.12	48.01	23.52	8.596
95	61.47	32.44	22.06	6.974
105	44.83	18.4	18.23	8.196
115	34.05	11.94	16.58	5.526
125	29.78	5.72	15.78	8.284
135	23.08	2.513	12.8	7.769
145	24.79	2.817	13.8	8.169
155	22.94	1.147	12.62	9.175
165	18.73	0.6242	12.48	5.618
175	20.39	0	11.12	9.269

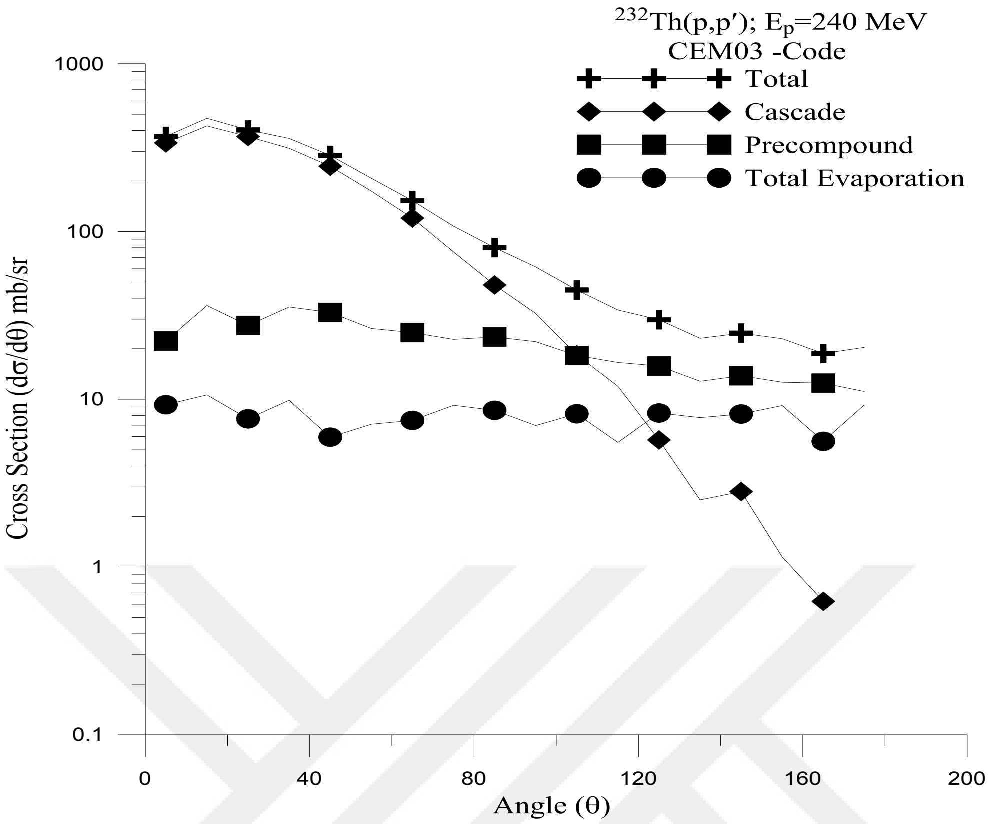

Figure 4.8. Angular Distributions (mb/sr) of the protons (p′) generated as a result of bombardment of element $_{90}Th^{232}$ with 240 MeV energetic protons

4.4.1.9. Proton Angular Distribution for p + $_{90}Th^{232}$ Reaction at E_p = 270 MeV

The CEM03 indicate asymmetrical angular distributions for secondary nucleons. This is because of high asymmetry of the cascade component. A convenient to have asymmetrical distributions for particles emitted throughout the pre-equilibrium interaction stage is connected to keeping several memory of the direction of a projectile.

Figure 4.9. and Table 4.9. Shows the evaluated results and angle-integrated emission Spectra measurements at E_p= 270 MeV. Number of inelastic interactions is 10000, number of elastic interactions is 5960, reaction cross section is 1749.90 mb, and elastic cross section is 1042.94 mb. The calculation obtained for proton emitted has been made for four steps (Total, Cascade, Precompound, Total evaporation) at angle (5°, 15°......... 175°). As can be seen in Figure (4.9) cascade cross section is decreasing when angular distributions are increasing. Similarly, total cross section slightly decreases while angular distribution increases and there is no change at Precompound and total evaporation cross

section. The cross section of proton produced in the cascade is higher than precompound and total evaporation cross section of proton produced.

Table 4.9. Proton scattered angular distributions (mb/sr) for p + $_{90}Th^{232}$ reaction, E_p= 270 MeV energy. Calculations have been made by CEM03 code program

$^{232}Th(p,p')$; E_p=270 MeV CEM03 – Code				
Ang.p [deg.]	Total	Cascade	Precompound	Total Evaporation
	Cross Section (mb/sr)	Cross Section (mb/sr)	Cross Section (mb/sr)	Cross Section (mb/sr)
5	436.3	372.1	53.16	11
15	464.2	426	32.1	6.173
25	414	369	32.89	12.1
35	363.2	322.8	32.31	8.078
45	291	249.2	32.31	9.49
55	222	179.8	34.13	7.997
65	166.2	126.4	29.26	10.58
75	124.9	86.51	28.95	9.428
85	90.62	56.62	23.1	10.91
95	68.97	35.12	23.58	10.26
105	48.63	21.5	17.53	9.594
115	44.6	14.46	19.04	11.11
125	35.3	9.167	17.16	8.972
135	29.37	6.553	13.11	9.716
145	27.58	3.9	12.54	11.14
155	24.2	2.646	12.48	9.073
165	22.84	1.235	15.43	6.173
175	18.33	1.833	3.666	12.83

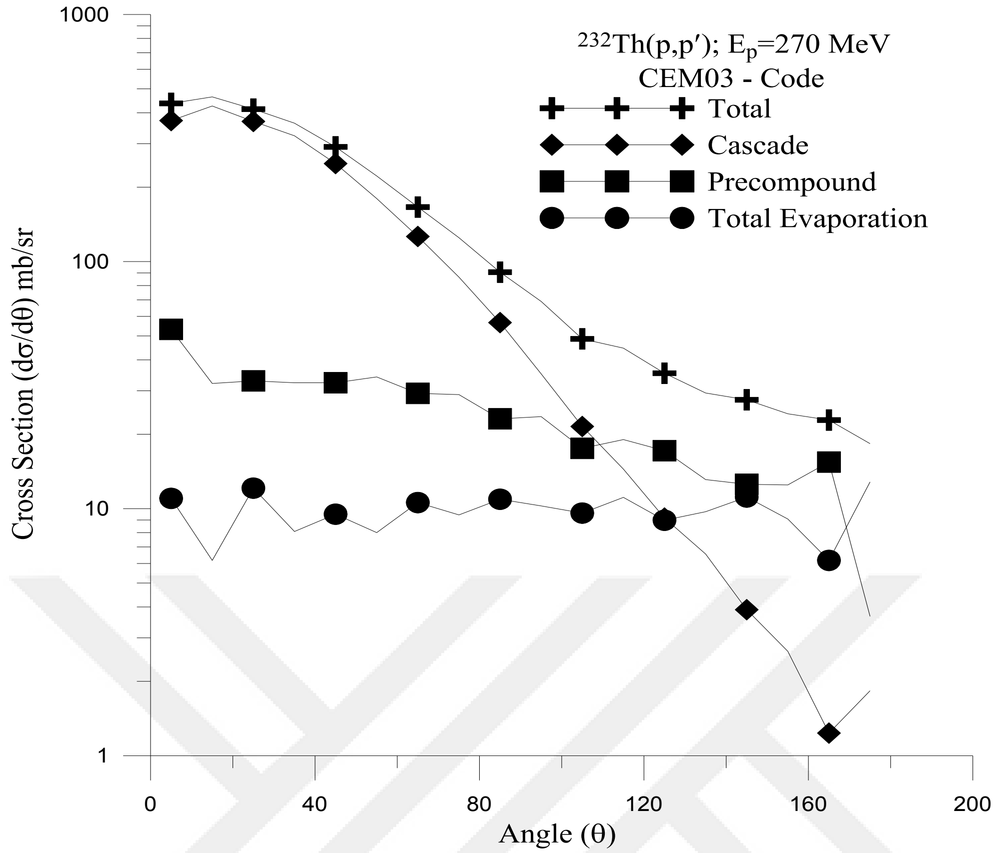

Figure 4.9. Angular Distributions (mb/sr) of the protons (p′) generated as a result of bombardment of element ${}_{90}Th^{232}$ with 270 MeV energetic protons

4.4.1.10. Neutron Angular Distribution for p + ${}_{90}Th^{232}$ Reaction at E_p = 300 MeV

The CEM03 indicate asymmetrical angular distributions for secondary nucleons. This is because of high asymmetry of the cascade component. A convenient to have asymmetrical distributions for particles emitted throughout the pre-equilibrium interaction stage is connected to keeping several memory of the direction of a projectile.

Figure 4.10. and Table 4.10. Shows the evaluated results and angle-integrated emission Spectra measurements at E_p= 300 MeV. Number of inelastic interactions is 10000, number of elastic interactions is 5744, reaction cross section is 1737.67 mb, and elastic cross section is 998.11 mb. The calculation obtained for neutron emitted has been made for four steps steps (Total, Cascade, Precompound, Total evaporation) at angle (5°, 15°......... 175°). As can be seen in Figure (4.10) cascade cross section is decreasing when angular distributions are increasing and there is no change at Precompound, total cross section and total evaporation cross section. The cross section of neutron produced in the

total evaporation is higher than cascade and precompound cross section of neutron produced.

Table 4.10. Neutron scattered angular distributions (mb/sr) for p + $_{90}Th^{232}$ reaction, E_p= 300 MeV energy. Calculations have been made by CEM03 code program

$^{232}Th(p,n)$; E_p=300 MeV CEM03 – Code				
Ang.n [deg.]	Total	Cascade	Precompound	Total Evaporation
	Cross Section (mb/sr)	Cross Section (mb/sr)	Cross Section (mb/sr)	Cross Section (mb/sr)
5	2164	618.9	103.8	1442
15	2140	665.1	115.9	1359
25	2054	582.3	97.61	1374
35	2033	561.2	96.81	1374
45	1939	501	92.67	1345
55	1881	455.4	85.22	1341
65	1835	387.9	89.98	1357
75	1746	322.1	81.31	1343
85	1667	272.3	75.97	1319
95	1600	222.3	65.46	1312
105	1547	173	64.88	1309
115	1463	131.8	59.35	1271
125	1435	111	62.37	1262
135	1383	87.06	53.85	1242
145	1360	74.13	47.3	1239
155	1330	55.19	49.93	1225
165	1359	52.11	50.27	1257
175	1272	45.51	58.25	1169

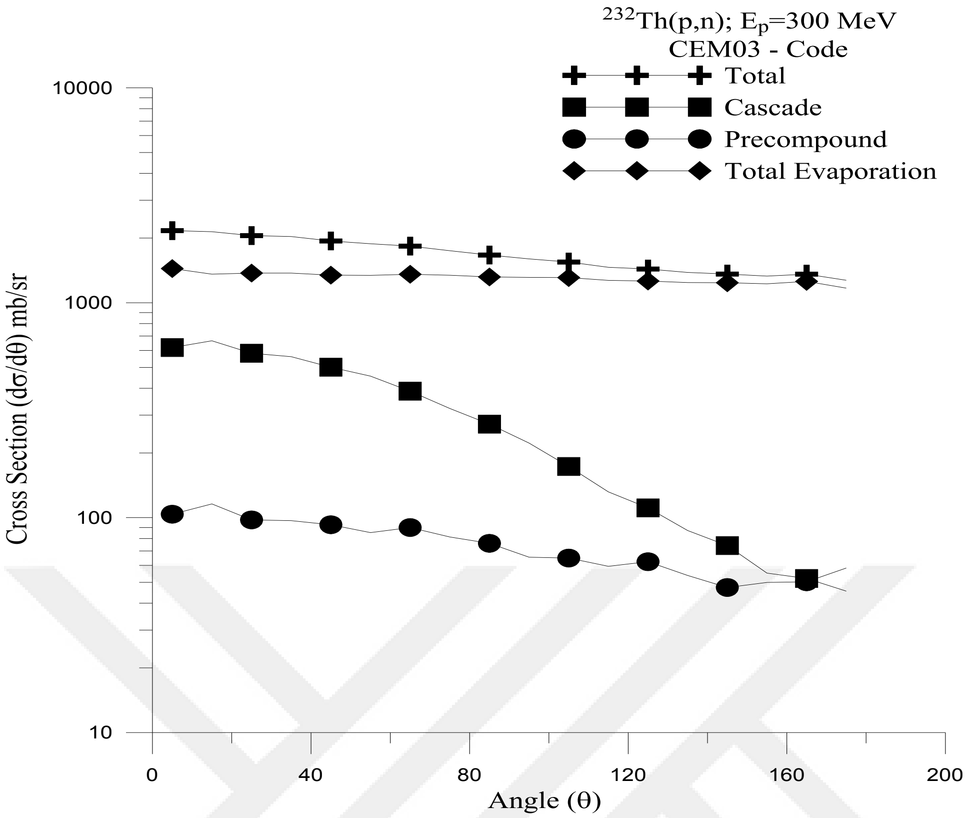

Figure 4.10. Angular Distributions (mb/sr) of the neutrons generated as a result of bombardment of element $_{90}Th^{232}$ with 300 MeV energetic protons

4.4.1.11. Neutron Angular Distribution for p + $_{90}Th^{232}$ Reaction at E_p = 350 MeV

The CEM03 indicate asymmetrical angular distributions for secondary nucleons. This is because of high asymmetry of the cascade component. A convenient to have asymmetrical distributions for particles emitted throughout the pre-equilibrium interaction stage is connected to keeping several memory of the direction of a projectile.

Figure 4.11. and Table 4.11. Shows the evaluated results and angle-integrated emission Spectra measurements at E_p= 350 MeV. Number of inelastic interactions is 10000, number of elastic interactions is 5744, reaction cross section is 1737.67 mb, and elastic cross section is 998.11 mb. The calculation obtained for neutron emitted has been made for four steps (Total, Cascade, Precompound, Total evaporation) at angle (5°, 15°......... 175°). As can be seen in Figure (4.11) cascade cross section is decreasing when angular distributions are increasing and there is no change at Precompound, total cross section

and total evaporation cross section. The cross section of neutron produced in the total evaporation is higher than cascade and precompound cross section of neutron produced.

Table 4.11. Neutron scattered angular distributions (mb/sr) for p + $_{90}Th^{232}$ reaction, E_p= 350 MeV energy. Calculations have been made by CEM03 code program

$^{232}Th(p,n)$; E_p=350 MeV CEM03 – Code				
Ang.n	Total	Cascade	Precompound	Total Evaporation
[deg.]	Cross Section (mb/sr)	Cross Section (mb/sr)	Cross Section (mb/sr)	Cross Section (mb/sr)
5	2119	603.2	99.62	1416
15	2259	723.4	114.7	1421
25	2185	630.9	102	1452
35	2138	552.1	103.8	1482
45	2039	526.4	93.32	1419
55	1965	459.8	93.85	1411
65	1892	387.6	84.83	1420
75	1805	319.5	82.7	1403
85	1753	273	75.27	1404
95	1663	219.5	70.99	1373
105	1589	183	72.89	1333
115	1536	141.1	62.18	1333
125	1531	129.5	58.2	1343
135	1471	100.2	50.9	1320
145	1426	75.41	54.22	1296
155	1417	67.98	45.95	1303
165	1406	68.31	47.58	1290
175	1328	61.58	41.66	1224

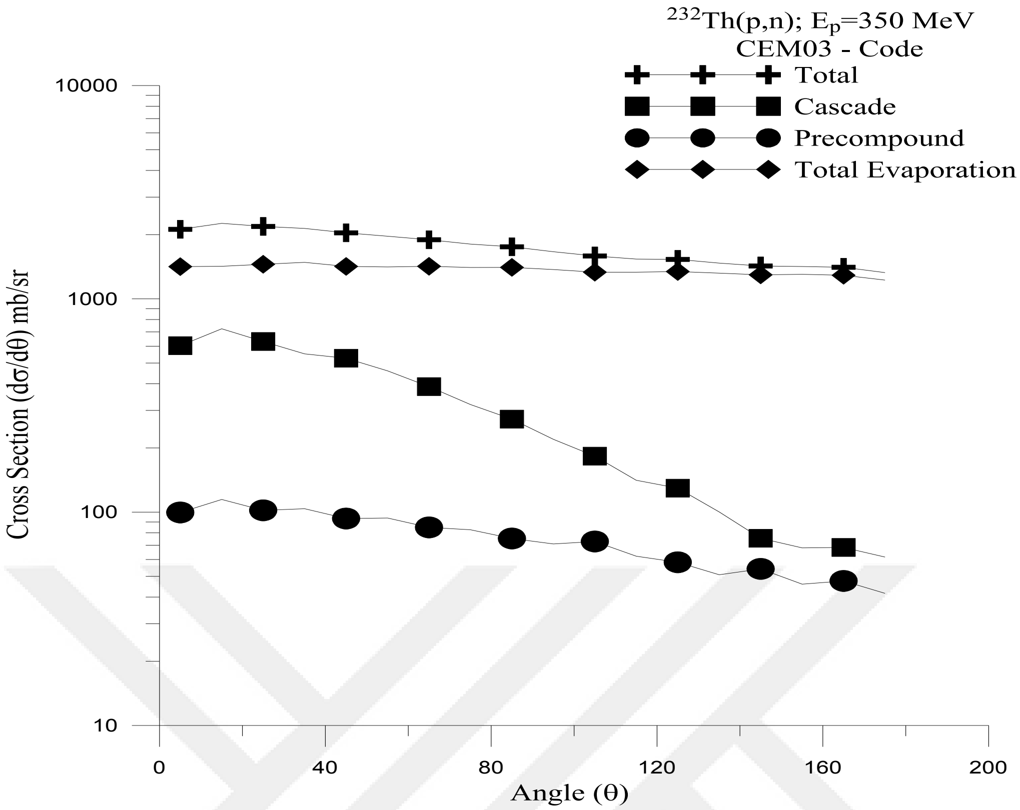

Figure 4.11. Angular Distributions (mb/sr) of the neutrons generated as a result of bombardment of element $_{90}Th^{232}$ with 350 MeV energetic protons

4.4.1.12. Neutron Angular Distribution for p + $_{90}Th^{232}$ Reaction at E_p = 400 MeV

The CEM03 indicate asymmetrical angular distributions for secondary nucleons. This is because of high asymmetry of the cascade component. A convenient to have asymmetrical distributions for particles emitted throughout the pre-equilibrium interaction stage is connected to keeping several memory of the direction of a projectile.

Figure 4.12. and Table 4.12. Shows the evaluated results and angle-integrated emission Spectra measurements at E_p = 400 MeV. Number of inelastic interactions is 10000, number of elastic interactions is 5557, reaction cross section is 1729.89 mb, and elastic cross section is 961.30 mb. The calculation obtained for neutron emitted has been made for four steps (Total, Cascade, Precompound, Total evaporation) at angle (5°, 15°......... 175°). As can be seen in Figure (4.12) cascade cross section is decreasing when angular distributions are increasing and there is no change at Precompound, total cross section

and total evaporation cross section. The cross section of neutron produced in the total evaporation is higher than cascade and precompound cross section of neutron produced.

Table 4.12. Neutron scattered angular distributions (mb/sr) for p + $_{90}Th^{232}$ reaction, E_p= 400 MeV energy. Calculations have been made by CEM03 code program

$^{232}Th(p,n)$; E_p=400 MeV CEM03 – Code				
Ang.n [deg.]	Total	Cascade	Precompound	Total Evaporation
	Cross Section (mb/sr)	Cross Section (mb/sr)	Cross Section (mb/sr)	Cross Section (mb/sr)
5	2450	801	114.2	1535
15	2426	742.7	112.9	1570
25	2277	692.2	94.18	1490
35	2248	609.7	106.8	1531
45	2187	564.2	113.5	1509
55	2074	472.4	103.7	1498
65	1996	410.2	98.64	1487
75	1892	356.1	94.68	1441
85	1810	296.6	80.23	1433
95	1764	234.7	79.43	1450
105	1693	206.9	75.87	1410
115	1619	163.6	65.88	1390
125	1577	127.6	67.49	1382
135	1539	103.2	61.43	1374
145	1504	87.29	56.73	1360
155	1492	74.75	49.33	1368
165	1453	56.75	54.92	1341
175	1490	83.36	39.87	1366

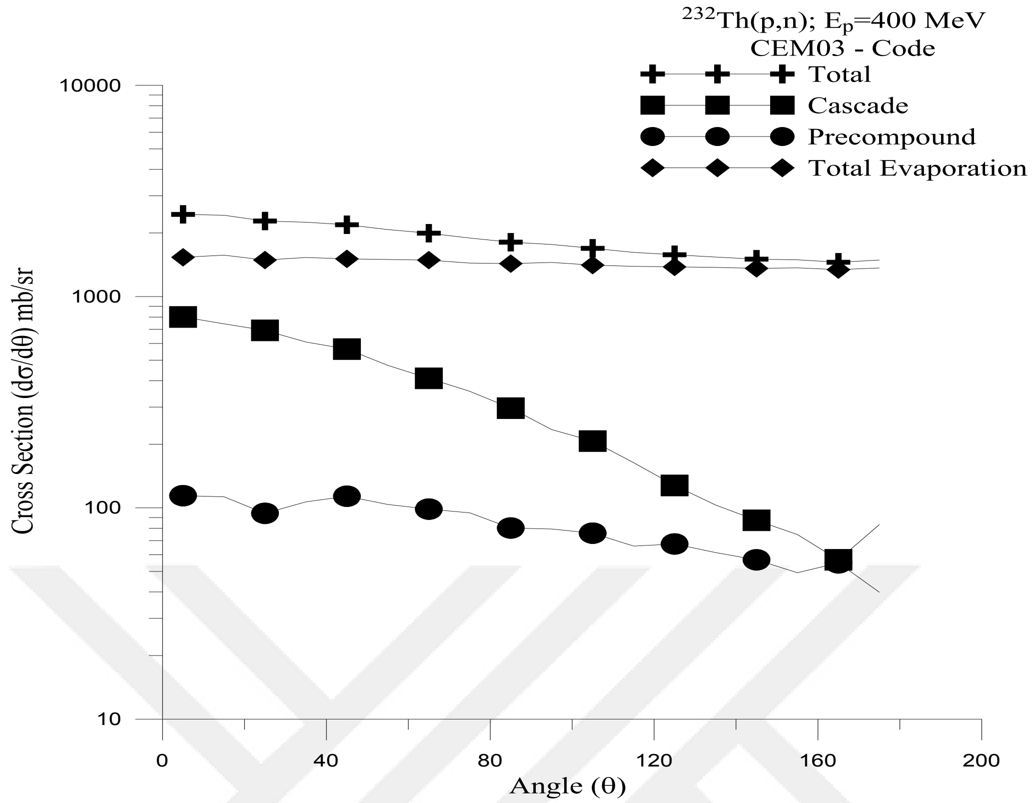

Figure 4.12. Angular Distributions (mb/sr) of the neutrons generated as a result of bombardment of element ${}_{90}Th^{232}$ with 400 MeV energetic protons

4.4.1.13. Neutron Angular Distribution for p + ${}_{90}Th^{232}$ Reaction at E_p = 450 MeV

The CEM03 indicate asymmetrical angular distributions for secondary nucleons. This is because of high asymmetry of the cascade component. A convenient to have asymmetrical distributions for particles emitted throughout the pre-equilibrium interaction stage is connected to keeping several memory of the direction of a projectile.

Figure 4.13.and Table 4.13. Shows the evaluated results and angle-integrated emission Spectra measurements at E_p= 450 MeV. Number of inelastic interactions is 10000, number of elastic interactions is 5487, reaction cross section is 1736.51 mb, and elastic cross section is 952.82 mb. The calculation obtained for neutron emitted has been made for four steps (Total, Cascade, Precompound, Total evaporation) at angle (5°, 15°......... 175°). As can be seen in Figure (4.13) cascade cross section is decreasing when angular distributions are increasing and there is no change at Precompound total cross section and

total evaporation cross section. The cross section of neutron produced in the total evaporation is higher than cascade and precompound cross section of neutron produced.

Table 4.13. Neutron scattered angular distributions (mb/sr) for p + $_{90}Th^{232}$ reaction, E_p= 450 MeV energy. Calculations have been made by CEM03 code program

$^{232}Th(p,n)$; E_p=450 MeV CEM03 – Code				
Ang.n [deg.]	Total Cross Section (mb/sr)	Cascade Cross Section (mb/sr)	Precompound Cross Section (mb/sr)	Total Evaporation Cross Section (mb/sr)
5	2674	840.5	118.2	1715
15	2536	831.9	126.8	1577
25	2487	755.2	130.9	1600
35	2375	662	118.6	1594
45	2301	573.6	111.9	1615
55	2166	503.1	116.5	1547
65	2095	432.5	101.6	1561
75	1987	379.3	97.99	1510
85	1924	333	82.76	1508
95	1862	259.9	79.1	1523
105	1771	215.7	82.56	1473
115	1711	187.4	66.48	1457
125	1644	147.9	63.87	1432
135	1626	130.3	61.44	1435
145	1605	101.4	57.5	1446
155	1560	96.04	50.27	1414
165	1556	82.09	55.75	1418
175	1515	67.31	49.12	1399

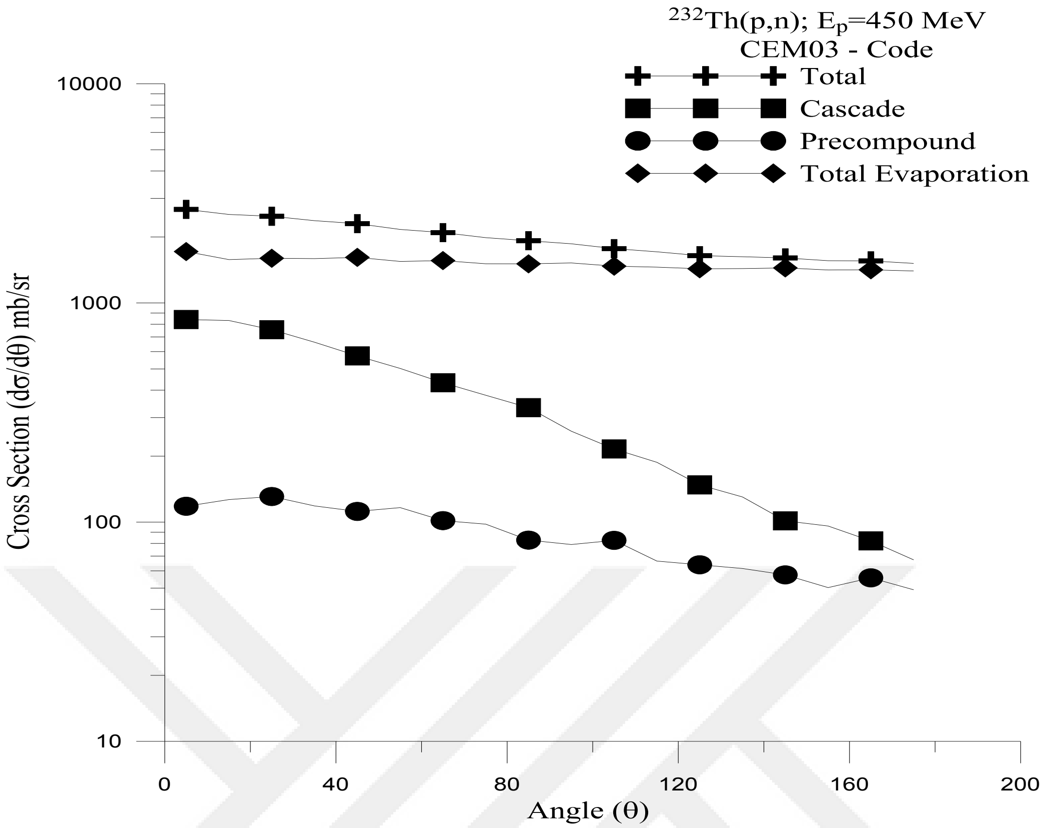

Figure 4.13. Angular Distributions (mb/sr) of the neutrons generated as a result of bombardment of element $_{90}Th^{232}$ with 450 MeV energetic protons

4.4.2. p + $_{82}Pb^{206}$ Reaction

Lead is a chemical element with atomic number 82 and denoted by Pb (after the Latin plumbum). When recently cut, it is bluish-white; it tarnishes to a dull gray leading exposure to air. It is a soft, malleable, and heavy metal with a density exceeding that of the majority common materials. Lead has the second-maximum atomic number of the classically constant elements and lies at the end of three core decay groups of heavier elements.

Lead has numerous properties that make it useful: low melting point, high density, ductility, and relative inertness to oxidation (https://en.wikipedia.org/wiki/Lead).

4.4.2.1. Neutron Angular Distribution for p + $_{82}Pb^{206}$ Reaction at E_p = 30 MeV

The CEM03 indicate asymmetrical angular distributions for secondary nucleons. This is because of high asymmetry of the cascade component. A convenient to have asymmetrical distributions for particles emitted throughout the pre-equilibrium interaction stage is connected to keeping several memory of the direction of a projectile.

Figure 4.14. and Table 4.14. Shows the evaluated results and angle-integrated emission Spectra measurements at E_p= 30 MeV. Number of inelastic interactions is 10000, number of elastic interactions is 3686, reaction cross section is 1787.24 mb, and elastic cross section is 658.78 mb. The calculation obtained for neutron emitted has been made for four steps steps (Total, Cascade, Precompound, Total evaporation) at angle (5°, 15°......... 175°). As can be seen in Figure (4.14) cascade cross section is decreasing when angular distributions are increasing. Similarly, Precompound slightly decreases while angular distribution increases and there is no change at total cross section and total evaporation cross section. The cross section of neutron produced in the total evaporation is higher than cascade and precompound cross section of neutron produced

Table 4.14. Neutron scattered angular distributions (mb/sr) for p + $_{82}Pb^{206}$ reaction, E_p= 30 MeV energy. Calculations have been made by CEM03 code program

$^{206}Pb(p,n)$; E_p=30 MeV CEM03 –Code				
Ang.n [deg.]	Total Cross Section (mb/sr)	Cascade Cross Section (mb/sr)	Precompound Cross Section (mb/sr)	Total Evaporation Cross Section (mb/sr)
5	572.4	44.81	79.44	448.1
15	607.7	75.45	67.22	465
25	626.3	98.71	82.75	444.8
35	632.6	83.57	74.59	474.5
45	576.2	72.3	61.26	442.6
55	542.9	50.06	52.45	440.4
65	532.8	39.37	47.6	445.8
75	498.2	24.26	37.86	436.1
85	489.3	14.79	34.93	439.6
95	459	7.663	27.8	423.6
105	462	4.778	23.52	433.7
115	445.4	2.938	21.94	420.5
125	443.2	0.4334	22.76	420
135	435.8	0	18.33	417.5
145	417.5	0.9285	13.62	403
155	431.8	0.4201	22.68	408.7
165	404	0	12.35	391.6
175	450.1	0	10.18	440

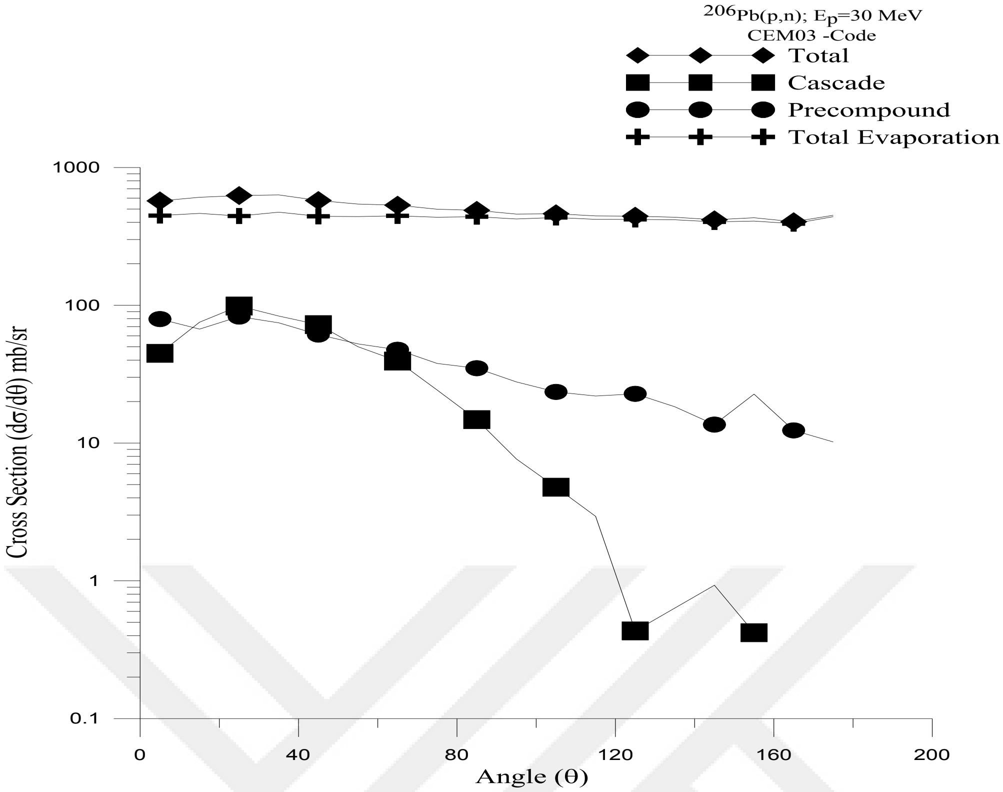

Figure 4.14. Angular Distributions (mb/sr) of the neutrons generated as a result of bombardment of element $_{82}Pb^{206}$ with 30 MeV energetic protons

4.4.2.2. Neutron Angular Distribution for p + $_{82}$Pb^{206} Reaction at E$_p$ = 60 MeV

The CEM03 indicate asymmetrical angular distributions for secondary nucleons. This is because of high asymmetry of the cascade component. A convenient to have asymmetrical distributions for particles emitted throughout the pre-equilibrium interaction stage is connected to keeping several memory of the direction of a projectile.

Figure 4.15. and Table 4.15. Shows the evaluated results and angle-integrated emission Spectra measurements at E_p= 60 MeV. Number of inelastic interactions is 10000, number of elastic interactions is 5096, reaction cross section is 1948.41 mb, and elastic cross section is 992.91 mb. The calculation obtained for neutron emitted has been made for four steps (Total, Cascade, Precompound, Total evaporation) at angle (5°, 15°......... 175°). As can be seen in Figure (4.15) cascade cross section is decreasing when angular distributions are increasing. Similarly, Precompound slightly decreases while angular distribution increases and there is no change at total cross section and total evaporation

cross section. The cross section of neutron produced in the total evaporation is higher than cascade and precompound cross section of neutron produced.

Table 4.15. Neutron scattered angular distributions (mb/sr) for p + $_{82}Pb^{206}$ reaction, E_p= 60 MeV energy. Calculations have been made by CEM03 code program

$^{206}Pb(p,n)$; E_p=60 MeV CEM03 – Code				
Ang.n [deg.]	Total	Cascade	Precompound	Total Evaporation
	Cross Section (mb/sr)	Cross Section (mb/sr)	Cross Section (mb/sr)	Cross Section (mb/sr)
5	561.3	57.15	95.93	408.2
15	672.9	121.7	93.48	457.8
25	684.5	138.1	85.03	461.4
35	685.5	142.4	71.03	472.1
45	651.9	104.9	67.68	479.3
55	580.3	74.27	59.51	446.5
65	557.3	55.35	50.25	451.7
75	544.1	35.55	49.73	458.8
85	511.6	20.72	35.18	455.7
95	499.5	17.14	32.14	450.2
105	503.2	9.393	26.52	467.3
115	469.5	2.552	22.77	444.2
125	434.6	2.389	17.59	414.6
135	438	1.258	20.38	416.4
145	431.1	1.241	20.47	409.4
155	427.7	0	16.42	411.3
165	429.6	0.6874	17.18	411.7
175	430.7	0	14.29	416.4

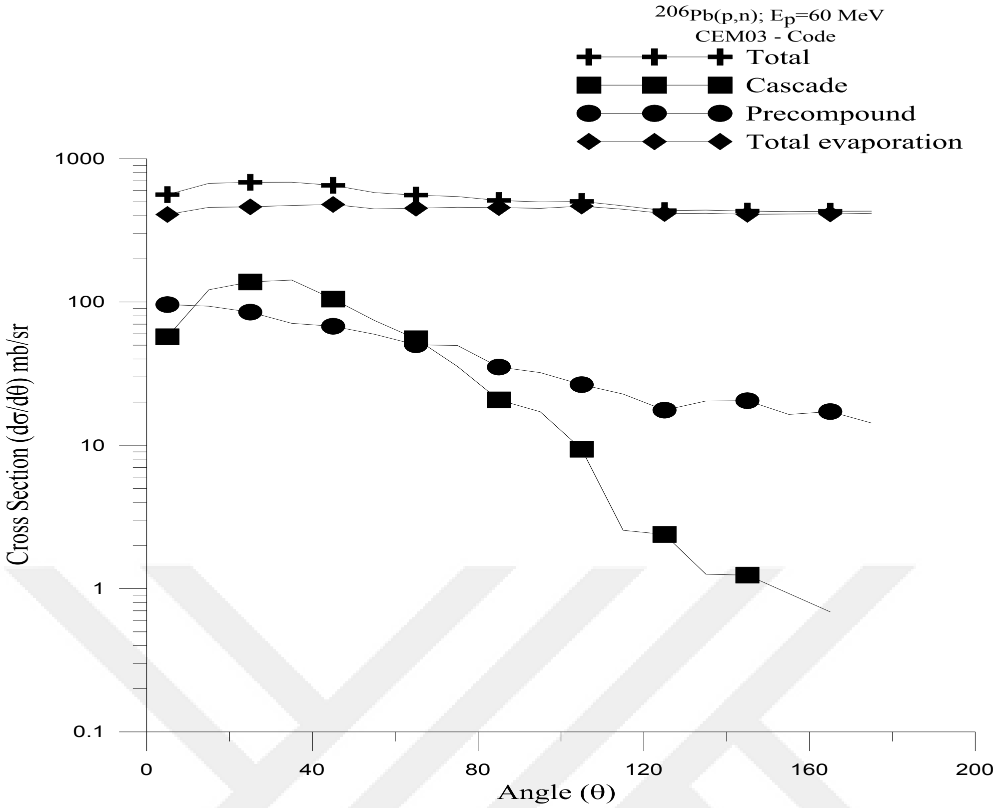

Figure 4.15. Angular Distributions (mb/sr) of the neutrons generated as a result of bombardment of element $_{82}Pb^{206}$ with 60 MeV energetic protons

4.4.2.3. Neutron Angular Distribution for p + $_{82}Pb^{206}$ Reaction at E_p = 90 MeV

The CEM03 indicate asymmetrical angular distributions for secondary nucleons. This is because of high asymmetry of the cascade component. A convenient to have asymmetrical distributions for particles emitted throughout the pre-equilibrium interaction stage is connected to keeping several memory of the direction of a projectile.

Figure 4.16. and Table 4.16. Shows the evaluated results and angle-integrated emission Spectra measurements at E_p= 90 MeV. Number of inelastic interactions is 10000, number of elastic interactions is 5510, reaction cross section is 1888.04 mb, and elastic cross section is 1040.31 mb. The calculation obtained for neutron emitted has been made for four steps (Total, Cascade, Precompound, Total evaporation) at angle (5°, 15°......... 175°). As can be seen in Figure (4.16) cascade cross section is decreasing when angular distributions are increasing. Similarly, Precompound slightly decreases while angular distribution increases and there is no change at total cross section and total evaporation

cross section. The cross section of neutron produced in the total evaporation is higher than cascade and precompound cross section of neutron produced.

Table 4.16. Neutron scattered angular distributions (mb/sr) for p + $_{82}Pb^{206}$ reaction, E_p= 90 MeV energy. Calculations have been made by CEM03 code program

$^{206}Pb(p,n)$; E_p=90 MeV CEM03 –Code				
Ang.n [deg.]	Total	Cascade	Precompound	Total Evaporation
	Cross Section (mb/sr)	Cross Section (mb/sr)	Cross Section (mb/sr)	Cross Section (mb/sr)
5	763.5	120.7	138.5	504.4
15	921.8	195.8	141.9	584.1
25	868	188.9	107.3	571.9
35	817.8	174.3	104.6	538.9
45	821.8	151.4	88.5	581.9
55	761.2	112.8	70.5	577.9
65	696.9	89.4	62.39	545.1
75	661.6	60.32	52.29	549
85	627.5	41.7	41.36	544.4
95	610.7	29.94	40.49	540.2
105	587	17.67	34.27	535
115	573.1	10.65	29.67	532.8
125	548.8	5.261	25.25	518.3
135	543.9	4.632	19.75	519.5
145	539.5	2.404	18.63	518.4
155	525.4	0.4079	17.13	507.8
165	546.2	0.6661	15.32	530.2
175	514.3	3.956	13.85	496.5

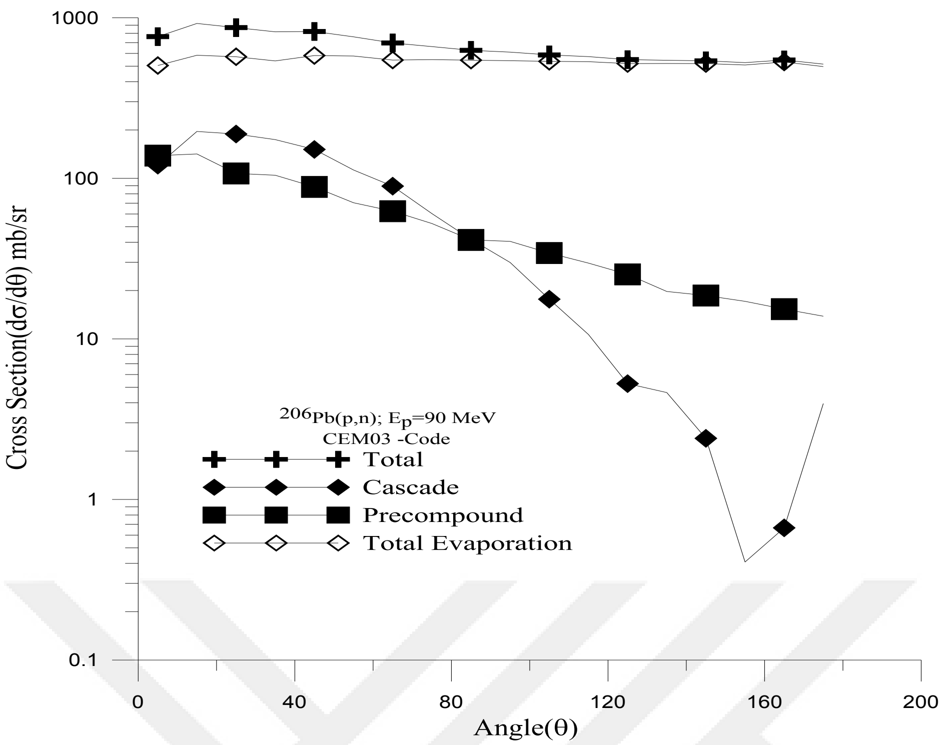

Figure 4.16. Angular Distributions (mb/sr) of the neutrons generated as a result of bombardment of element $_{82}Th^{206}$ with 90 MeV energetic protons

4.4.2.4. Proton Angular Distribution for p + $_{82}Pb^{206}$ Reaction at E_p = 120 MeV

The CEM03 indicate asymmetrical angular distributions for secondary nucleons. This is because of high asymmetry of the cascade component. A convenient to have asymmetrical distributions for particles emitted throughout the pre-equilibrium interaction stage is connected to keeping several memory of the direction of a projectile.

Figure 4.17. and Table 4.17. Shows the evaluated results and angle-integrated emission Spectra measurements at E_p= 120 MeV. Number of inelastic interactions is 10000, number of elastic interactions is 5769, reaction cross section is 1808.56 mb, and elastic cross section is 1043.36 mb. The calculation obtained for proton emitted has been made for four steps (Total, Cascade, Precompound, Total evaporation) at angle (5°, 15°......... 175°). As can be seen in Figure (4.17) cascade cross section is decreasing when angular distributions are increasing. Similarly, Precompound and total cross section slightly decreases while angular distribution increases and there is no change at total evaporation cross section. The cross section of proton produced in the cascade is higher than precompound and total evaporation cross section of proton produced.

Table 4.17. Proton scattered angular distributions (mb/sr) for p + $_{82}Pb^{206}$ reaction, E_p= 120 MeV energy. Calculations have been made by CEM03 code program

$^{206}Pb(p,p')$; E_p=120 MeV CEM03 – Code				
Ang.p [deg.]	Total Cross Section (mb/sr)	Cascade Cross Section (mb/sr)	Precompound Cross Section (mb/sr)	Total Evaporation Cross Section (mb/sr)
5	388.4	236.8	142.1	9.473
15	439	304.3	129.5	5.104
25	413.8	305.6	103.2	5.08
35	342	249	88.38	4.606
45	252.9	175.6	73.09	4.204
55	170.7	108.9	55.23	6.652
65	121.9	71.42	45	5.466
75	79.32	37.78	34.53	7.009
85	55.7	18.73	31.66	5.304
95	40.45	10.77	24.37	5.304
105	31.11	5.642	19.49	5.983
115	22.41	2.369	14.39	5.648
125	16.73	1.21	11.29	4.233
135	18.22	0.2335	11.21	6.772
145	15.55	0.5758	8.349	6.622
155	11.72	0.3907	8.205	3.126
165	8.932	0	7.018	1.914
175	15.16	0	11.37	3.789

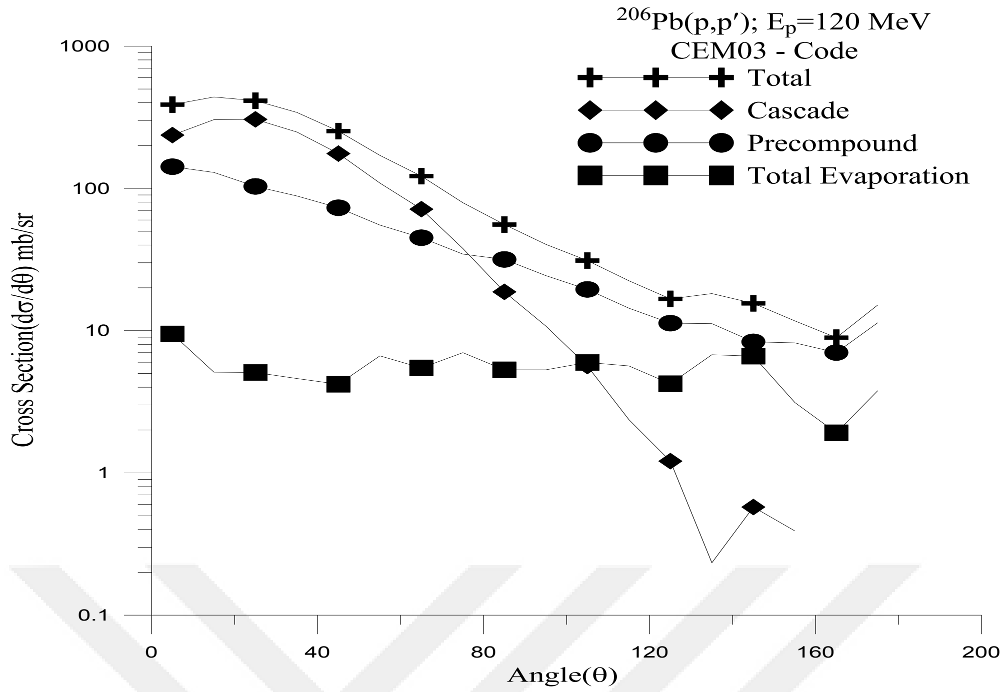

Figure 4.17. Angular Distributions (mb/sr) of the protons (p′) generated as a result of bombardment of element $_{82}Pb^{206}$ with 120 MeV energetic protons

4.4.2.5. Neutron Angular Distribution for p + $_{82}Pb^{206}$ Reaction at E_p = 150 MeV

The CEM03 indicate asymmetrical angular distributions for secondary nucleons. This is because of high asymmetry of the cascade component. A convenient to have asymmetrical distributions for particles emitted throughout the pre-equilibrium interaction stage is connected to keeping several memory of the direction of a projectile.

Figure 4.18. and Table 4.18. shows the evaluated results and angle-integrated emission Spectra measurements at E_p= 150 MeV. Number of inelastic interactions is 10000, number of elastic interactions is 5778, reaction cross section is 1740.38 mb, and elastic cross section is 1005.59 mb. The calculation obtained for neutron emitted has been made for four steps (Total, Cascade, Precompound, Total evaporation) at angle (5°, 15°......... 175°). As can be seen in Figure (4.18) cascade cross section is decreasing when angular distributions are increasing. Similarly, Precompound slightly decreases while angular distribution increases and there is no change at total cross section and total evaporation cross section. The cross section of neutron produced in the total evaporation is higher than cascade and precompound cross section of neutron produced.

Table 4.18. Neutron scattered angular distributions (mb/sr) for p + $_{82}Pb^{206}$ reaction, E_p= 150 MeV energy. Calculations have been made by CEM03 code program

$^{206}Pb(p,n)$; E_p=150 MeV CEM03 – Code				
Ang.n [deg.]	Total	Cascade	Precompound	Total Evaporation
	Cross Section (mb/sr)	Cross Section (mb/sr)	Cross Section (mb/sr)	Cross Section (mb/sr)
5	1147	279	125.8	742.1
15	1162	329.1	145.5	687.6
25	1146	330.1	121.1	694.8
35	1074	292.6	95.3	686.2
45	1054	247.4	85.85	721.1
55	990.3	220.6	83.8	685.9
65	938.6	168.5	70.48	699.6
75	875.9	133.9	55.11	686.8
85	815.3	100.8	45.62	668.8
95	760.6	67.63	42.75	650.2
105	754.1	51.82	35.7	666.6
115	728.3	36.82	29.28	662.2
125	687.7	28.71	27.35	631.6
135	684.5	22.7	26.07	635.7
145	704.5	14.41	25.21	664.9
155	627.2	10.53	23.31	593.3
165	636.1	4.912	17.8	613.3
175	672.8	3.646	16.41	652.7

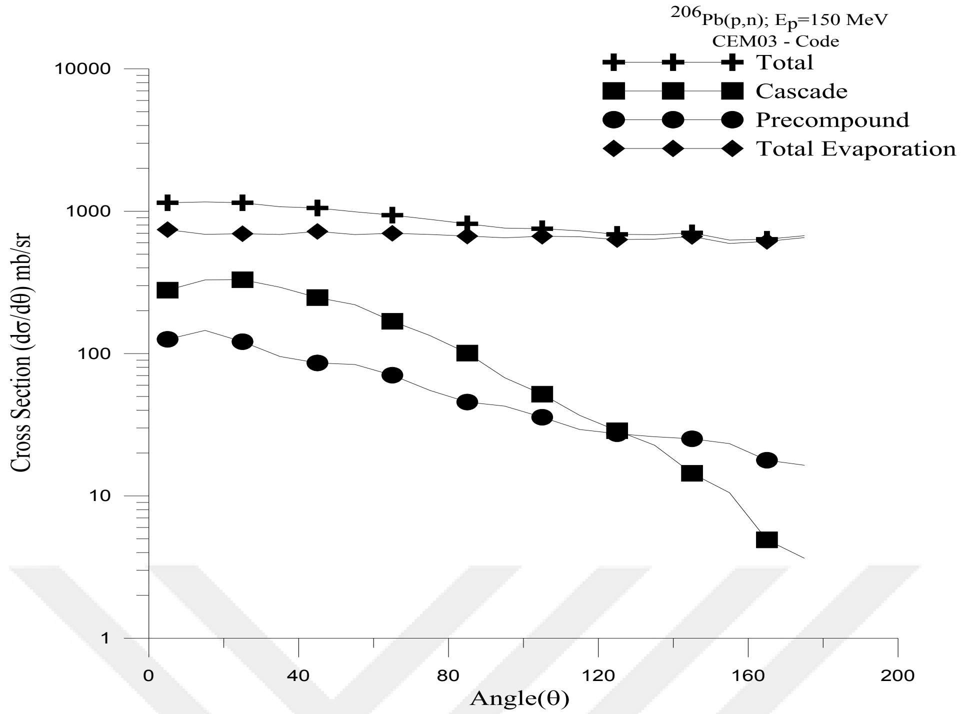

Figure 4.18. Angular Distributions (mb/sr) of the neutrons generated as a result of bombardment of element $_{82}Pb^{206}$ with 150 MeV energetic protons

4.4.2.6. Proton Angular distribution for p + $_{82}Pb^{206}$ Reaction at E_p = 180 MeV

The CEM03 indicate asymmetrical angular distributions for secondary nucleons. This is because of high asymmetry of the cascade component. A convenient to have asymmetrical distributions for particles emitted throughout the pre-equilibrium interaction stage is connected to keeping several memory of the direction of a projectile.

Figure 4.19. and Table 4.19. Shows the evaluated results and angle-integrated emission Spectra measurements at E_p= 180 MeV. Number of inelastic interactions is 10000, number of elastic interactions is 6288, reaction cross section is 1687.86 mb, and elastic cross section is 1061.33 mb. The calculation obtained for proton emitted has been made for four steps (Total, Cascade, Precompound, Total evaporation) at angle (5°, 15°......... 175°). As can be seen in figure (4.19) cascade cross section is decreasing when angular distributions are increasing. Similarly, Precompound and total cross section slightly decreases while angular distribution increases and there is no change at total evaporation cross section. The cross section of proton produced in the cascade is higher than precompound and total evaporation cross section of proton produced.

Table 4.19. Proton scattered angular distributions (mb/sr) for p + $_{82}Pb^{206}$ reaction, E_p= 180 MeV energy. Calculations have been made by CEM03 code program

$^{206}Pb(p,p')$; E_p=180 MeV CEM03 – Code				
Ang.p [deg.]	Total Cross Section (mb/sr)	Cascade Cross Section (mb/sr)	Precompound Cross Section (mb/sr)	Total Evaporation Cross Section (mb/sr)
5	389	295.3	83.11	10.61
15	457.9	369.8	75.02	13.1
25	419.7	343.5	64.18	12.03
35	363.8	296.1	60.99	6.717
45	273.5	213.1	51	9.372
55	204.5	153.1	42.14	9.219
65	140.6	99.98	30.95	9.692
75	100.2	64.78	26.33	9.094
85	69.46	40.53	20.27	8.663
95	47.18	21.19	16.09	9.901
105	41	13.72	17.71	9.573
115	31.97	8.842	12.58	10.54
125	27.66	4.139	12.23	11.29
135	20.92	2.833	8.282	9.807
145	15.85	2.956	7.792	5.105
155	14.95	0.3647	6.199	8.387
165	16.67	0.5954	8.336	7.741
175	19.45	0	7.073	12.38

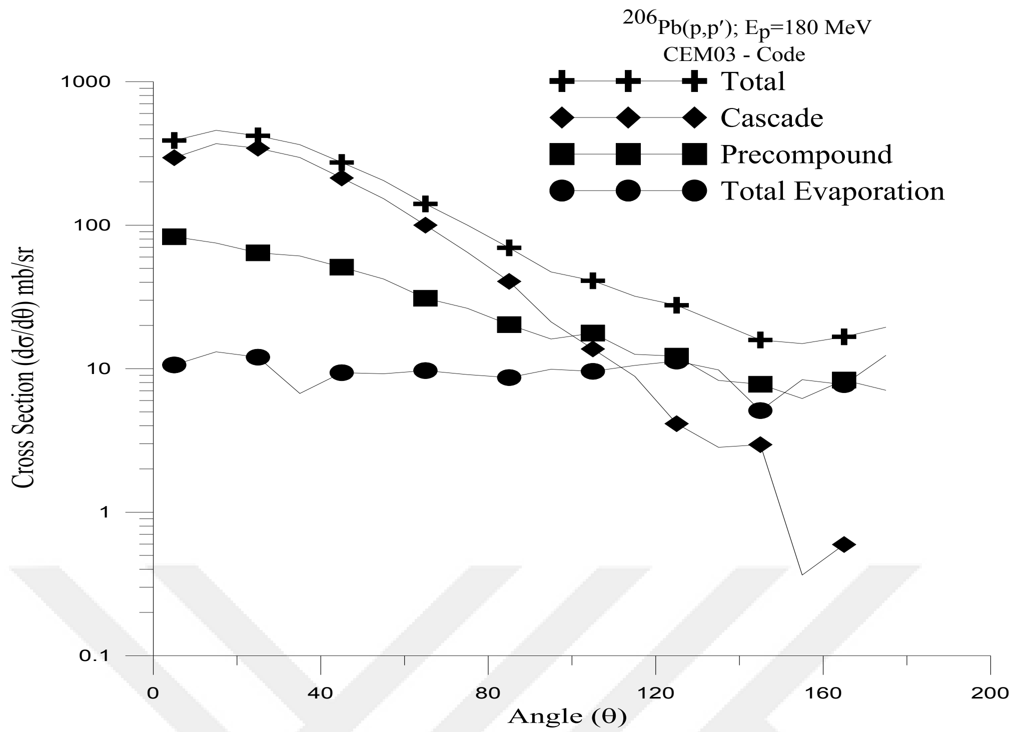

Figure 4.19. Angular Distributions (mb/sr) of the protons (p′) generated as a result of bombardment of element ${}_{82}Pb^{206}$ with 180 MeV energetic protons

4.4.2.7. Proton Angular Distribution for p + ${}_{82}Pb^{206}$ Reaction at E_p = 210 MeV

The CEM03 indicate asymmetrical angular distributions for secondary nucleons. This is because of high asymmetry of the cascade component. A convenient to have asymmetrical distributions for particles emitted throughout the pre-equilibrium interaction stage is connected to keeping several memory of the direction of a projectile.

Figure 4.20. and Table 4.20. Shows the evaluated results and angle-integrated emission Spectra measurements at E_p= 210 MeV. Number of inelastic interactions is 10000, number of elastic interactions is 6050, reaction cross section is 1649.68 mb, and elastic cross section is 998.06 mb. The calculation obtained for proton emitted has been made for four steps (Total, Cascade, Precompound, Total evaporation) at angle (5°, 15°......... 175°). As can be seen in Figure (4.20) cascade cross section is decreasing when angular distributions are increasing. Similarly, Precompound and total cross section slightly decreases while angular distribution increases and there is no change at total evaporation cross section. The cross section of proton produced in the cascade is higher than precompound and total evaporation cross section of proton produced.

Table 4.20. Proton scattered angular distributions (mb/sr) for p + $_{82}Pb^{206}$ reaction, E_p= 210 MeV energy. Calculations have been made by CEM03 code program

$^{206}Pb(p,p')$; E_p=210 MeV CEM03 – Code				
Ang.p	Total	Cascade	Precompound	Total Evaporation
[deg.]	Cross Section (mb/sr)	Cross Section (mb/sr)	Cross Section (mb/sr)	Cross Section (mb/sr)
5	376.8	305.9	58.76	12.1
15	463.2	385.3	69.25	8.729
25	413.8	350	53.82	9.979
35	360	293.9	52.78	13.39
45	284.2	226.9	44.73	12.57
55	217.9	166.8	38.06	13.06
65	159.5	114	33.74	11.8
75	105.3	69.39	23.86	12.01
85	75.3	44.3	21.32	9.677
95	57.76	31.15	13.76	12.85
105	40.7	16.53	11.7	12.47
115	33.07	11.3	9.806	11.97
125	26.66	6.62	8.642	11.4
135	27.48	3.195	10.22	14.06
145	20.22	1.576	5.515	13.13
155	20.32	1.782	6.772	11.76
165	16.3	2.328	4.656	9.311
175	17.28	5.185	3.456	8.641

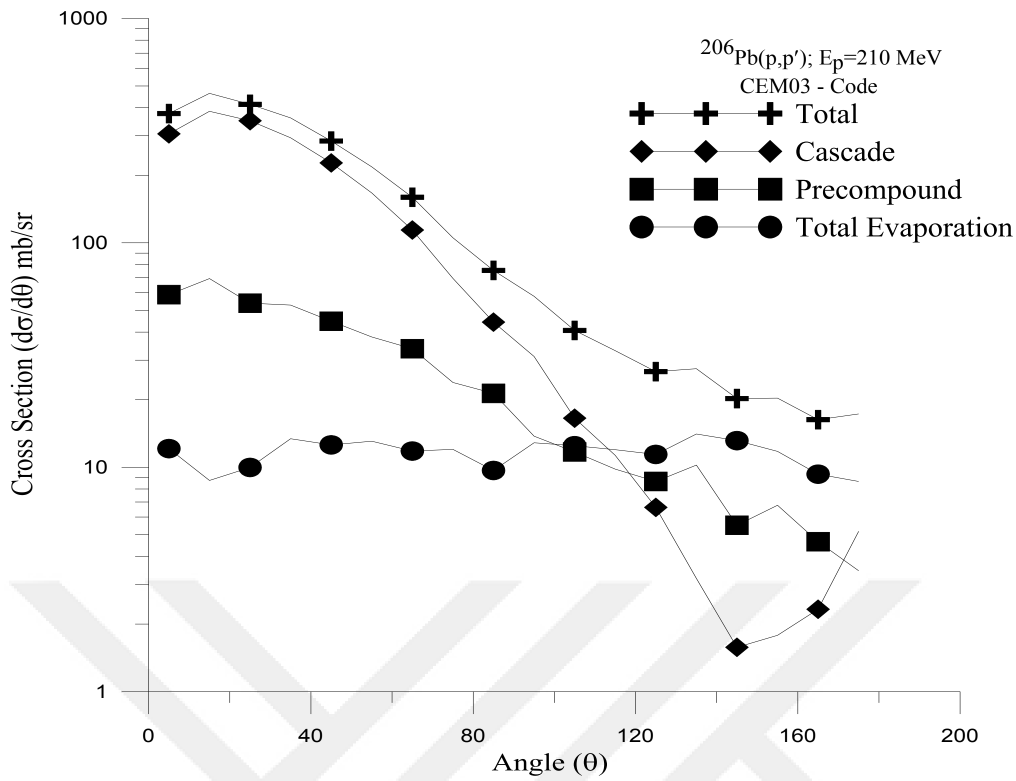

Figure 4.20. Angular Distributions (mb/sr) of the protons (p′) generated as a result of bombardment of element $_{82}Pb^{206}$ with 210 MeV energetic protons

4.4.2.8. Proton Angular distribution for p + $_{82}Pb^{206}$ Reaction at E_p = 240 MeV

The CEM03 indicate asymmetrical angular distributions for secondary nucleons. This is because of high asymmetry of the cascade component. A convenient to have asymmetrical distributions for particles emitted throughout the pre-equilibrium interaction stage is connected to keeping several memory of the direction of a projectile.

Figure 4.21. and Table 4.21. Shows the evaluated results and angle-integrated emission Spectra measurements at E_p= 240 MeV. Number of inelastic interactions is 10000, number of elastic interactions is 6176, reaction cross section is 1623.32 mb, and elastic cross section is 1002.56 mb. The calculation obtained for proton emitted has been made for four steps (Total, Cascade, Precompound, Total evaporation) at angle (5°, 15°......... 175°). As can be seen in Figure (4.21) cascade cross section is decreasing when angular distributions are increasing. Similarly, total cross section slightly decreases while angular distribution increases and there is no change at Precompound and total evaporation cross

section. The cross section of proton produced in the cascade is higher than precompound and total evaporation cross section of proton produced.

Table 4.21. Proton scattered angular distributions (mb/sr) for p + $_{82}Pb^{206}$ reaction, E_p= 240 MeV energy. Calculations have been made by CEM03 code program

$^{206}Pb(p,p')$; E_p=240 MeV CEM03 – Code				
Ang.p [deg.]	Total Cross Section (mb/sr)	Cascade Cross Section (mb/sr)	Precompound Cross Section (mb/sr)	Total Evaporation Cross Section (mb/sr)
5	392.8	335	40.81	17.01
15	473	416.3	40.09	16.61
25	395.6	346.9	36.47	12.27
35	353.5	300.5	32.56	20.41
45	290.5	244	29.76	16.77
55	222.9	178.6	29.49	14.84
65	167.5	125.1	24.55	15.65
85	94.48	53.86	25.44	15.18
95	70.97	30.05	25.14	15.77
105	49.26	19.79	15.04	14.42
115	48.24	15.05	19.95	13.25
125	38.72	6.876	17.37	14.48
135	37.31	5.24	14.67	17.4
145	32.56	2.067	16.28	14.21
155	36.47	1.052	17.18	18.24
165	38.94	1.145	16.61	21.19
175	37.41	1.701	13.6	22.11

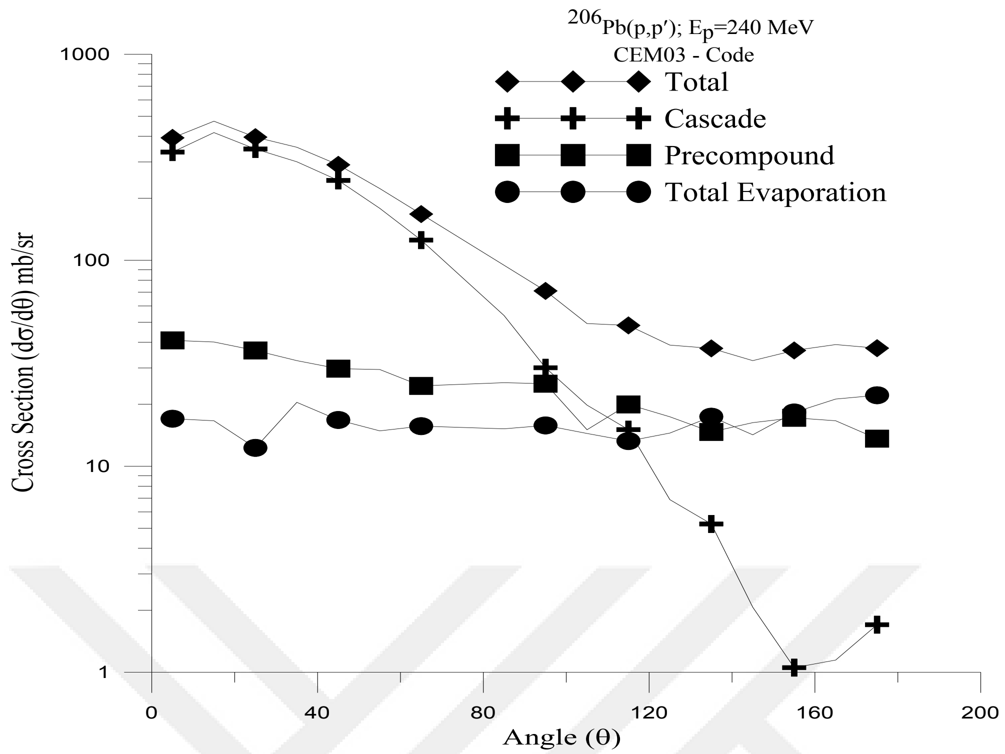

Figure 4.21. Angular Distributions (mb/sr) of the protons (p′) generated as a result of bombardment of element $_{82}Pb^{206}$ with 240 MeV energetic protons

4.4.2.9. Proton Angular distribution for p + $_{82}Pb^{206}$ Reaction at E_p = 270 MeV

The CEM03 indicate asymmetrical angular distributions for secondary nucleons. This is because of high asymmetry of the cascade component. A convenient to have asymmetrical distributions for particles emitted throughout the pre-equilibrium interaction stage is connected to keeping several memory of the direction of a projectile.

Figure 4.22. and Table 4.22. Shows the evaluated results and angle-integrated emission Spectra measurements at E_p= 270 MeV. Number of inelastic interactions = 10000, number of elastic interactions = 6198, reaction cross section = 1606.23 mb, and elastic cross section = 995.54 mb. The calculation obtained for proton emitted has been made for four steps (Total, Cascade, Precompound, Total evaporation) at angle (5°, 15°......... 175°). As can be seen in Figure (4.22) cascade cross section is decreasing when angular distributions are increasing. Similarly, total cross section slightly decreases while angular distribution increases and there is no change at Precompound and total evaporation cross

section. The cross section of proton produced in the cascade is higher than precompound and total evaporation cross section of proton produced.

Table 4.22. Proton scattered angular distributions (mb/sr) for p + $_{82}Pb^{206}$ reaction, E_p= 270 MeV energy. Calculations have been made by CEM03 code program

$^{206}Pb(p,p')$; E_p=270 MeV CEM03 – Cod				
Ang.p [deg.]	Total Cross Section (mb/sr)	Cascade Cross Section (mb/sr)	Precompound Cross Section (mb/sr)	Total Evaporation Cross Section (mb/sr)
5	429.1	371.9	43.75	13.46
15	459	407.4	39.66	11.9
25	435.9	381.4	35.05	19.43
35	362.8	307.3	37.33	18.15
45	302.8	240.2	39.2	23.44
55	230.1	176.7	32.23	21.13
65	174.8	124.8	29.94	20.07
75	140.6	92.92	28.39	19.28
85	100.5	55.06	26.06	19.43
95	80.97	37.25	23.85	19.87
105	67.11	24.9	22.32	19.89
115	56.96	13.11	22.33	21.52
125	47.62	7.519	21.84	18.26
135	44.59	4.978	17.01	22.61
145	38.86	4.602	17.64	16.62
155	36.44	1.041	12.15	23.25
165	41.36	1.133	20.97	19.27
175	21.88	0	8.413	13.46

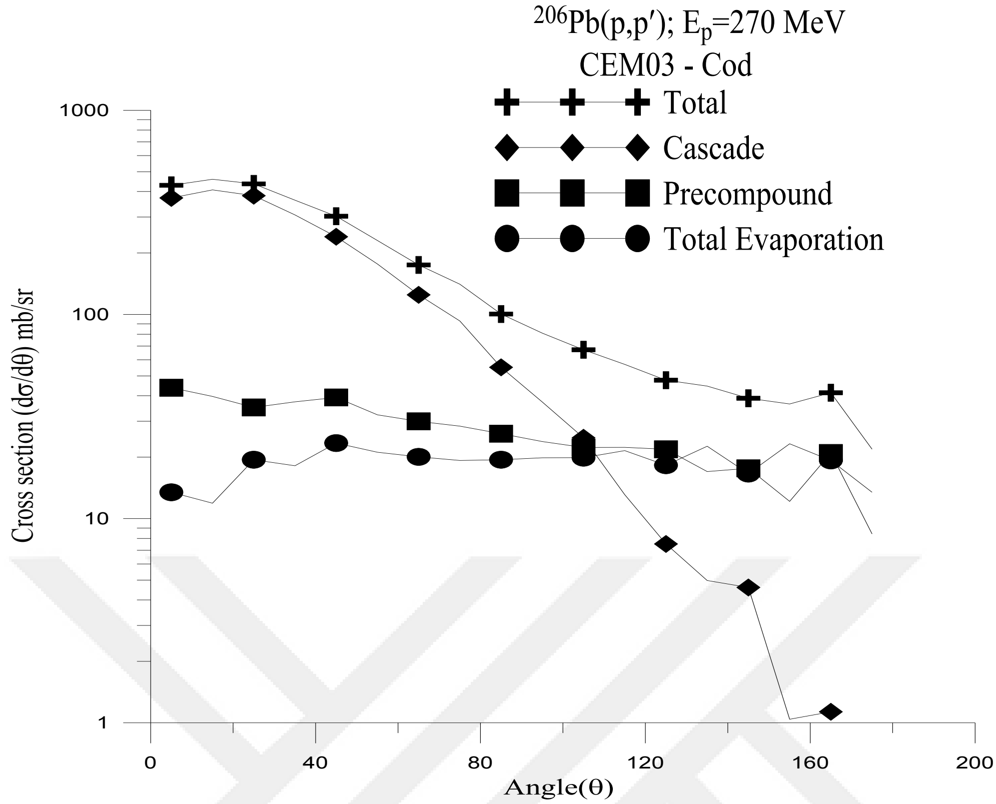

Figure 4.22. Angular Distributions (mb/sr) of the proton generated as a result of bombardment of element $_{82}Pb^{206}$ with 270 MeV energetic protons

4.4.2.10. Neutron Angular distribution for p + $_{82}Pb^{206}$ Reaction at E_p = 300 MeV

The CEM03 indicate asymmetrical angular distributions for secondary nucleons. This is because of high asymmetry of the cascade component. A convenient to have asymmetrical distributions for particles emitted throughout the pre-equilibrium interaction stage is connected to keeping several memory of the direction of a projectile.

Figure 4.23. and Table 4.23. Shows the evaluated results and angle-integrated emission Spectra measurements at E_p= 300 MeV. Number of inelastic interactions is 10000, number of elastic interactions is 6265, reaction cross section is 1596.20 mb, and elastic cross section is 1000.02 mb. The calculation obtained for neutron emitted has been made for four steps (Total, Cascade, Precompound, Total evaporation) at angle (5°, 15°......... 175°). As can be seen in Figure (4.23) cascade cross section is decreasing when angular distributions are increasing. Similarly, Precompound slightly decreases while angular distribution increases and there is no change at total cross section and total evaporation

cross section. The cross section of neutron produced in the total evaporation is higher than cascade and precompound cross section of neutron produced.

Table 4.23. Neutron scattered angular distributions (mb/sr) for p + $_{82}Pb^{206}$ reaction, E_p= 300 MeV energy. Calculations have been made by CEM03 code program

$^{206}Pb(p,n)$; E_p=300 MeV CEM03 – Code				
Ang.n [deg.]	Total	Cascade	Precompound	Total Evaporation
	Cross Section (mb/sr)	Cross Section (mb/sr)	Cross Section (mb/sr)	Cross Section (mb/sr)
5	1532	525.1	73.58	933.1
15	1590	617.2	75.46	897
25	1499	528	74.49	897
35	1414	452.8	72.92	888.3
45	1347	420	66.16	860.3
55	1297	366.7	66.01	864
65	1271	320.6	60.79	889.9
75	1187	269.5	63.52	853.8
85	1152	221.1	61.3	870
95	1087	164.3	48.42	874.4
105	1023	134.9	51.15	836.6
115	972.6	102	45.35	825.3
125	948.7	81.31	40.56	826.8
135	891.6	67.6	37.72	786.3
145	851.7	53.87	30.75	767.1
155	881.4	39.31	37.24	804.9
165	882.9	40.54	31.53	810.9
175	916.4	45.15	48.49	822.7

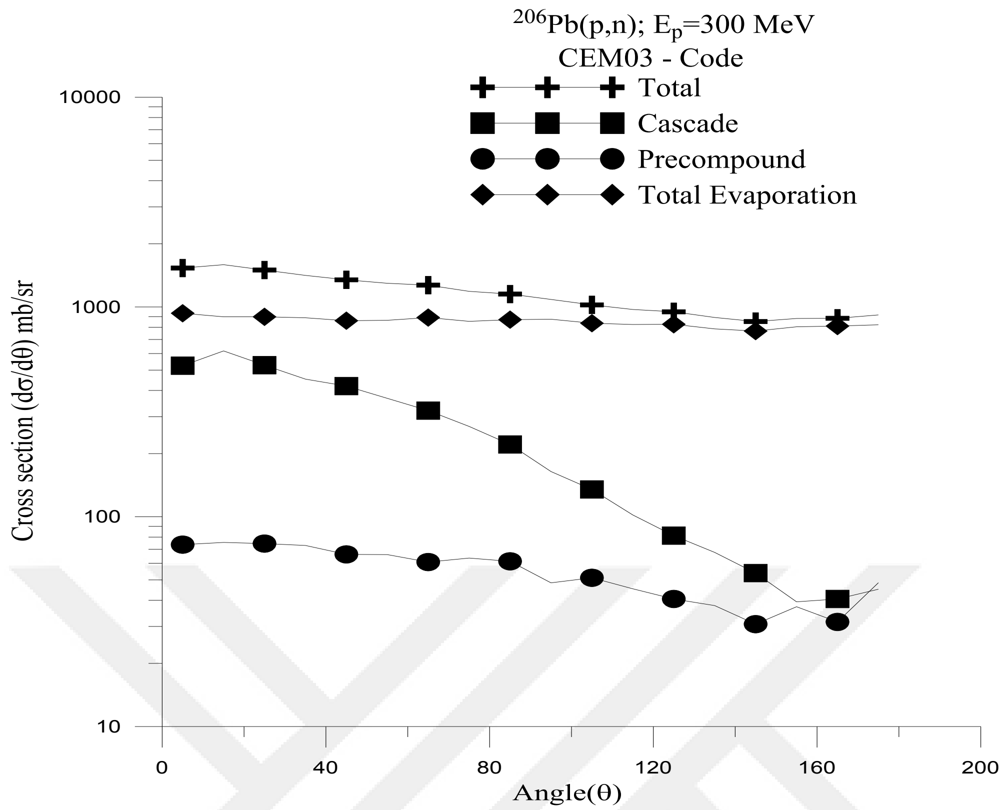

Figure 4.23. Angular Distributions (mb/sr) of the neutrons generated as a result of bombardment of element $_{82}Pb^{206}$ with 300 MeV energetic protons

4.4.2.11. Neutron Angular Distribution for p + $_{82}Pb^{206}$ Reaction at E_p = 350 MeV

The CEM03 indicate asymmetrical angular distributions for secondary nucleons. This is because of high asymmetry of the cascade component. A convenient to have asymmetrical distributions for particles emitted throughout the pre-equilibrium interaction stage is connected to keeping several memory of the direction of a projectile.

Figure 4.24. and Table 4.24. Shows the evaluated results and angle-integrated emission Spectra measurements at E_p= 350 MeV. Number of inelastic interactions is 10000, number of elastic interactions is 6103, reaction cross section is 1590.43 mb, and elastic cross section is 970.64 mb. The calculation obtained for neutron emitted has been made for four steps (Total, Cascade, Precompound, Total evaporation) at angle (5°, 15°......... 175°). As can be seen in Figure (4.24) cascade cross section is decreasing when angular distributions are increasing. Similarly, Precompound slightly decreases while angular distribution increases and there is no change at total cross section and total evaporation

cross section. The cross section of neutron produced in the total evaporation is higher than cascade and precompound cross section of neutron produced.

Table 4.24. Neutron scattered angular distributions (mb/sr) for p + $_{82}Pb^{206}$ reaction, E_p= 350 MeV energy. Calculations have been made by CEM03 code program

$^{206}Pb(p,n)$; E_p=350 MeV CEM03 – Code				
Ang.n [deg.]	Total Cross Section (mb/sr)	Cascade Cross Section (mb/sr)	Precompound Cross Section (mb/sr)	Total Evaporation Cross Section (mb/sr)
5	1578	521.5	99.97	956.4
15	1651	621.1	80.23	949.3
25	1574	526.1	77.31	970.3
35	1533	486.6	73.42	972.9
45	1438	410.5	77.22	949.8
55	1369	362.5	76.41	930.5
65	1294	304.8	68.9	920.7
75	1216	246.6	61.19	908
85	1178	210.3	59.77	908.1
95	1111	167.6	47.52	895.5
105	1086	134.1	51.87	900.4
115	1027	116.6	47.75	862.2
125	963.1	87.93	40.77	834.4
135	955.4	67.77	38.4	849.2
145	926.1	55.95	42.03	828.1
155	895.4	46.39	37.11	811.9
165	915.1	40.96	30.3	843.8
175	991.4	36.66	38.32	916.4

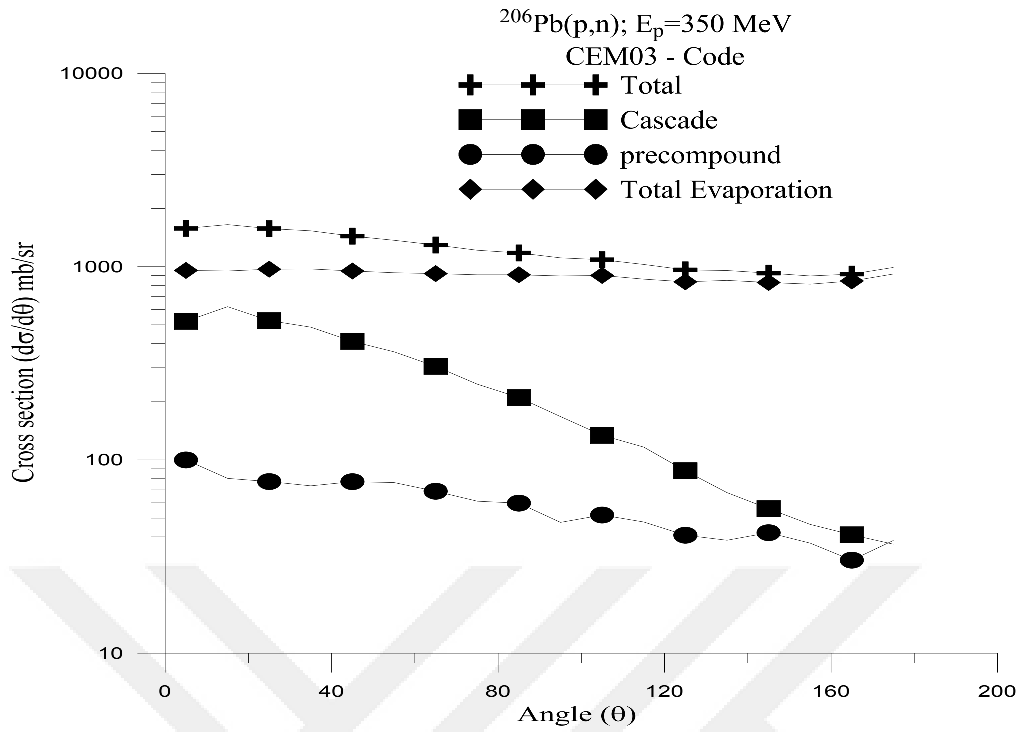

Figure 4.24. Angular Distributions (mb/sr) of the neutrons generated as a result of bombardment of element $_{82}Pb^{206}$ with 350 MeV energetic protons

4.4.2.12. Neutron Angular Distribution for p + $_{82}Pb^{206}$ Reaction at E_p = 400 MeV

The CEM03 indicate asymmetrical angular distributions for secondary nucleons. This is because of high asymmetry of the cascade component. A convenient to have asymmetrical distributions for particles emitted throughout the pre-equilibrium interaction stage is connected to keeping several memory of the direction of a projectile.

Figure 4.25. and Table 4.25. Shows the evaluated results and angle-integrated emission Spectra measurements at E_p= 400 MeV. Number of inelastic interactions is 10000, number of elastic interactions is 5893, reaction cross section is 1593.39 mb, and elastic cross section is 938.98 mb. The calculation obtained for neutron emitted has been made for four steps (Total, Cascade, Precompound, Total evaporation) at angle (5°, 15°......... 175°). As can be seen in figure (4.25) cascade cross section is decreasing when angular distributions are increasing and there is no change at Precompound, total cross section and total evaporation cross section. The cross section of neutron produced in the total evaporation is higher than cascade and precompound cross section of neutron produced.

Table 4.25. Neutron scattered angular distributions (mb/sr) for p + $_{82}Pb^{206}$ reaction, E_p= 400 MeV energy. Calculations have been made by CEM03 code program

$^{206}Pb(p,n)$; E_p=400 MeV CEM03 – Code				
Ang.n [deg.]	Total	Cascade	Precompound	Total Evaporation
	Cross Section (mb/sr)	Cross Section (mb/sr)	Cross Section (mb/sr)	Cross Section (mb/sr)
5	1664	604.3	85.13	974.8
15	1791	659.9	88.25	1043
25	1663	573.2	80.21	1010
35	1610	496.1	82.43	1031
45	1553	450.4	81.27	1022
55	1447	378.1	72.64	996.5
65	1381	320.7	70.63	989.5
75	1321	271.6	63.56	985.5
85	1269	235.4	63.09	970.7
95	1213	186.1	59.58	967.8
105	1125	144.3	52.87	927.6
115	1124	126.5	50.57	947.1
125	1051	95.55	47.6	907.7
135	1018	83.12	43.82	890.9
145	1022	66.96	38.05	917.2
155	989	57.49	37.52	894
165	947.2	50.59	43.84	852.7
175	978.2	48.41	31.72	898.1

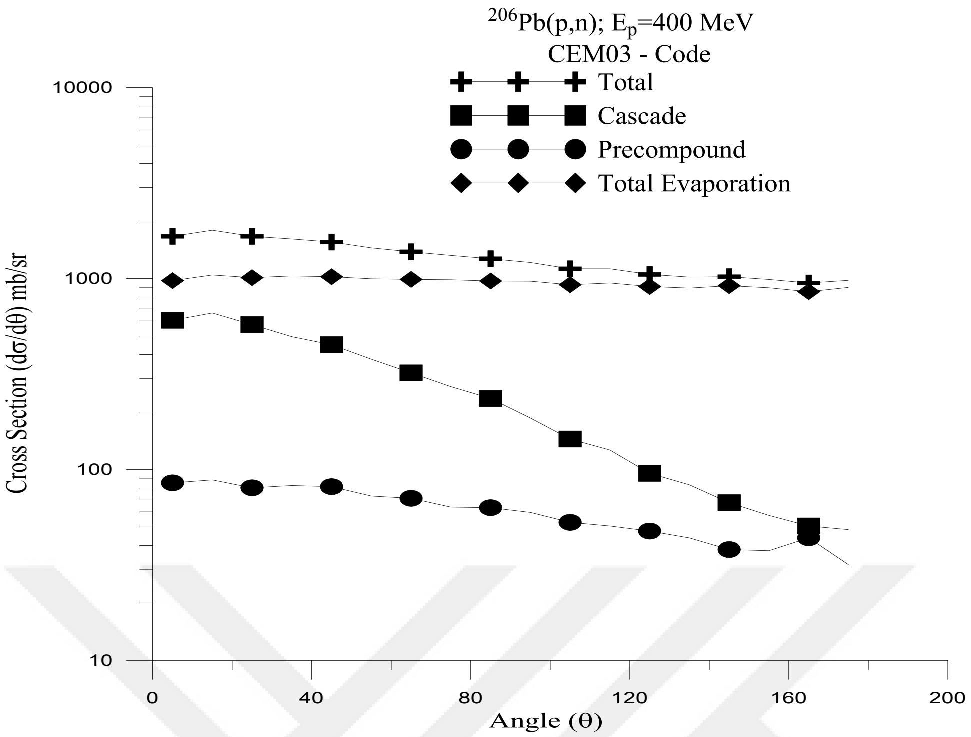

Figure 4.25. Angular Distributions (mb/sr) of the neutrons generated as a result of bombardment of element $_{82}Pb^{206}$ with 400 MeV energetic protons

4.4.2.13. Neutron Angular Distribution for p + $_{82}Pb^{206}$ Reaction at E_p = 450 MeV

The CEM03 indicate asymmetrical angular distributions for secondary nucleons. This is because of high asymmetry of the cascade component. A convenient to have asymmetrical distributions for particles emitted throughout the pre-equilibrium interaction stage is connected to keeping several memory of the direction of a projectile.

Figure 4.26. and Table 4.26. Shows the evaluated results and angle-integrated emission Spectra measurements at E_p= 450 MeV. Number of inelastic interactions is 10000, number of elastic interactions is 5633, reaction cross section is 1601.33 mb, and elastic cross section is 902.03 mb. The calculation obtained for neutron emitted has been made for four steps (Total, Cascade, Precompound, Total evaporation) at angle (5°, 15°......... 175°). As can be seen in Figure (4.26) cascade cross section is decreasing when angular distributions are increasing and there is no change at Precompound, total cross section and total evaporation cross section. The cross section of neutron produced in the total evaporation is higher than cascade and precompound cross section of neutron produced.

Table 4.26. Neutron scattered angular distributions (mb/sr) for p + $_{82}Pb^{206}$ reaction, E_p= 450 MeV energy. Calculations have been made by CEM03 code program

$^{206}Pb(p,n)$; E_p=450 MeV CEM03 – Code				
Ang.n [deg.]	Total Cross Section (mb/sr)	Cascade Cross Section (mb/sr)	Precompound Cross Section (mb/sr)	Total Evaporation Cross Section (mb/sr)
5	1891	659.3	100.7	1131
15	1943	751.3	98.29	1093
25	1852	641.1	96.18	1115
35	1719	534.3	92.28	1093
45	1616	475.8	82.09	1058
55	1551	411.1	83.35	1056
65	1485	366.2	76.14	1043
75	1397	297.6	72.66	1027
85	1334	252.1	66.19	1016
95	1257	205.3	65.16	986.3
105	1235	165.4	62.06	1008
115	1194	134.4	54.04	1006
125	1136	120.8	49.44	966
135	1081	83.54	48.59	948.7
145	1070	80.04	40.79	949.3
155	1057	67.81	47.4	942.1
165	1050	40.67	37.28	971.6
175	1062	57.04	50.33	954.5

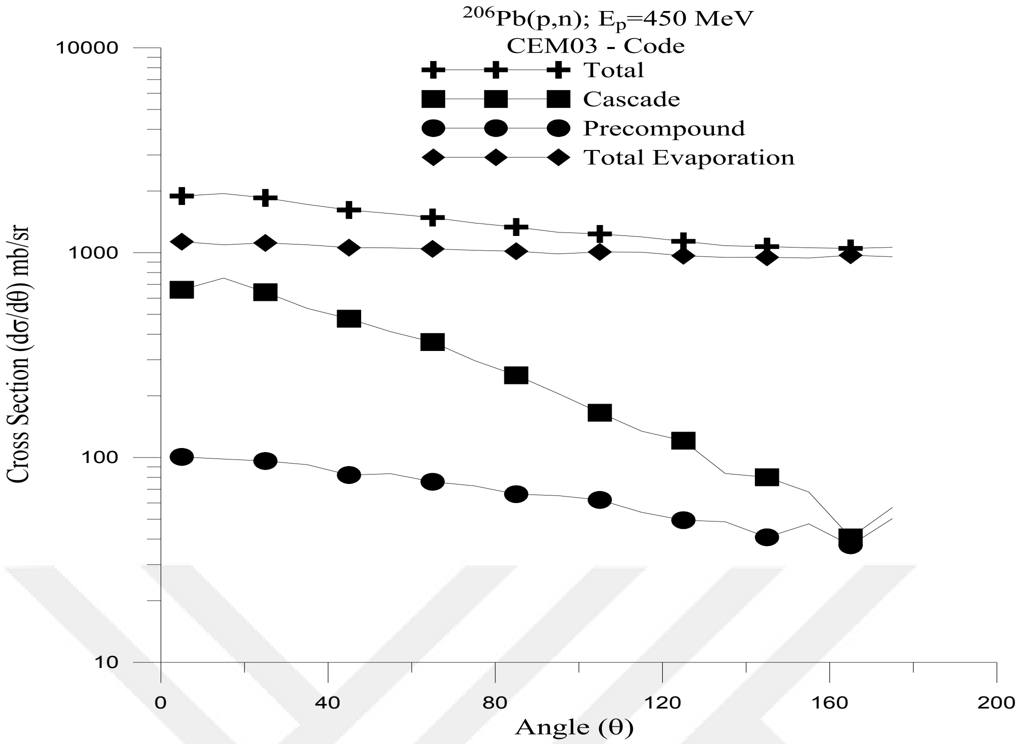

Figure 4.26. Angular Distributions (mb/sr) of the neutrons generated as a result of bombardment of element $_{82}Pb^{206}$ with 450 MeV energetic protons

4.4.2.14. Angular Distribution for p + $_{82}Pb^{206}$ Reaction at 35 MeV and 295 MeV (Compare between CEM03 and Experimental Data)

The calculated angular distribution of ^{206}Pb reactions are compared with the experimental values in figures 27 and 28. The equilibrium calculations of ^{206}Pb(p, xn) reaction are in good agreement with the measurements at 35 MeV and 295 MeV. For ^{206}Pb(p, xn) reaction the pre-equilibrium calculations (hybrid and GDH models) are in good agreement with the measurements. The cascade-exciton model calculations (CEM03) are in good agreement with the experimental values at energies below 35 MeV and 295 MeV respectively.

Table 4.27. Neutron scattered angular distributions (mb/sr) for p + $_{82}Pb^{206}$ reaction, E_p= 35 MeV energy. Calculations have been made by CEM03 code program compare by the experimental data

	^{206}Pb(p,n); E_p=35 MeV CEM03 –Code	E=35 MeV Pb Experimental DATA
Ang.n [deg.]	Total Cross Section mb	Experimental mb
5	572.4	
10.1		192000
12.1		59600
15	607.7	
16.1		17000
20.1		5970
24.1		1910
25	626.3	
28.1		790
32.2		340
34.2		225
35	632.6	
38.2		149
40.2		140
44.2		122
45	576.2	
48.2		78.9
52.2		31.7
55	542.9	
56.3		10.4
60.3		13.8
64.3		21.1
65	532.8	
68.3		18
72.3		9.92
75	498.2	
76.3		3.12
80.3		2.06
84.3		3.88
85	489.3	
88.3		4.66
92.3		3.66
95	459	
96.3		1.86
100.3		0.744
104.3		0.642

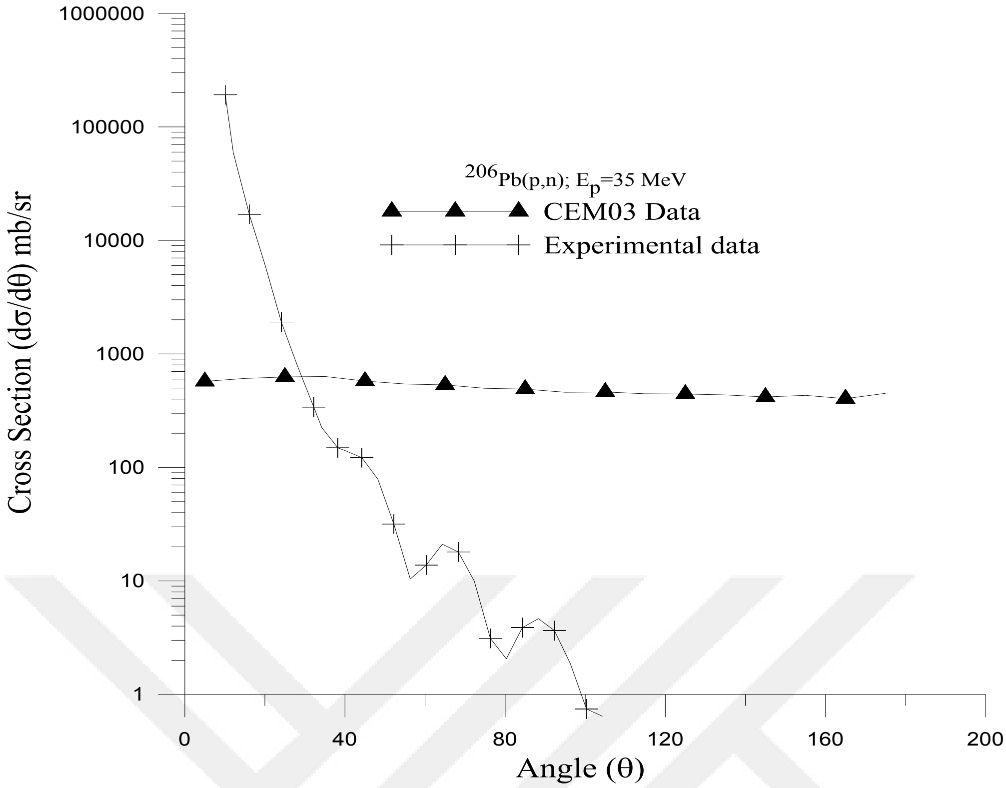

Figure 4.27. Angular Distributions (mb/sr) of the neutrons generated as a result of bombardment of element $_{82}Pb^{206}$ with 35 MeV energetic protons

Table 4.28. Neutron scattered angular distributions (mb/sr) for p + $_{82}Pb^{206}$ reaction, E_p= 295 MeV energy. Calculations have been made by CEM03 code program compare by the experimental data.

	$^{206}Pb(p,n)$; E_p=295 MeV CEM03 – Code	Experimental Data, E=295 MeV
Ang.n	Total cross section, mb	Mb
[deg.]		DATA-CM
5	1532	
7.72		1520
9.25		599
10.68		696
15	1590	
15.26		19.6
16.7		51.1
18.24		43.9
25	1499	
25.7		3.98
27.33		1.39
28.86		0.677
35	1414	
36.33		0.122
37.76		0.155
39.4		0.102
45	1347	
45.33		0.0201
46.86		0.0101
48.38		0.00239
55	1297	
65	1271	
75	1187	

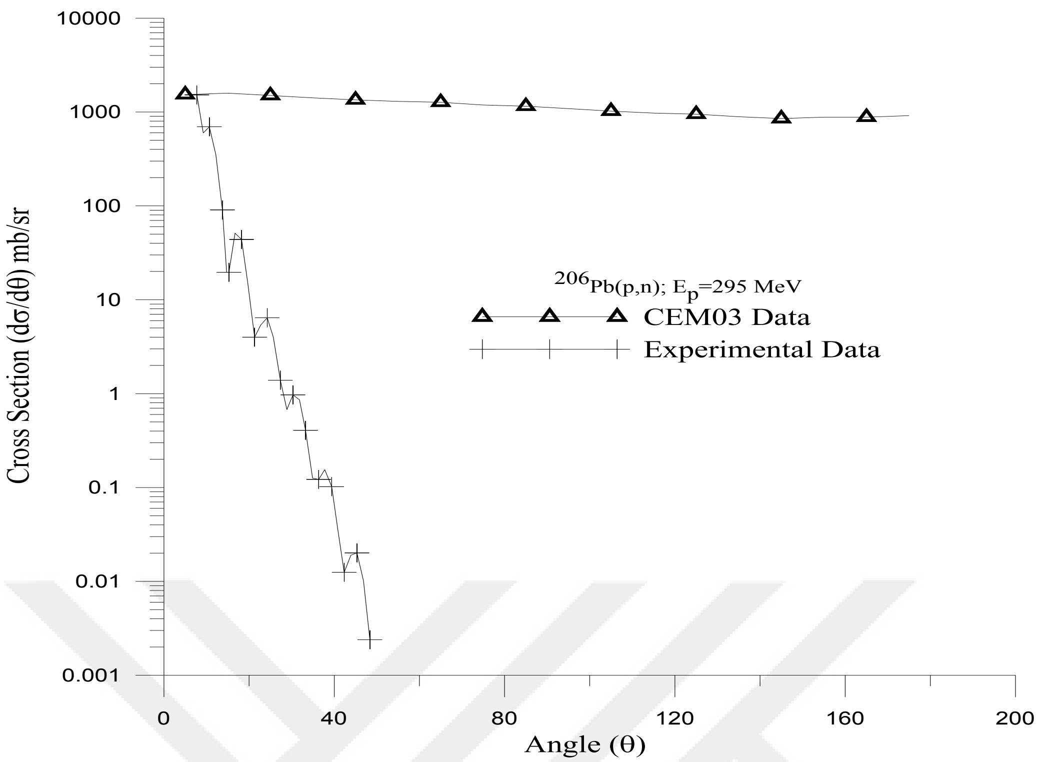

Figure 4.28. Angular Distributions (mb/sr) of the neutrons generated as a result of bombardment of element $_{82}Pb^{206}$ with 295 MeV energetic protons

4.4.2.15. Angular distribution for p+ $_{90}Th^{232}$ Reaction at65 MeV and 95 MeV (Compare between CEM03 and Experimental Data)

The calculated angular distributions of ^{232}Th reactions are compared with the experimental values in figures 29 and 30. The equilibrium calculations of ^{232}Th (p, xn) reaction are in good agreement with the measurements at 65 MeV and 95 MeV. For ^{232}Th(p, xn) reaction the pre-equilibrium calcuculations (hybrid and GDH models) are in good agreement with the measurements. The cascade-exciton model calculations (CEM03) are in good agreement with the experimental values at energies 65 MeV and 95 MeV.

Table 4.29. Proton scattered angular distributions (mb/sr) for p + $_{90}Th^{232}$ reaction, E_p= 65 MeV energy. Calculations have been made by CEM03 code program compare by the experimental data

Ang.p	Th^{232}(p,p′): E_p=65 MeV CEM03 - Code	Experimental E=65 MeV Th
[deg.]	Total Cross Section mb	DATA-CM
5	191.7	
11.11		29740
12.11		18900
13.11		12350
14.11		6277
15	306.6	
15.11		3319
16.11		2063
24.12		817.1
25	299.6	
25.12		568.3
32.14		120.7
33.14		154.2
35	261.8	
35.15		161.5
36.15		136.3
42.18		9.228
45	161.6	
46.19		19.61
48.19		23.96
54.2		5.839
55	100.4	
56.21		2.48
58.21		2.347
64.22		3.816
65	55.51	
66.22		2.612
68.23		1.327
70.23		0.6583
75	38.52	
85	28.01	
95	21.34	

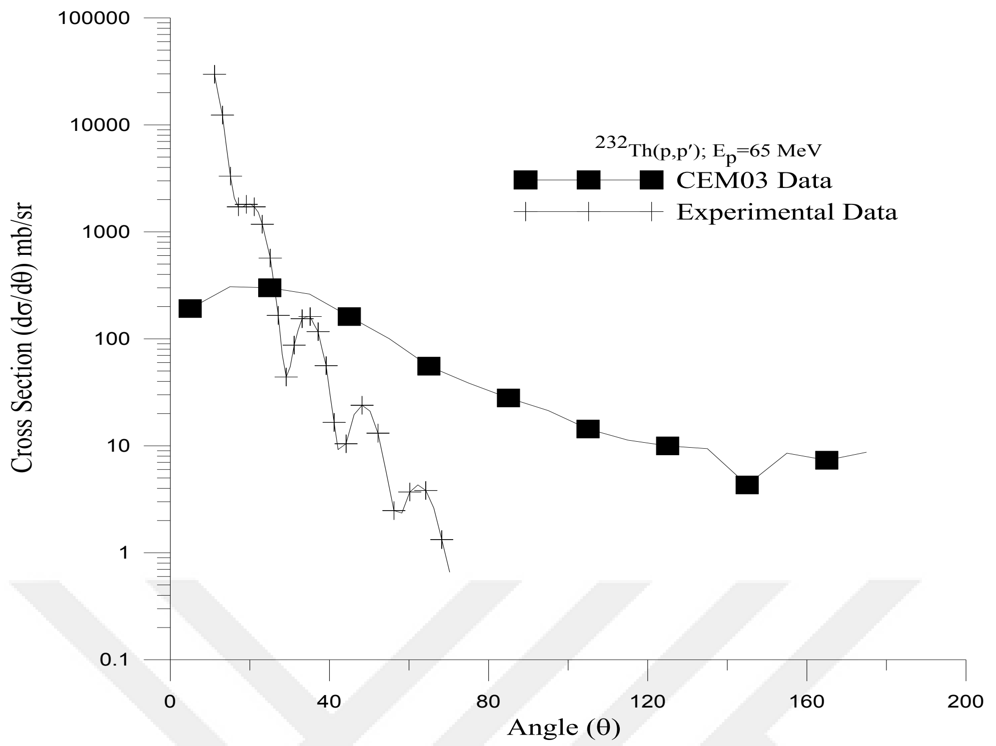

Figure 4.29. Angular Distributions (mb/sr) of the neutrons generated as a result of bombardment of element ${}_{90}Th^{232}$ with 65 MeV energetic protons

Table 4.30. Neutron scattered angular distributions (mb/sr) for p + ${}_{90}Th^{232}$ reaction, E_p= 65 MeV energy. Calculations have been made by CEM03 code program compare by the experimental data

	${}^{232}Th(p, n)$; E_p=95 MeV CEM03 - Code	Experimental E=95 MeV
Ang.n	Total Cross Section mb	Experimental
[deg.]		DATA-CM
5	1387	
5.806		185200
6.957		85190
14.63		1146
15	1401	
17.03		1203
17.94		1099
24.5		85.39
25	1404	
26.69		101.2
28.19		112.7
31.41		82.14
35	1377	
45	1273	
175	981.4	

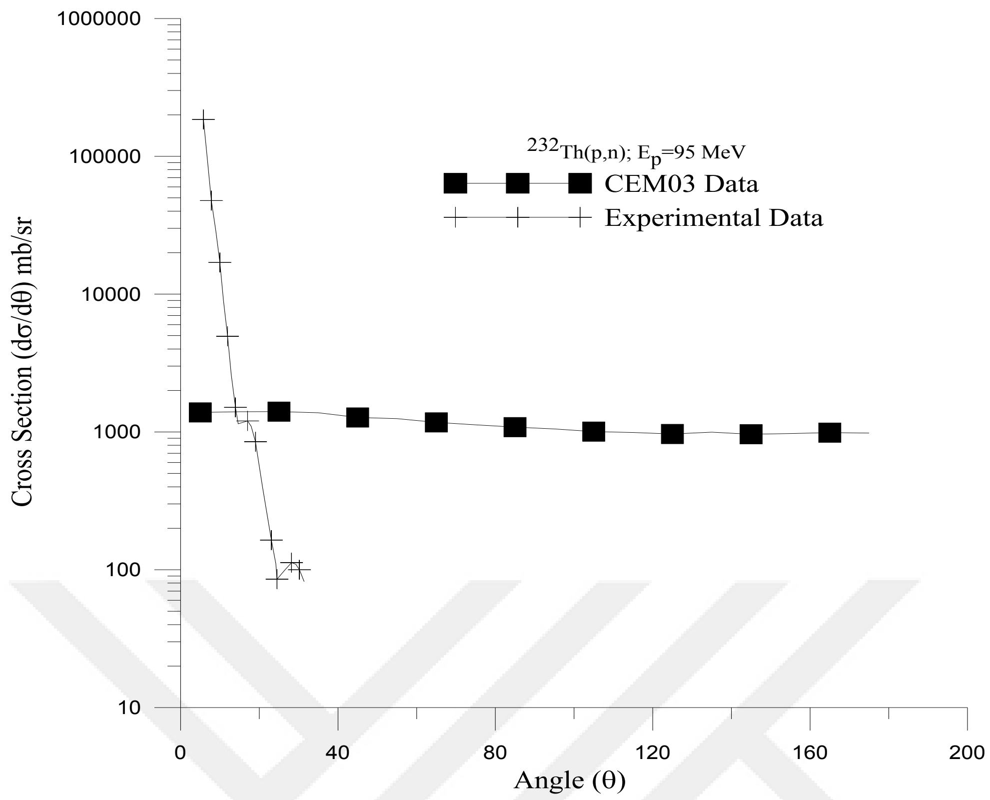

Figure 4.30. Angular Distributions (mb/sr) of the neutrons generated as a result of bombardment of element $_{90}Th^{232}$ with 95 MeV energetic protons

4.4.3.1. α Angular Distribution for p + $_{82}Pb^{206}$ Reaction at E_p = 30 MeV

The calculation for the angular distribution of $^{206}Pb(p,\alpha)$ reaction has been see in the Fig. 4.31. In this reaction α- particle emitted at these angles (2.5°, 7.5°......... 177.5°). In this reaction, when E_α= 5.50 MeV the maximum point of reaction cross section equal to (6.65 mb), located at this angle (12.5°), and the minimum point of reaction cross section equal to (0.563 mb), located at this angle (177.5°). When E_α= 10.5 MeV the maximum point of reaction cross section equal to (4.61 mb) located at this angle (2.5°), and the minimum point of reaction cross section equal to (0.0905 mb), located at this angle (172.5°). When E_α= 15.5 MeV the maximum point of reaction cross section equal to (3.4 mb) located at this angle (2.5°), and the minimum point of reaction cross section equal to (0.00853 mb), located at this angle (177.5°). Figure (4.31) represents the evaluated results and angle-integrated emission spectra at E_p =30 MeV.

Table 4.31. Alpha scattered angular distributions (mb/sr) for p + $_{82}Pb^{206}$ reaction, E_p= 30 MeV energy. Calculations have been made by ALICE/ASH code program

^{206}pb(p, α); E_p=30 MeV ALICE/ASH Code			
ANGLE/DEG.	E_α=5.50 MeV	E_α=10.5 MeV	E_α=15.5 MeV
	Cross section mb	Cross section mb	Cross section mb
2.5	6.54	4.61	3.4
7.5	6.54	4.55	3.28
12.5	6.65	4.53	3.29
17.5	6.54	4.51	3.2
22.5	6.22	4.22	2.91
27.5	6.4	4.2	2.89
32.5	6.24	4.11	2.67
37.5	6.23	3.96	2.46
42.5	6.31	3.91	2.34
47.5	5.83	3.44	1.99
52.5	5.36	3.11	1.71
57.5	5	2.78	1.46
62.5	4.56	2.44	1.26
67.5	4.24	2.19	1.09
72.5	3.97	1.98	0.97
77.5	3.77	1.81	0.85
82.5	3.32	1.58	0.71
87.5	3.12	1.4	0.61
92.5	2.81	1.25	0.506
97.5	2.63	1.08	0.425
102.5	2.36	0.965	0.35
107.5	2.14	0.82	0.289
112.5	1.99	0.72	0.211
117.5	1.79	0.593	0.151
122.5	1.66	0.509	0.115
127.5	1.53	0.439	0.0826
132.5	1.39	0.341	0.0454
137.5	1.29	0.292	0.0267
142.5	1.06	0.199	0.0147
147.5	0.929	0.156	0.0117
152.5	0.847	0.127	0.0109
157.5	0.692	0.103	0.0094
162.5	0.681	0.1	0.0095
167.5	0.629	0.0953	0.009
172.5	0.576	0.0905	0.0085
177.5	0.563	0.0909	0.0085

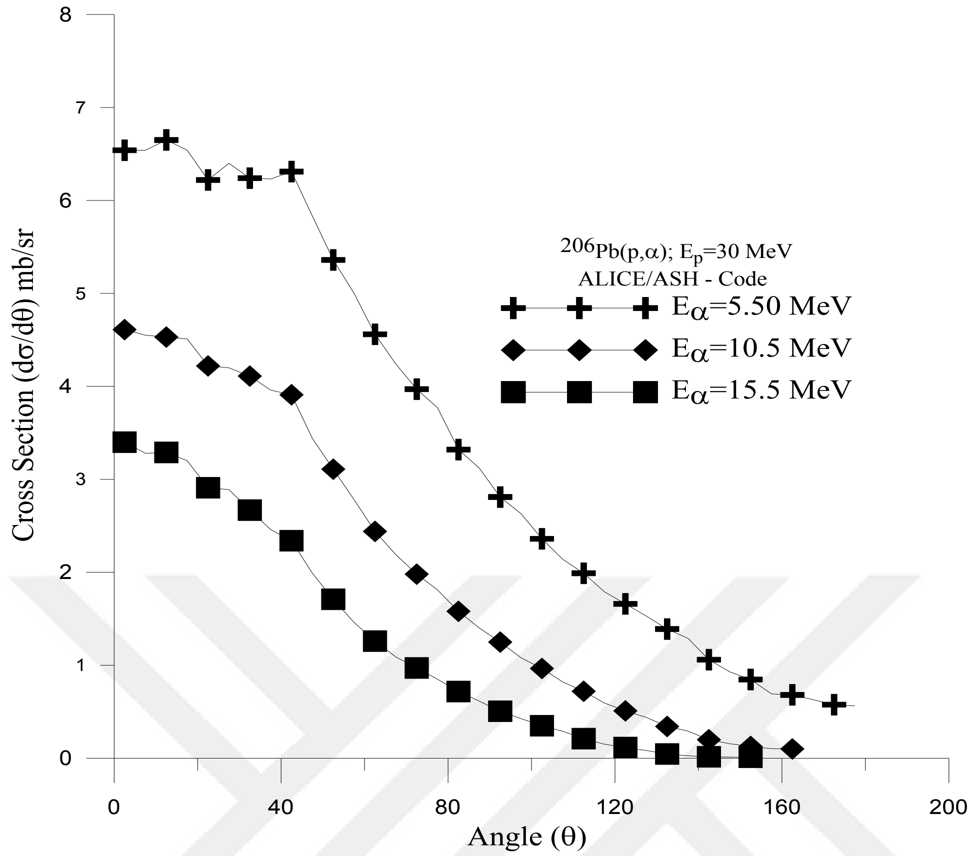

Figure 4.31. Angular Distributions (mb/sr) of the alpha generated as a result of bombardment of element $_{82}Pb^{206}$ with 30 MeV energetic protons

4.4.3.2. α Angular Distribution for p + $_{82}$Pb^{206} Reaction at E_p = 60 MeV

The calculation for the angular distribution of ^{206}Pb(p,α) reaction has been see in the Fig. 4.32. In this reaction α- particle emitted at angle (2.5°, 7.5°......... 177.5°). In this reaction, when E_α= 5.50 MeV the maximum point of reaction cross section equal to (6.33 mb), located at this angle (12.5°), and the minimum point of reaction cross section equal to (0.815 mb), located at this angle (172.5°). When E_α= 10.5 MeV the maximum point of reaction cross section equal to (5.81 mb) located at this angle (2.5°), and the minimum point of reaction cross section equal to (0.341 mb), located at this angle (172.5°). When E_α= 15.5 MeV the maximum point of reaction cross section equal to (4.98 mb) located at this angle (2.5°), and the minimum point of reaction cross section equal to (0.131 mb), located at this angle (172.5°). Figure (4.32) represents the evaluated results and angle-integrated emission Spectra measurements at E_p= 60 MeV.

Table 4.32. Alpha scattered angular distributions (mb/sr) for p + $_{82}Pb^{206}$ reaction, E_p= 60 MeV energy. Calculations have been made by ALICE/ASH code program

^{206}pb(p, α); E_p=60 MeV ALICE/ASH –Code			
ANGLE/DEG	E_α=5.50 MeV	E_α=10.5 MeV	E_α=15.5 MeV
	Cross Section mb	Cross Section mb	Cross Section mb
2.5	6.27	5.81	4.98
7.5	6.24	5.7	4.79
12.5	6.33	5.68	4.87
17.5	6.2	5.66	4.82
22.5	5.92	5.31	4.44
27.5	6.02	5.28	4.55
32.5	5.83	5.22	4.47
37.5	5.86	5.13	4.45
42.5	5.92	5.23	4.58
47.5	5.49	4.82	4.22
52.5	5.13	4.52	3.9
57.5	4.89	4.28	3.5
62.5	4.49	3.88	3.11
67.5	4.31	3.62	2.77
72.5	4.13	3.36	2.5
77.5	3.96	3.07	2.2
82.5	3.67	2.77	1.9
87.5	3.48	2.47	1.63
92.5	3.17	2.23	1.36
97.5	3	1.97	1.17
102.5	2.63	1.72	0.964
107.5	2.45	1.51	0.825
112.5	2.31	1.36	0.666
117.5	2.06	1.14	0.531
122.5	1.96	1.05	0.478
127.5	1.81	0.939	0.408
132.5	1.68	0.808	0.33
137.5	1.56	0.743	0.29
142.5	1.33	0.601	0.232
147.5	1.16	0.506	0.192
152.5	1.09	0.456	0.175
157.5	0.941	0.395	0.152
162.5	0.92	0.38	0.147
167.5	0.87	0.36	0.139
172.5	0.815	0.341	0.131
177.5	0.816	0.345	0.132

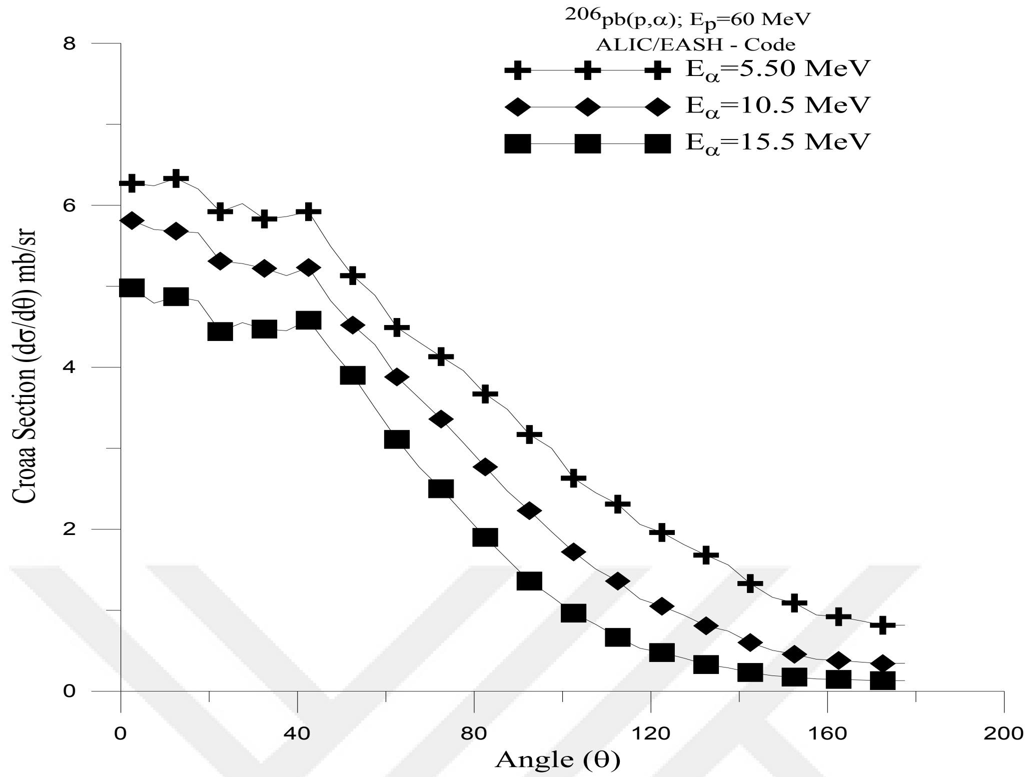

Figure 4.32. Angular Distributions (mb/sr) of the alpha generated as a result of bombardment of element $_{82}Pb^{206}$ with 60 MeV energetic protons

4.4.3.3. α Angular Distribution for p + $_{82}Pb^{206}$ Reaction at E_p = 90 MeV

The calculation for the angular distribution of $^{206}Pb(p,\alpha)$ reaction has been see in the Fig. 4.33. In this reaction α- particle emitted at angle (2.5°, 7.5°......... 177.5°). In this reaction, when E_α= 5.50 MeV the maximum point of reaction cross section equal to (3.72 mb), located at this angle (12.5°), and the minimum point of reaction cross section equal to (0.656 mb), located at this angle (177.5°). When E_α= 10.5 MeV the maximum point of reaction cross section equal to (3.58 mb) located at this angle (2.5°), and the minimum point of reaction cross section equal to (0.376 mb), located at this angle (172.5°). When E_α= 15.5 MeV the maximum point of reaction cross section equal to (3.19 mb) located at this angle (47.5°), and the minimum point of reaction cross section equal to (0.207 mb), located at this angle (177.5°). When E_α= 80.5 MeV the maximum point of reaction cross section equal to (5.97 mb) located at this angle (2.5°), and the minimum point of reaction cross section equal to (0.00177 mb), located at this angle (82.5°). Figure (4.33) represents the evaluated results and angle-integrated emission Spectra measurements at E_p= 90 MeV.

Table 4.33. Alpha scattered angular distributions (mb/sr) for p + $_{82}Pb^{206}$ reaction, E_p= 90 MeV energy. Calculations have been made by ALICE/ASH code program

$^{206}Pb(p, \alpha)$; E_p=90 MeV ALICE/ASH – Code				
ANGLE/DEG.	E_α =5.50 MeV	E_α=10.5 MeV	E_α =15.5 MeV	E_α =80.5 MeV
	Cross Section mb	Cross Section mb	Cross Section mb	Cross Section mb
2.5	3.67	3.58	3.08	5.97
7.5	3.69	3.55	2.99	5.65
12.5	3.72	3.52	3.05	5
17.5	3.62	3.51	3.07	4.07
22.5	3.46	3.33	2.9	2.98
27.5	3.52	3.34	3.05	2.23
32.5	3.41	3.35	3.11	1.47
37.5	3.45	3.37	3.2	1.03
42.5	3.54	3.54	3.4	0.71
47.5	3.3	3.29	3.19	0.424
52.5	3.1	3.14	3.06	0.256
57.5	2.95	2.99	2.82	0.156
62.5	2.77	2.79	2.61	0.0946
67.5	2.67	2.66	2.4	0.0531
72.5	2.59	2.52	2.22	0.026
77.5	2.56	2.38	2.04	0.00918
82.5	2.38	2.19	1.81	0.00177
87.5	2.31	2	1.6	
92.5	2.14	1.84	1.38	
107.5	1.72	1.32	0.908	
112.5	1.63	1.2	0.759	
117.5	1.49	1.05	0.207	
122.5	1.41	0.963	0.207	
127.5	1.34	0.891	0.207	
132.5	1.27	0.796	0.207	
137.5	1.2	0.75	0.207	
142.5	1.01	0.602	0.207	
147.5	0.887	0.519	0.207	
152.5	0.841	0.475	0.207	
157.5	0.732	0.419	0.207	
162.5	0.722	0.407	0.207	
167.5	0.693	0.391	0.207	
172.5	0.661	0.376	0.207	
177.5	0.656	0.378	0.207	

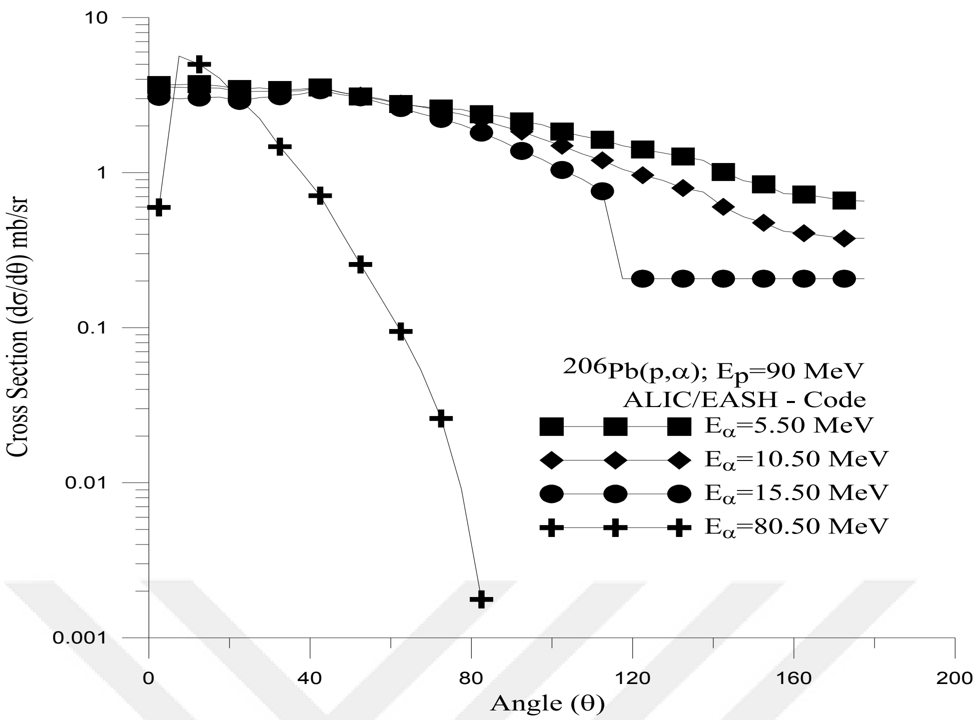

Figure 4.33. Angular Distributions (mb/sr) of the alpha generated as a result of bombardment of element $_{82}Pb^{206}$ with 90 MeV energetic protons

4.4.3.4. α Angular Distribution for p + $_{82}Pb^{206}$ Reaction at E_p = 120 MeV

The calculation for the angular distribution of $^{206}Pb(p,\alpha)$ reaction has been see in the Fig. 4.34. In this reaction α- particle emitted at angle (2.5°, 7.5°......... 177.5°). In this reaction, when E_α= 5.50 MeV the maximum point of reaction cross section equal to (2.31 mb), located at this angle (12.5°), and the minimum point of reaction cross section equal to (0.481 mb), located at this angle (177.5°). When E_α= 15.5 MeV the maximum point of reaction cross section equal to (2.37 mb) located at this angle (42.5°), and the minimum point of reaction cross section equal to (0.205 mb), located at this angle (177.5°). When E_α= 85.5 MeV the maximum point of reaction cross section equal to (3.82 mb) located at this angle (27.5°), and the minimum point of reaction cross section equal to (0.00231 mb), located at this angle (87.5°). When E_α= 95.5 MeV the maximum point of reaction cross section equal to (4.68 mb) located at this angle (2.5°), and the minimum point of reaction cross section equal to (0.00015 mb), located at this angle (87.5°). When E_α= 105.5 MeV the maximum point of reaction cross section equal to (6.72 mb) located at this angle (2.5°), and the minimum point of reaction cross section equal to (0.00227 mb), located at this angle (72.5°). Figure (4.34) represents the evaluated results and angle-integrated emission Spectra measurements at E_p=120 MeV.

Table 4.34. Alpha scattered angular distributions (mb/sr) for p + $_{82}Pb^{206}$ reaction, E_p= 120 MeV energy. Calculations have been made by ALICE/ASH code program

$^{206}Pb(p, \alpha)$; E_p=120 MeV ALICE/ASH – Code					
ANGLE/DEG.	E_α=5.50 MeV	E_α=15.5 MeV	E_α=85.5 MeV	E_α=95.5 MeV	E_α=105.5MeV
	Cross Section mb	Cross Section mb	Cross Section mb	Cross Section mb	Cross Section mb
2.5	2.28	1.93	2.72	4.68	6.72
7.5	2.3	1.88	2.86	4.59	6.31
12.5	2.31	1.92	3.25	4.58	5.78
17.5	2.22	1.94	3.58	4.42	5.04
22.5	2.14	1.89	3.69	4.13	3.82
27.5	2.18	2.02	3.82	3.86	2.76
32.5	2.12	2.1	3.35	3.04	1.74
37.5	2.19	2.22	2.92	2.39	1.19
42.5	2.21	2.37	2.34	1.72	0.758
47.5	2.11	2.27	1.52	1.01	0.433
52.5	1.98	2.21	0.94	0.595	0.239
57.5	1.86	2.05	0.564	0.342	0.117
62.5	1.76	1.93	0.332	0.193	0.0518
67.5	1.74	1.83	0.181	0.0941	0.0174
72.5	1.67	1.71	0.0891	0.0375	0.00227
77.5	1.68	1.61	0.0362	0.0107	
82.5	1.56	1.45	0.0115	0.0016	
87.5	1.54	1.31	0.00231	0.00015	
92.5	1.44	1.15			
97.5	1.37	1.02			
102.5	1.26	0.895			
107.5	1.18	0.78			
112.5	1.15	0.671			
117.5	1.04	0.56			
132.5	0.922	0.422			
137.5	0.851	0.378			
142.5	0.738	0.315			
147.5	0.635	0.261			
152.5	0.602	0.242			
157.5	0.531	0.218			
162.5	0.513	0.21			
167.5	0.503	0.208			
172.5	0.487	0.205			
177.5	0.481	0.205			

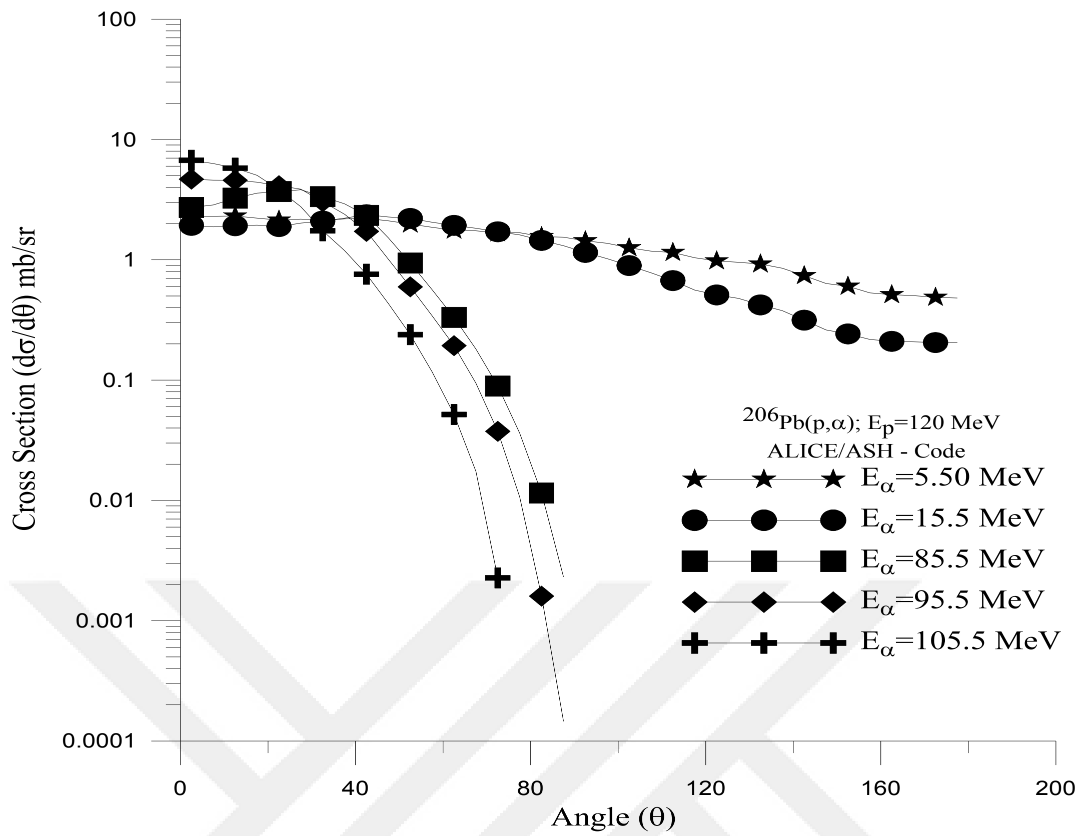

Figure 4.34. Angular Distributions (mb/sr) of the alpha generated as a result of bombardment of element $_{82}Pb^{206}$ with 120 MeV energetic protons

4.4.3.5. α Angular Distribution for p + $_{82}Pb^{206}$ Reaction at E_p = 150 MeV

The calculation for the angular distribution of ^{206}Pb(p,α) reaction has been see in the Fig. 4.35. In this reaction α- particle emitted at angle (2.5°, 7.5°......... 177.5°). In this reaction, when E_α= 5.50 MeV the maximum point of reaction cross section equal to (1.25 mb), located at this angle (12.5°), and the minimum point of reaction cross section equal to (0.356 mb), located at this angle (177.5°). When E_α= 85.5 MeV the maximum point of reaction cross section equal to (2.43 mb) located at this angle (37.5°), and the minimum point of reaction cross section equal to (0.042 mb), located at this angle (82.5°). When E_α= 105.5 MeV the maximum point of reaction cross section equal to (3.54 mb) located at this angle (27.5°), and the minimum point of reaction cross section equal to (0.324 mb), located at this angle (57.5°). When E_α= 120.5 MeV the maximum point of reaction cross section equal to (4.34 mb) located at this angle (17.5°), and the minimum point of reaction cross section equal to (0.161 mb), located at this angle (57.5°). When E_α= 140.5

MeV the maximum point of reaction cross section equal to (6.31 mb) located at this angle (2.5°), and the minimum point of reaction cross section equal to (0.0205 mb), located at this angle (57.5°). Figure (4.35) represents the evaluated results and angle-integrated emission Spectra measurements at E_p= 150 MeV.

Table 4.35. Alpha scattered angular distributions (mb/sr) for p + $_{82}Pb^{206}$ reaction, E_p= 150 MeV energy. Calculations have been made by ALICE/ASH code program

^{206} Pb(p, α); E_p=150 MeV ALICE/ASH – Code					
ANGLE/DEG.	E_α=5.50MeV	E_α= 85.5 MeV	E_α= 105.5 MeV	E_α= 120.5 MeV	E_α= 140.5 MeV
	Cross Section mb	Cross Section mb	Cross Section mb	Cross Section mb	Cross Section mb
2.5	1.5	0.543	0.896	2.88	6.31
7.5	1.51	0.703	1.23	3.18	5.69
12.5	1.52	1.06	1.95	3.89	4.5
17.5	1.47	1.48	2.69	4.34	3.06
22.5	1.42	1.86	3.24	4.22	1.8
27.5	1.45	2.28	3.54	3.76	1.09
32.5	1.41	2.38	3.09	2.73	0.61
37.5	1.46	2.43	2.67	2	0.379
42.5	1.48	2.32	1.93	1.26	0.219
47.5	1.42	1.81	1.15	0.686	0.111
52.5	1.34	1.29	0.636	0.353	0.0533
57.5	1.27	0.853	0.324	0.161	0.0205
62.5	1.2	0.539			
67.5	1.19	0.319			
72.5	1.14	0.177			
77.5	1.16	0.0909			
82.5	1.08	0.042			
87.5	1.07				
92.5	1.01				
97.5	0.968				
102.5	0.898				
107.5	0.842				
112.5	0.823				
117.5	0.75				
122.5	0.71				
127.5	0.693				
132.5	0.673				
147.5	0.469				
152.5	0.445				
157.5	0.393				
162.5	0.38				
167.5	0.374				
172.5	0.362				
177.5	0.356				

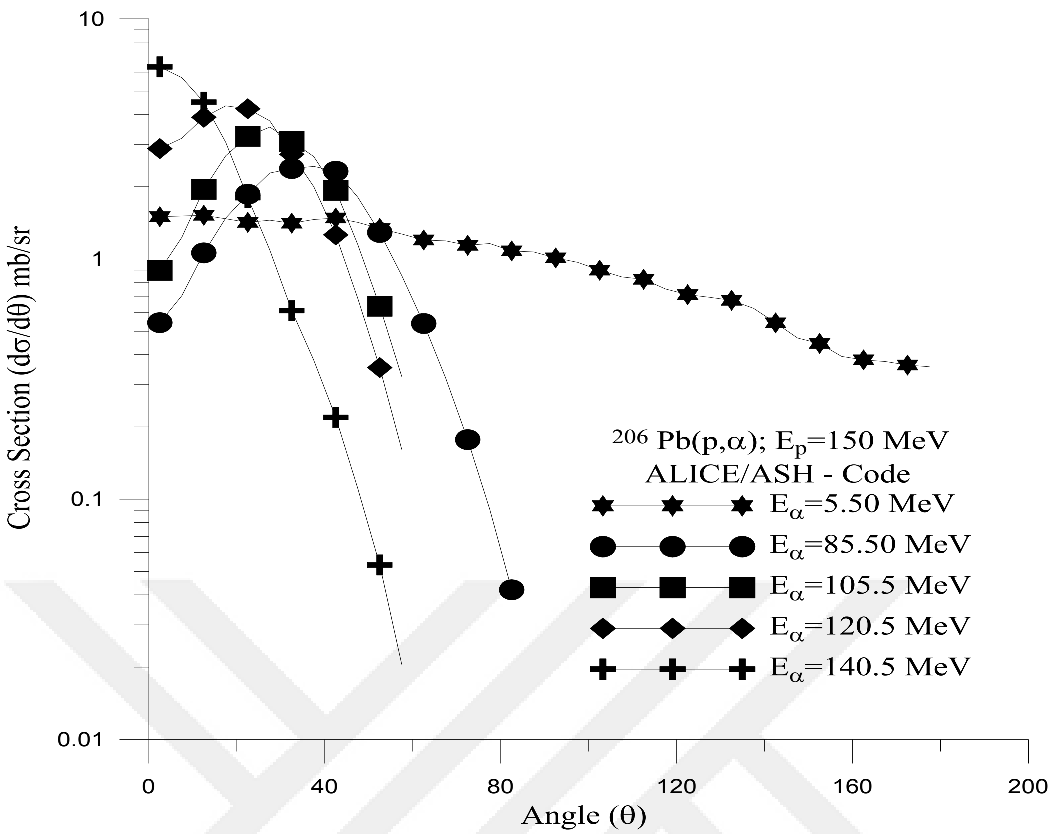

Figure 4.35. Angular Distributions (mb/sr) of the alpha generated as a result of bombardment of element $_{82}Pb^{206}$ with 150 MeV energetic protons

4.4.3.6. α Angular Distribution for p + $_{82}Pb^{206}$ Reaction at E_p = 180 MeV

The calculation for the angular distribution of ^{206}Pb(p,α) reaction has been see in the Fig. 4.36. In this reaction α- particle emitted at angle (2.5°, 7.5°......... 177.5°). In this reaction, when E_α= 80.50 MeV the maximum point of reaction cross section equal to (1.93 mb), located at this angle (42.5°), and the minimum point of reaction cross section equal to (0.164 mb), located at this angle (2.5°). When E_α= 110.5 MeV the maximum point of reaction cross section equal to (2.41 mb) located at this angle (37.5°), and the minimum point of reaction cross section equal to (0.158 mb), located at this angle (2.5°). When E_α= 135.5 MeV the maximum point of reaction cross section equal to (3.21 mb) located at this angle (27.5°), and the minimum point of reaction cross section equal to (0.061 mb), located at this angle (62.5°). When E_α= 150.5 MeV the maximum point of reaction cross section equal to (4.07 mb) located at this angle (17.5°), and the minimum point of reaction cross section equal to (0.0191 mb), located at this angle (62.5°). When E_α=

155.5 MeV the maximum point of reaction cross section equal to (4.39 mb) located at this angle (12.5°), and the minimum point of reaction cross section equal to (0.13 mb), located at this angle (52.5°). When E_{α}= 165.5 MeV the maximum point of reaction cross section equal to (6.05 mb) located at this angle (2.5°), and the minimum point of reaction cross section equal to (0.0544 mb), located at this angle (52.5°). Figure (4.36) represents the evaluated results and angle-integrated emission Spectra measurements at E_p= 180 MeV.

Table 4.36. Alpha scattered angular distributions (mb/sr) for p + $_{82}Pb^{206}$ reaction, E_p= 180 MeV energy. Calculations have been made by ALICE/ASH code program

$^{206}Pb(p, \alpha)$; E_p=180 MeV ALICE/ASH – Code						
ANGLE/DEG.	E_{α}=80.5 MeV	E_{α}=110.5 MeV	E_{α}=135.5 MeV	E_{α}=150.5 MeV	E_{α}=155.5 MeV	E_{α}=165.5 MeV
	Cross Section mb	Cross Section mb	Cross Section mb	Cross Section mb	Cross Section mb	Cross Section mb
2.5	0.164	0.158	1.04	3.13	4.26	6.05
7.5	0.25	0.325	1.39	3.34	4.26	5.51
12.5	0.422	0.674	2.13	3.84	4.39	4.65
17.5	0.65	1.16	2.79	4.07	4.27	3.72
22.5	0.923	1.73	3.15	3.72	3.57	2.47
27.5	1.27	2.27	3.21	3.11	2.75	1.56
32.5	1.52	2.38	2.59	2.09	1.73	0.871
37.5	1.77	2.41	2.04	1.42	1.12	0.535
42.5	1.93	2.03	1.32	0.821	0.636	0.296
47.5	1.71	1.4	0.694	0.399	0.304	0.138
52.5	1.43	0.841	0.339	0.177	0.13	0.0544
57.5	1.09	0.452	0.15 m	0.0654		
62.5	0.794	0.241	0.061	0.0191		
67.5	0.537					
72.5	0.334					
77.5	0.2					

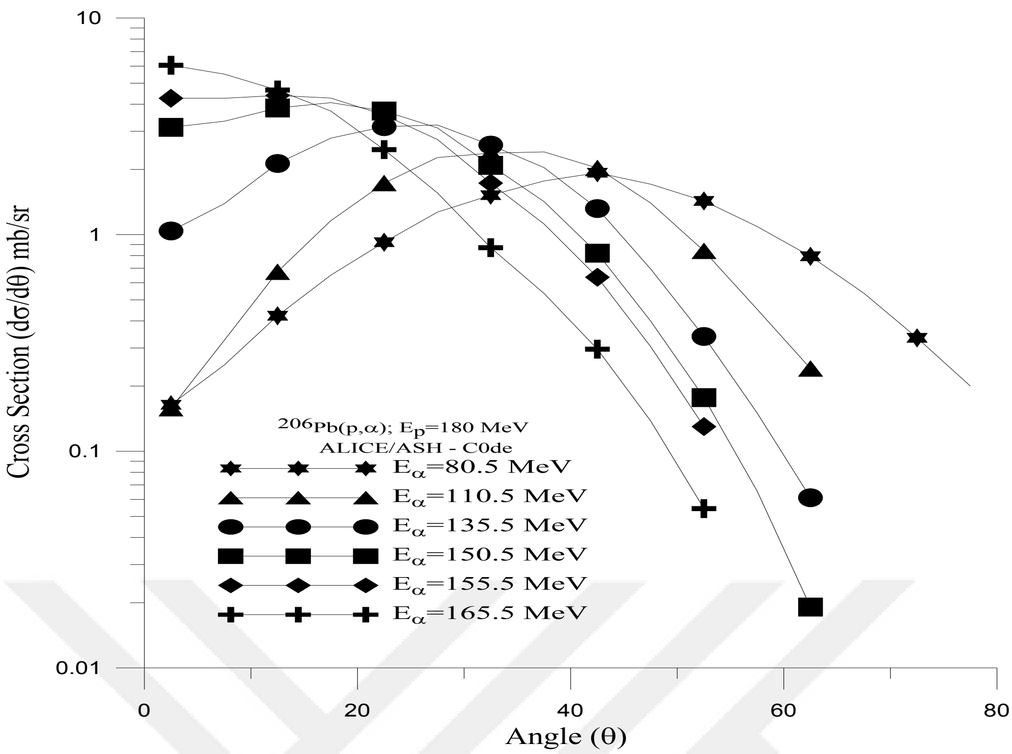

Figure 4.36. Angular Distributions (mb/sr) of the alpha generated as a result of bombardment of element $_{82}Pb^{206}$ with 180 MeV energetic protons

4.4.3.7. α Angular Distribution for p + $_{82}Pb^{206}$ Reaction at E_p = 210 MeV

The calculation for the angular distribution of $^{206}Pb(p,\alpha)$ reaction has been see in the Fig. 4.37. In this reaction α- particle emitted at angle (2.5°, 7.5°......... 177.5°). In this reaction, when E_α= 5.50 MeV the maximum point of reaction cross section equal to (0.782 mb), located at this angle (12.5°), and the minimum point of reaction cross section equal to (0.215 mb), located at this angle (177.5°). When E_α= 90.5 MeV the maximum point of reaction cross section equal to (1.58 mb) located at this angle (42.5°), and the minimum point of reaction cross section equal to (0.101 mb), located at this angle (2.5°). When E_α= 125.5 MeV the maximum point of reaction cross section equal to (2.01 mb) located at this angle (37.5°), and the minimum point of reaction cross section equal to (0.0784 mb), located at this angle (2.5°). When E_α= 155.5 MeV the maximum point of reaction cross section equal to (2.62 mb) located at this angle (27.5°), and the minimum point of reaction cross section equal to (0.281 mb), located at this angle (52.5°). When E_α= 180.5 MeV the maximum point of reaction cross section equal to (3.64 mb) located at this angle (17.5°), and the minimum point of reaction cross section equal to (0.0881 mb), located at this angle (52.5°). When E_α= 195.5 MeV the maximum point of reaction cross section equal to (5.39 mb) located at this angle (2.5°), and the minimum point of reaction cross section equal to (0.0234 mb), located at this angle (52.5°). Figure (4.37) represents the evaluated results and angle-integrated emission Spectra measurements at E_p= 210 MeV.

Table 4.37. Alpha scattered angular distributions (mb/sr) for p + $_{82}Pb^{206}$ reaction, E_p= 210 MeV energy. Calculations have been made by ALICE/ASH code program

$^{206}Pb(p, \alpha)$; E_p=210 MeV ALICE/ASH – Code						
ANGLE/DEG .	E_α=5.50 MeV	E_α= 90.5 MeV	E_α= 125.5 MeV	E_α= 155.5 MeV	E_α= 180.5 MeV	E_α= 195.5 MeV
	Cross Section mb	Cross Section mb	Cross Section mb	Cross Section mb	Cross Section mb	Cross Sectio n mb
2.5	0.763	0.101	0.0784	0.567	3.23	5.39
7.5	0.775	0.157	0.177	0.866	3.31	4.9
12.5	0.782	0.276	0.414	1.46	3.6	3.99
17.5	0.753	0.445	0.776	2.05	3.64	3.05
22.5	0.731	0.658	1.25	2.45	3.16	1.91
27.5	0.75	0.941	1.73	2.62	2.49	1.18
32.5	0.732	1.16	1.91	2.19	1.58	0.633
37.5	0.762	1.4	2.01	1.77	1 .0	0.368
42.5	0.778	1.58	1.76	1.16	0.539	0.188
47.5	0.75	1.44	1.25	0.602	0.236	0.0763
52.5	0.712	1.22	0.76	0.281	0.0881	0.0234
57.5	0.678	0.948	0.403			
62.5	0.644	0.704	0.209			
67.5	0.642	0.482	0.106			
72.5	0.619	0.298				
77.5	0.632	0.176				
82.5	0.594					
87.5	0.593					
92.5	0.563					
97.5	0.544					
102.5	0.509					
107.5	0.48					
112.5	0.472					
117.5	0.433					
122.5	0.413					
127.5	0.405					
132.5	0.396					
137.5	0.369					
142.5	0.323					
147.5	0.281					
152.5	0.268					
157.5	0.236					
162.5	0.23					
167.5	0.226					
177.5	0.215					

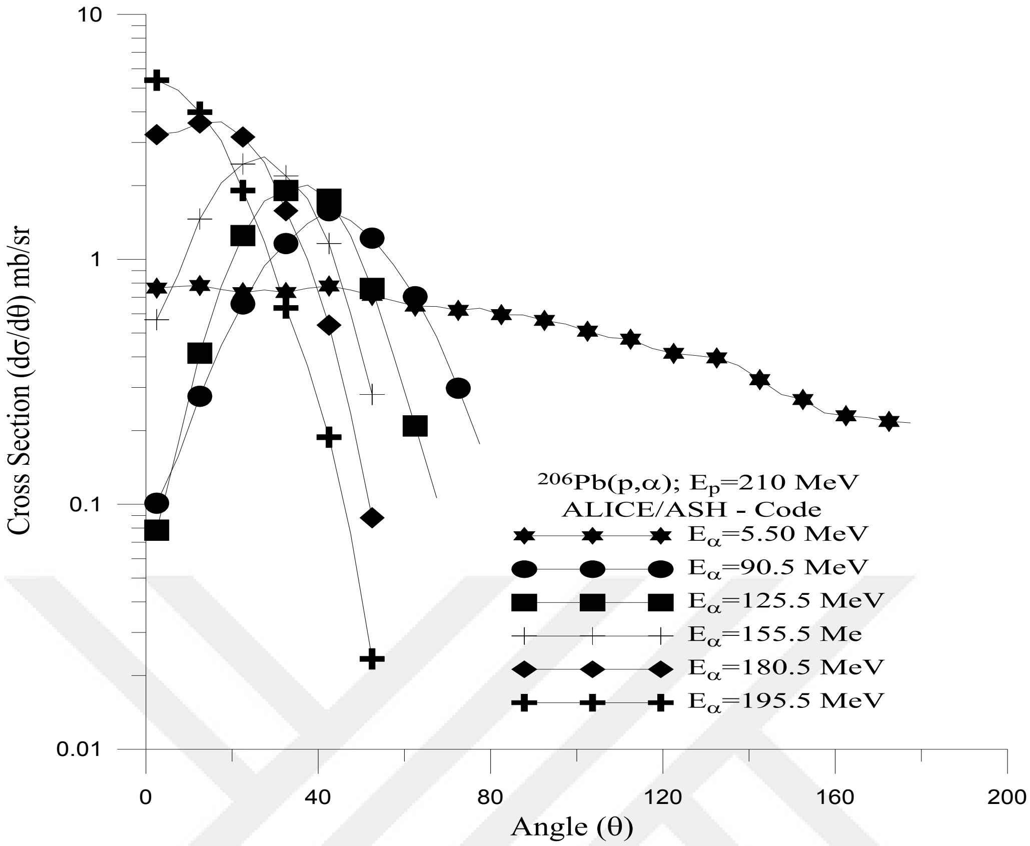

Figure 4.37. Angular Distributions (mb/sr) of the alpha generated as a result of bombardment of element $_{82}Pb^{206}$ with 210 MeV energetic protons

4.4.3.8. α Angular Distribution for p + $_{82}Pb^{206}$ Reaction at E_p = 240 MeV

The calculation for the angular distribution of $^{206}Pb(p,\alpha)$ reaction has been see in the Fig. 4.38. In this reaction α- particle emitted at angle (2.5°, 7.5°......... 177.5°). In this reaction, when E_α= 5.50 MeV the maximum point of reaction cross section equal to (0.6 mb), located at this angle (42.5°), and the minimum point of reaction cross section equal to (0.176 mb), located at this angle (177.5°). When E_α= 85.5 MeV the maximum point of reaction cross section equal to (1.21 mb) located at this angle (42.5°), and the minimum point of reaction cross section equal to (0.086 mb), located at this angle (2.5°). When E_α= 165.5 MeV the maximum point of reaction cross section equal to (1.9 mb) located at this angle (27.5°), and the minimum point of reaction cross section equal to (0.148 mb), located at this angle (57.5°). When E_α= 205.5 MeV the maximum point of reaction cross section equal to (2.98 mb) located at this angle (17.5°), and the minimum point of reaction cross section equal to (0.0582 mb), located at this angle (52.5°). When E_α=

225.5 MeV the maximum point of reaction cross section equal to (5.13 mb) located at this angle (2.5°), and the minimum point of reaction cross section equal to (0.00156 mb), located at this angle (52.5°). Figure (4.38) represents the evaluated results and angle-integrated emission Spectra measurements at E_p= 240 MeV.

Table 4.38. Alpha scattered angular distributions (mb/sr) for p + $_{82}Pb^{206}$ reaction, E_p= 240 MeV energy. Calculations have been made by ALICE/ASH code program

$^{206}Pb(p, \alpha)$; E_p=240 MeV ALICE/ASH – Code					
ANGLE/DEG.	E_α=5.50 MeV	E_α= 85.5 MeV	E_α= 165.5 MeV	E_α= 205.5 MeV	E_α= 225.5 MeV
	Cross Section mb	Cross Section mb	Cross Section mb	Cross Section mb	Cross Section mb
2.5	0.583	0.086	0.156	2.41	5.13
7.5	0.596	0.11	0.335	2.52	4.73
12.5	0.59	0.167	0.696	2.87	3.73
17.5	0.566	0.268	1.15	2.98	2.32
22.5	0.557	0.403	1.57	2.67	1.34
27.5	0.564	0.595	1.9	2.14	0.744
32.5	0.561	0.776	1.78	1.36	0.412
37.5	0.578	0.985	1.61	0.855	0.217
42.5	0.6	1.21	1.18	0.439	0.0947
47.5	0.576	1.17	0.688	0.176	0.0201
52.5	0.551	1.08	0.341	0.0582	0.00156
57.5	0.529	0.906	0.148		
62.5	0.492	0.73			
67.5	0.486	0.559			
72.5	0.48	0.391			
77.5	0.488	0.256			
82.5	0.462	0.157			
87.5	0.464				
92.5	0.443				
97.5	0.426				
127.5	0.325				
132.5	0.317				
137.5	0.299				
142.5	0.256				
147.5	0.227				
152.5	0.212				
157.5	0.191				
162.5	0.182				
177.5	0.176				

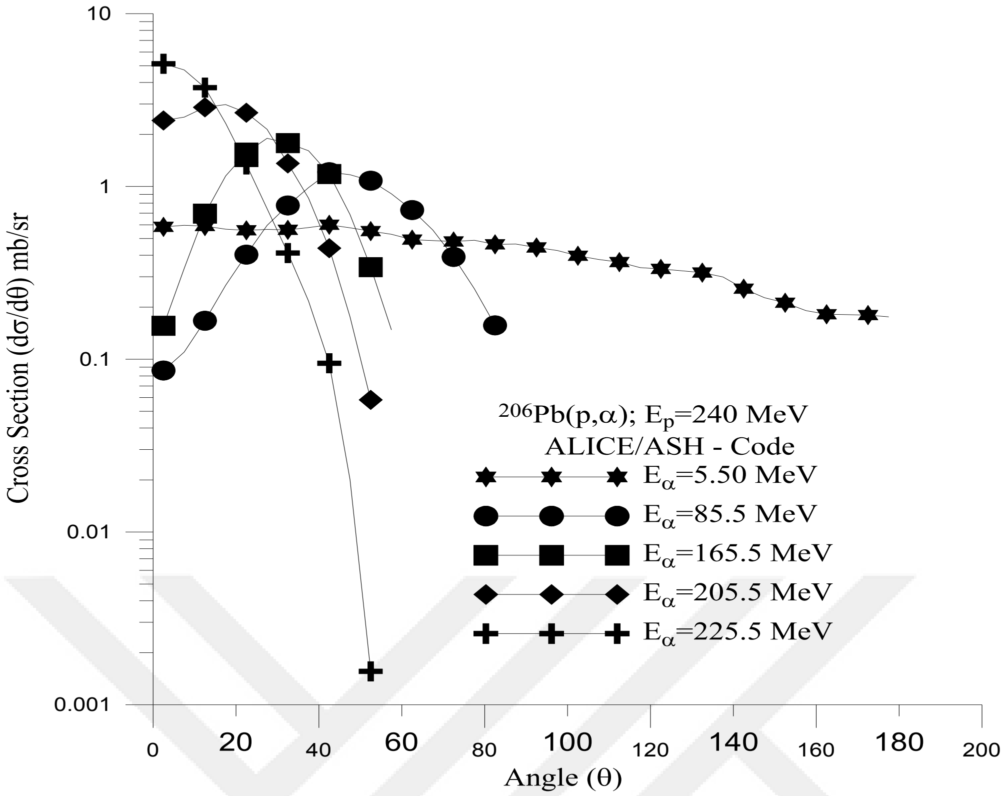

Figure 4.38. Angular Distributions (mb/sr) of the alpha generated as a result of bombardment of element $_{82}Pb^{206}$ with 240 MeV energetic protons

4.4.3.9. α Angular Distribution for p + $_{82}Pb^{206}$ Reaction at E_p = 270 MeV

The calculation for the angular distribution of ^{206}Pb(p,α) reaction has been see in the Fig. 4.39. In this reaction α- particle emitted at angle (2.5°, 7.5°......... 177.5°). In this reaction, when E_α= 5.50 MeV the maximum point of reaction cross section equal to (0.47 mb), located at this angle (42.5°), and the minimum point of reaction cross section equal to (0.145 mb), located at this angle (177.5°). When E_α= 105.5 MeV the maximum point of reaction cross section equal to (1.1 mb) located at this angle (47.5°), and the minimum point of reaction cross section equal to (0.0521 mb), located at this angle (2.5°). When E_α= 160.5 MeV the maximum point of reaction cross section equal to (1.34 mb) located at this angle (37.5°), and the minimum point of reaction cross section equal to (0.0217 mb), located at this angle (2.5°). When E_α= 205.5 MeV the maximum point of reaction cross section equal to (1.77 mb) located at this angle (27.5°), and the minimum point of reaction cross section equal to (0.136 mb), located at this angle (52.5°). When E_α= 255.5 MeV the maximum point of reaction cross section equal to (4.2 mb) located at this angle

(2.5°), and the minimum point of reaction cross section equal to (0.0533 mb), located at this angle (42.5°). Figure (4.39) represents the evaluated results and angle-integrated emission Spectra measurements at E_p= 270 MeV.

Table 4.39. Alpha scattered angular distributions (mb/sr) for p + $_{82}Pb^{206}$ reaction, E_p= 270 MeV energy. Calculations have been made by ALICE/ASH code program

$^{206}Pb(p, \alpha)$; E_p=270 MeV ALICE/ASH – Code					
ANGLE/DEG.	E_α= 5.50 MeV	E_α= 105.5 MeV	E_α= 160.5 MeV	E_α= 205.5 MeV	E_α= 255.5 MeV
	Cross Section mb	Cross Section mb	Cross Section mb	Cross Section mb	Cross Section mb
2.5	0.453	0.0521	0.0217	0.377	4.2
7.5	0.463	0.0543	0.0662	0.619	3.77
12.5	0.459	0.0693	0.205	1.05	2.79
17.5	0.44	0.135	0.44	1.44	1.72
22.5	0.433	0.264	0.757	1.68	1.02
27.5	0.44	0.464	1.09	1.77	0.571
32.5	0.438	0.677	1.24	1.44	0.308
37.5	0.452	0.933	1.34	1.12	0.147
42.5	0.47	1.1	1.19	0.701	0.0533
47.5	0.452	1.1	0.858	0.339	
52.5	0.433	0.95	0.531	0.136	
57.5	0.417	0.721	0.279		
62.5	0.388	0.53			
67.5	0.384	0.386			
72.5	0.38	0.223			
77.5	0.386				
82.5	0.367				
87.5	0.369				
92.5	0.353				
97.5	0.341				
102.5	0.318				
107.5	0.303				
112.5	0.293				
117.5	0.273				
132.5	0.257				
147.5	0.187				
152.5	0.175				
157.5	0.158				
162.5	0.151				
167.5	0.15				
177.5	0.145				

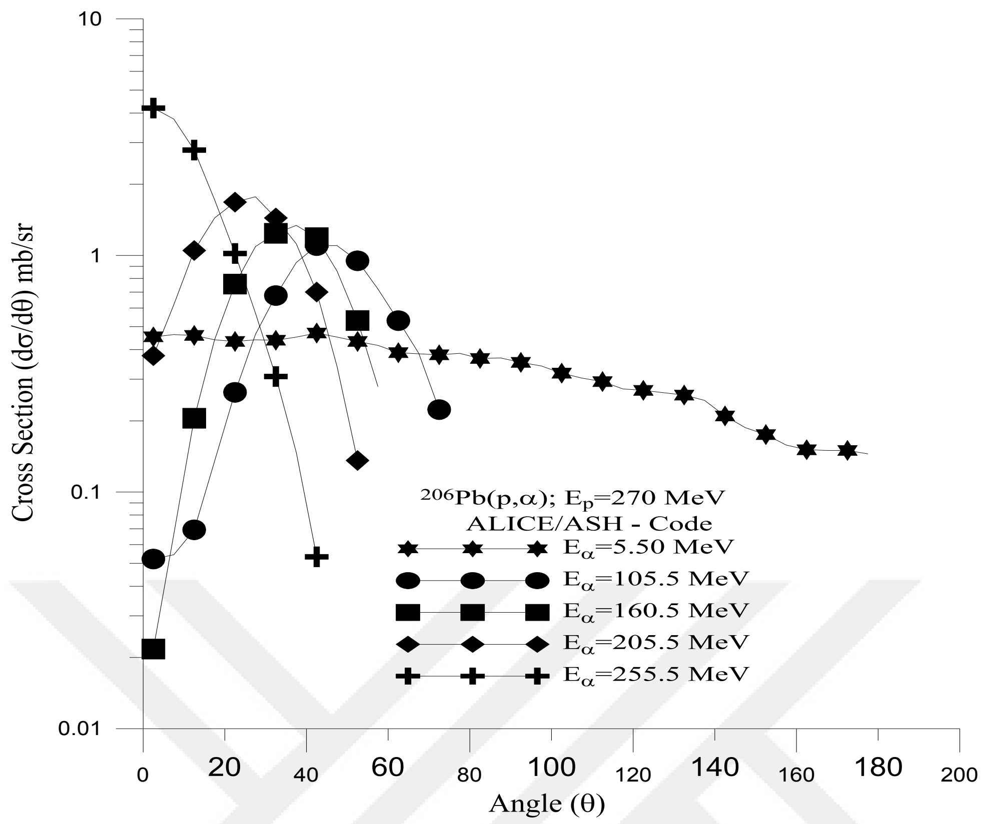

Figure 4.39. Angular Distributions (mb/sr) of the alpha generated as a result of bombardment of element $_{82}Pb^{206}$ with 270 MeV energetic protons

4.4.4.10. α Angular Distribution for p + $_{90}Th^{232}$ Reaction at E_p = 30 MeV

The calculation for the angular distribution of $^{232}Th(p,\alpha)$ reaction has been see in the Fig. 4.40. In this reaction α- particle emitted at angle (2.5°, 7.5°......... 177.5°). In this reaction, when E_α= 5.50 MeV the maximum point of reaction cross section equal to (10 mb), located at this angle (12.5°), and the minimum point of reaction cross section equal to (0.988 mb), located at this angle (177.5°). When E_α= 10.5 MeV the maximum point of reaction cross section equal to (6.83 mb) located at this angle (2.5°), and the minimum point of reaction cross section equal to (0.199 mb), located at this angle (172.5°). When E_α= 15.5 MeV the maximum point of reaction cross section equal to (4.44 mb) located at this angle (2.5°), and the minimum point of reaction cross section equal to (0.0273 mb), located at this angle (177.5°). Figure (4.40) represents the evaluated results and angle-integrated emission Spectra measurements at E_p= 30 MeV.

Table 4.40. Alpha scattered angular distributions (mb/sr) for p + $_{90}Th^{232}$ reaction, E_p= 30 MeV energy. Calculations have been made by ALICE/ASH code program

$^{232}Th(P, \alpha)$; E_p=30 MeV ALICE/ASH – Code			
ANGLE/DEG.	E_α= 5.50 MeV	E_α= 10.5 MeV	E_α= 15.5 MeV
	Cross Section mb	Cross Section mb	Cross Section mb
2.5	9.89	6.83	4.44
7.5	9.83	6.62	4.3
12.5	10	6.65	4.32
17.5	9.86	6.62	4.22
22.5	9.36	6.07	3.85
27.5	9.63	6.14	3.83
32.5	9.38	5.88	3.56
37.5	9.38	5.7	3.32
42.5	9.37	5.5	3.21
47.5	8.74	5.04	2.76
52.5	7.91	4.4	2.41
57.5	7.54	4.03	2.09
62.5	6.79	3.52	1.83
67.5	6.36	3.2	1.61
72.5	5.96	2.95	1.45
77.5	5.63	2.69	1.29
82.5	5.04	2.38	1.11
87.5	4.73	2.15	0.959
92.5	4.33	1.89	0.805
97.5	4.01	1.68	0.689
102.5	3.65	1.49	0.577
107.5	3.3	1.3	0.481
112.5	3.08	1.09	0.365
117.5	2.72	0.901	0.27
122.5	2.63	0.832	0.219
127.5	2.36	0.692	0.166
132.5	2.21	0.552	0.105
137.5	2.03	0.479	0.0739
142.5	1.71	0.364	0.0475
147.5	1.5	0.297	0.0378
152.5	1.38	0.258	0.0348
157.5	1.18	0.22	0.0305
162.5	1.15	0.219	0.0304
167.5	1.08	0.209	0.0288
172.5	0.999	0.199	0.0273
177.5	0.988	0.2	0.0273

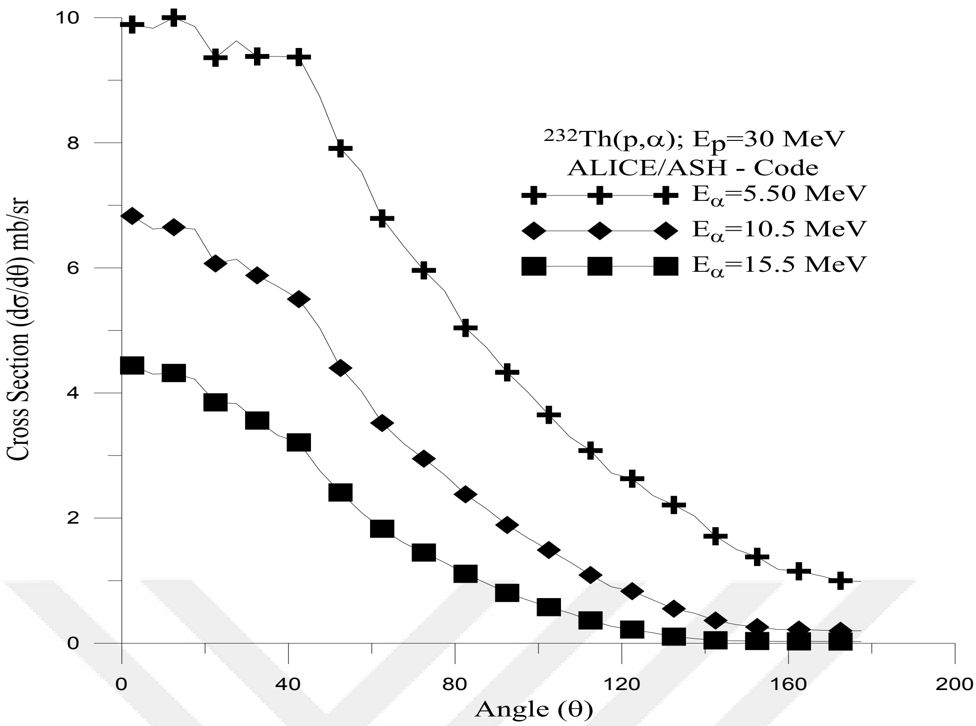

Figure 4.40. Angular Distributions (mb/sr) of the alpha generated as a result of bombardment of element $_{90}Th^{232}$ with 30 MeV energetic protons

4.4.4.11. α Angular Distribution for p + $_{90}Th^{232}$ Reaction at E_p = 60 MeV

The calculation for the angular distribution of ^{232}Th(p,α) reaction has been see in the Fig. 4.41. In this reaction α- particle emitted at angle (2.5°, 7.5°......... 177.5°). In this reaction, when E_α= 5.50 MeV the maximum point of reaction cross section equal to (8.32 mb), located at this angle (12.5°), and the minimum point of reaction cross section equal to (1.2 mb), located at this angle (177.5°). When E_α= 10.5 MeV the maximum point of reaction cross section equal to (7.19 mb) located at this angle (2.5°), and the minimum point of reaction cross section equal to (0.516 mb), located at this angle (172.5°). When E_α= 15.5 MeV the maximum point of reaction cross section equal to (5.82 mb) located at this angle (2.5°), and the minimum point of reaction cross section equal to (0.198 mb), located at this angle (177.5°). Figure (4.41) represents the evaluated results and angle-integrated emission Spectra measurements at E_p= 60 MeV.

Table 4.41. Alpha scattered angular distributions (mb/sr) for p + $_{90}Th^{232}$ reaction, E_p= 60 MeV energy. Calculations have been made by ALICE/ASH code program

$^{232}Th(P, \alpha)$; E_p=60 MeV ALICE/ASH – Code			
ANGLE/DEG.	E_α= 5.50 MeV	E_α= 10.5 MeV	E_α= 15.5 MeV
	Cross Section mb	Cross Section mb	Cross Section mb
2.5	8.3	7.19	5.82
7.5	8.27	6.96	5.61
12.5	8.32	6.96	5.68
17.5	8.12	6.94	5.61
22.5	7.7	6.39	5.17
27.5	7.86	6.53	5.32
32.5	7.62	6.39	5.23
37.5	7.71	6.47	5.24
42.5	7.82	6.62	5.45
47.5	7.33	6.24	5.03
52.5	6.8	5.75	4.66
57.5	6.47	5.43	4.18
62.5	6.03	4.94	3.77
67.5	5.74	4.55	3.37
72.5	5.55	4.25	3.06
77.5	5.3	3.9	2.74
82.5	4.87	3.51	2.38
87.5	4.63	3.18	2.08
92.5	4.26	2.82	1.76
97.5	3.96	2.53	1.53
102.5	3.56	2.23	1.29
107.5	3.29	1.99	1.11
112.5	3.09	1.73	0.909
117.5	2.78	1.5	0.748
122.5	2.63	1.4	0.669
127.5	2.47	1.27	0.588
132.5	2.35	1.12	0.489
137.5	2.2	1.04	0.435
142.5	1.86	0.837	0.336
147.5	1.62	0.708	0.279
152.5	1.52	0.65	0.255
157.5	1.34	0.568	0.222
162.5	1.31	0.555	0.216
167.5	1.26	0.535	0.207
172.5	1.2	0.516	0.198
177.5	1.2	0.518	0.198

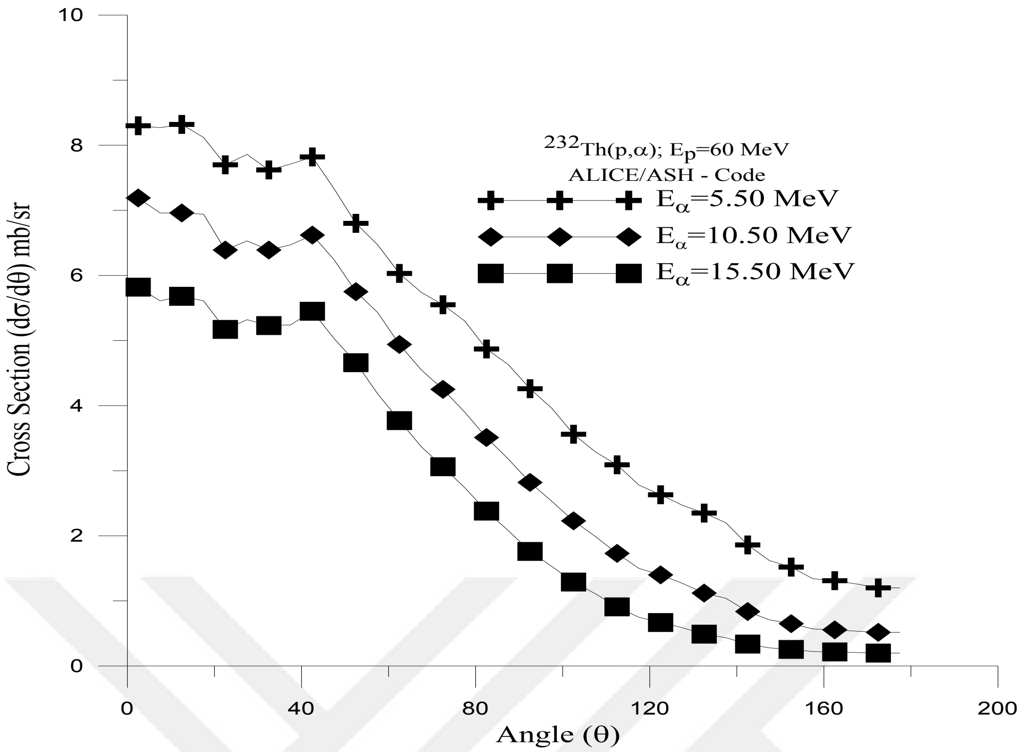

Figure 4.41. Angular Distributions (mb/sr) of the alpha generated as a result of bombardment of element $_{90}Th^{232}$ with 60 MeV energetic protons

4.4.4.12. α Angular Distribution for p + $_{90}Th^{232}$ Reaction at E_p = 90 MeV

The calculation for the angular distribution of $^{232}Th(p,\alpha)$ reaction has been see in the Fig. 4.42. In this reaction α- particle emitted at angle (2.5°, 7.5°......... 177.55°). In this reaction, when E_α= 5.50 MeV the maximum point of reaction cross section equal to (4.76 mb), located at this angle (12.5°), and the minimum point of reaction cross section equal to (0.933 mb), located at this angle (177.5°). When E_α= 10.5 MeV the maximum point of reaction cross section equal to (4.37 mb) located at this angle (42.5°), and the minimum point of reaction cross section equal to (0.534 mb), located at this angle (172.5°). When E_α= 15.5 MeV the maximum point of reaction cross section equal to (3.97 mb) located at this angle (42.5°), and the minimum point of reaction cross section equal to (0.294 mb), located at this angle (172.5°). When E_α= 80.5 MeV the maximum point of reaction cross section equal to (6.94 mb) located at this angle (2.5°), and the minimum point of reaction cross section equal to (0.171 mb), located at this angle (62.5°). When E_α= 85.5 MeV the maximum point of reaction cross section equal to (5.23 mb) located at this angle (2.5°), and the minimum point of reaction cross section equal to (0.0635 mb), located at this angle (62.5°). Figure (4.42) represents the evaluated results and angle-integrated emission Spectra measurements at E_p= 90 MeV.

Table 4.42. Alpha scattered angular distributions (mb/sr) for p + $_{90}Th^{232}$ reaction, E_p= 90 MeV energy. Calculations have been made by ALICE/ASH code program

$^{232}Th(p, \alpha)$; E_p=90 MeV ALICE/ASH – Code					
ANGLE/DEG.	E_α= 5.50 MeV	E_α= 10.5 MeV	E_α= 15.5 MeV	E_α= 80.5 MeV	E_α= 85.5 MeV
	Cross Section mb	Cross Section mb	Cross Section mb	Cross Section mb	Cross Section mb
2.5	4.73	4.28	3.59	6.94	5.23
7.5	4.73	4.15	3.48	6.59	4.94
12.5	4.76	4.17	3.55	5.94	4.37
17.5	4.64	4.2	3.57	5.05	3.49
22.5	4.42	3.91	3.37	4.12	2.33
27.5	4.52	4.06	3.55	3.36	1.64
32.5	4.4	4.05	3.61	2.34	1.04
37.5	4.49	4.2	3.72	1.71	0.714
42.5	4.57	4.37	3.97	1.2	0.479
47.5	4.34	4.17	3.72	0.727	0.281
52.5	4.07	3.93	3.58	0.451	0.169
57.5	3.91	3.78	3.32	0.279	0.102
62.5	3.67	3.5	3.07	0.171	0.0635
67.5	3.54	3.32	2.84		
72.5	3.46	3.15	2.65		
77.5	3.36	2.96	2.45		
82.5	3.14	2.72	2.19		
87.5	3.02	2.51	1.96		
92.5	2.83	2.27	1.71		
97.5	2.66	2.07	1.52		
102.5	2.42	1.86	1.33		
107.5	2.27	1.68	1.16		
112.5	2.15	1.49	0.987		
117.5	1.96	1.31	0.84		
147.5	1.22	0.698	0.388		
152.5	1.16	0.652	0.36		
157.5	1.03	0.576	0.319		
162.5	1.01	0.569	0.315		
167.5	0.98	0.551	0.304		
172.5	0.936	0.534	0.294		
177.5	0.933	0.537	0.295		

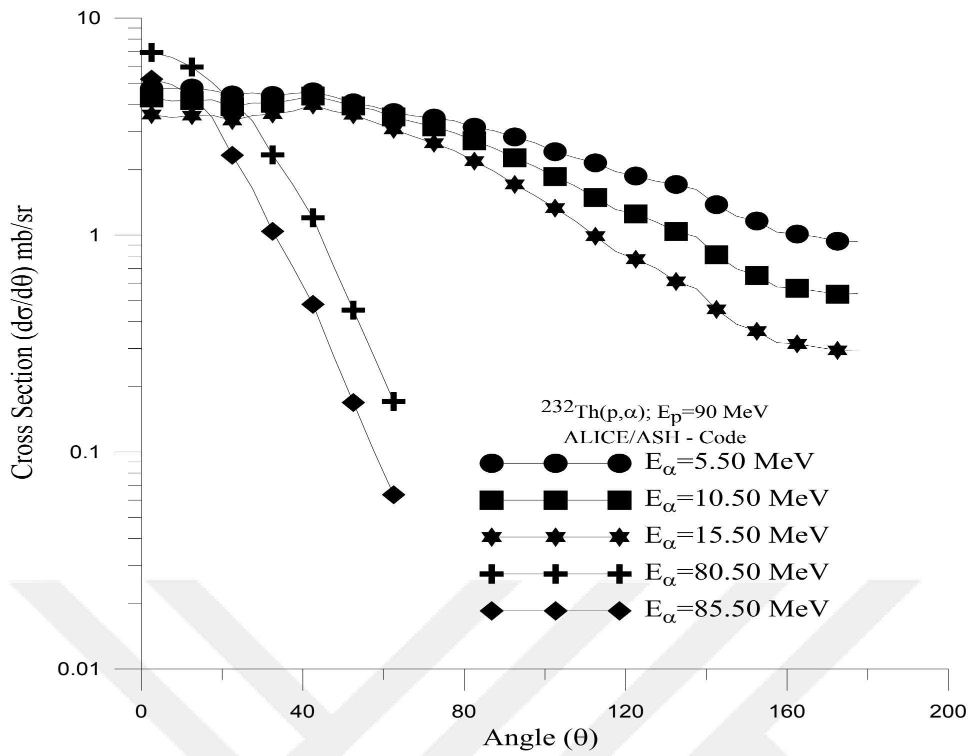

Figure 4.42. Angular Distributions (mb/sr) of the alpha generated as a result of bombardment of element ${}_{90}Th^{232}$ with 90 MeV energetic protons

4.4.4.13. α Angular Distribution for p + ${}_{90}Th^{232}$ Reaction at E_p = 120 MeV

The calculation for the angular distribution of ${}^{232}Th(p,\alpha)$ reaction has been see in the Fig. 4.43. In this reaction α- particle emitted at angle (2.5°, 7.5°......... 177.5°). In this reaction, when E_α= 5.50 MeV the maximum point of reaction cross section equal to (2.92 mb), located at this angle (12.5°), and the minimum point of reaction cross section equal to (0.67 mb), located at this angle (177.5°). When E_α= 10.5 MeV the maximum point of reaction cross section equal to (2.88 mb) located at this angle (42.5°), and the minimum point of reaction cross section equal to (0.436 mb), located at this angle (177.5°). When E_α= 85.5 MeV the maximum point of reaction cross section equal to (3.95 mb) located at this angle (27.5°), and the minimum point of reaction cross section equal to (0.113 mb), located at this angle (72.5°). When E_α= 100.5 MeV the maximum point of reaction cross section equal to (5.53 mb) located at this angle (17.5°), and the minimum point of reaction cross section equal to (0.125 mb), located at this angle (72.5°). When E_α= 120.5 MeV the maximum point of reaction cross section equal to (6.53 mb) located at this angle (2.5°), and the minimum point of reaction cross section equal to (0.0381 mb), located at this angle (57.5°). Figure 4.43 represents the evaluated results and angle-integrated emission Spectra measurements at E_p=120 MeV.

Table 4.43. Alpha scattered angular distributions (mb/sr) for p + $_{90}Th^{232}$ reaction, E_p= 120 MeV energy. Calculations have been made by ALICE/ASH code program

$^{232}Th(P, \alpha)$; E_p=120 MeV ALICE/ASH – Code					
ANGLE/DEG.	E_α= 5.50 MeV	E_α= 10.5 MeV	E_α= 85.5 MeV	E_α= 100.5 MeV	E_α= 120.5 MeV
	Cross Section mb	Cross Section mb	Cross Section mb	Cross Section mb	Cross Section mb
2.5	2.9	2.65	2.42	4.67	6.53
7.5	2.91	2.58	2.61	4.85	5.86
12.5	2.92	2.58	3.09	5.31	4.66
17.5	2.82	2.59	3.52	5.53	2.9
22.5	2.71	2.46	3.73	5.02	1.71
27.5	2.77	2.58	3.95	4.31	1.07
32.5	2.72	2.61	3.56	3.06	0.618
37.5	2.83	2.79	3.19	2.27	0.402
42.5	2.84	2.88	2.62	1.5	0.247
47.5	2.77	2.81	1.75	0.877	0.138
52.5	2.59	2.66	1.1	0.499	0.0769
57.5	2.46	2.55	0.67	0.257	0.0381
62.5	2.32	2.4	0.399	0.125	
67.5	2.3	2.33	0.222	0.0516	
72.5	2.22	2.21	0.113	0.0125	
77.5	2.2	2.13			
82.5	2.05	1.96			
87.5	2.01	1.84			
92.5	1.89	1.67			
112.5	1.49	1.15			
117.5	1.34	0.999			
142.5	0.996	0.657			
147.5	0.854	0.551			
152.5	0.811	0.514			
157.5	0.729	0.463			
162.5	0.702	0.447			
167.5	0.697	0.442			
172.5	0.675	0.436			
177.5	0.67	0.436			

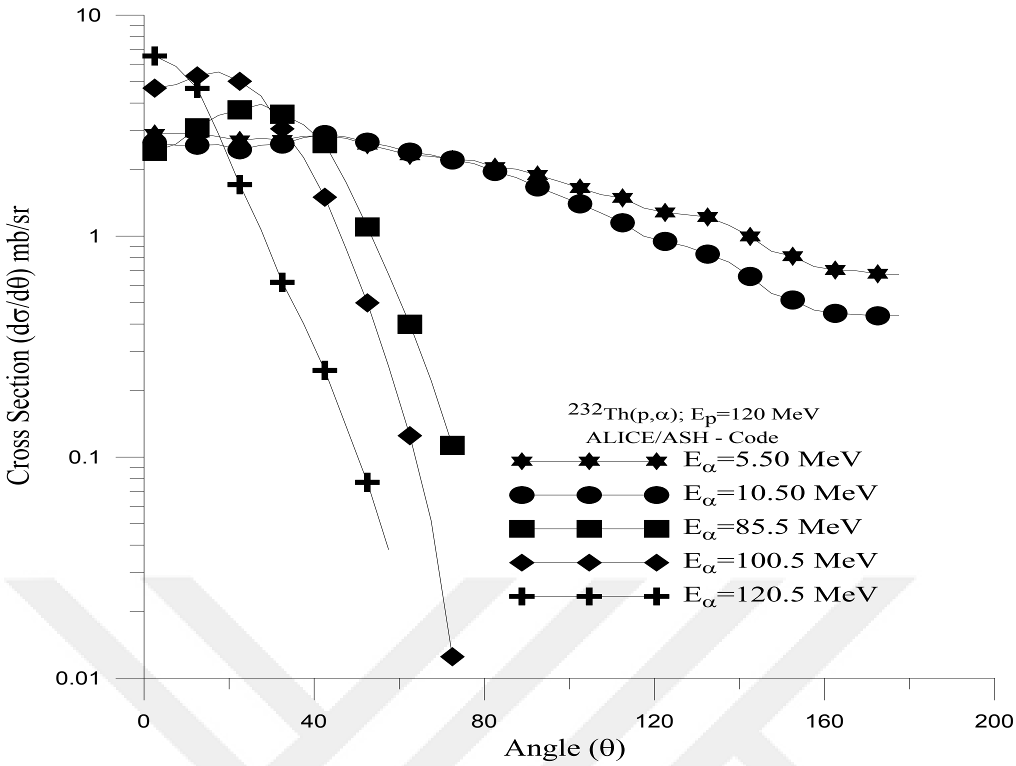

Figure 4.43. Angular Distributions (mb/sr) of the alpha generated as a result of bombardment of element $_{90}Th^{232}$ with 120 MeV energetic protons

4.4.4.14. α Angular Distribution for p + $_{90}Th^{232}$ Reaction at E_p = 150 MeV

The calculation for the angular distribution of $^{232}Th(p,\alpha)$ reaction has been see in the Fig. 4.44. In this reaction α- particle emitted at angle (2.5°, 7.5°......... 177.5°). In this reaction, when E_α= 5.50 MeV the maximum point of reaction cross section equal to (1.92 mb), located at this angle (12.5°), and the minimum point of reaction cross section equal to (0.488 mb), located at this angle (177.5°). When E_α= 15.5 MeV the maximum point of reaction cross section equal to (1.92 mb) located at this angle (42.5°), and the minimum point of reaction cross section equal to (0.241 mb), located at this angle (177.5°). When E_α= 95.5 MeV the maximum point of reaction cross section equal to (3.1 mb) located at this angle (32.5°), and the minimum point of reaction cross section equal to (0.0327 mb), located at this angle (77.5°). When E_α= 120.5 MeV the maximum point of reaction cross section equal to (4.45 mb) located at this angle (22.5°), and the minimum point of reaction cross section equal to (0.0898 mb), located at this angle (62.5°). When E_α= 140.5 MeV the maximum point of reaction cross section equal to

(7.34 mb) located at this angle (2.5°), and the minimum point of reaction cross section equal to (0.0108 mb), located at this angle (62.5°). Figure (4.44) represents the evaluated results and angle-integrated emission Spectra measurements at E_p= 150 MeV.

Table 4.44. Alpha scattered angular distributions (mb/sr) for p + $_{90}Th^{232}$ reaction, E_p= 150 MeV energy. Calculations have been made by ALICE/ASH code program

^{232}Th(P, α); E_p=150 MeV ALICE/ASH – Code					
ANGLE/DEG.	E_α= 5.50 MeV	E_α= 15.5 MeV	E_α= 95.5 MeV	E_α= 120.5 MeV	E_α= 140.5 MeV
	Cross Section mb	Cross Section mb	Cross Section mb	Cross Section mb	Cross Section mb
2.5	1.9	1.48	0.332	2.48	7.34
7.5	1.9	1.44	0.587	2.84	6.69
12.5	1.92	1.48	1.1	3.73	5.63
17.5	1.85	1.51	1.75	4.35	4.41
22.5	1.79	1.48	2.44	4.45	2.94
27.5	1.83	1.6	3.07	4.13	1.89
32.5	1.8	1.69	3.1	3.12	1.08
37.5	1.89	1.81	3.06	2.36	0.69
42.5	1.9	1.95	2.55	1.52	0.404
47.5	1.86	1.89	1.76	0.835	0.205
52.5	1.75	1.87	1.08	0.435	0.098
57.5	1.67	1.75	0.606	0.205	0.0377
62.5	1.58	1.67	0.342	0.0898	0.0108
67.5	1.57	1.61	0.194		
72.5	1.52	1.52	0.0832		
77.5	1.52	1.46	0.0327		
82.5	1.42	1.34			
87.5	1.4	1.23			
92.5	1.32	1.1			
97.5	1.25	0.991			
102.5	1.17	0.889			
122.5	0.918	0.54			
137.5	0.813	0.419			
142.5	0.722	0.355			
147.5	0.62	0.298			
152.5	0.59	0.278			
157.5	0.531	0.251			
162.5	0.512	0.244			
167.5	0.508	0.244			
172.5	0.493	0.241			
177.5	0.488	0.241			

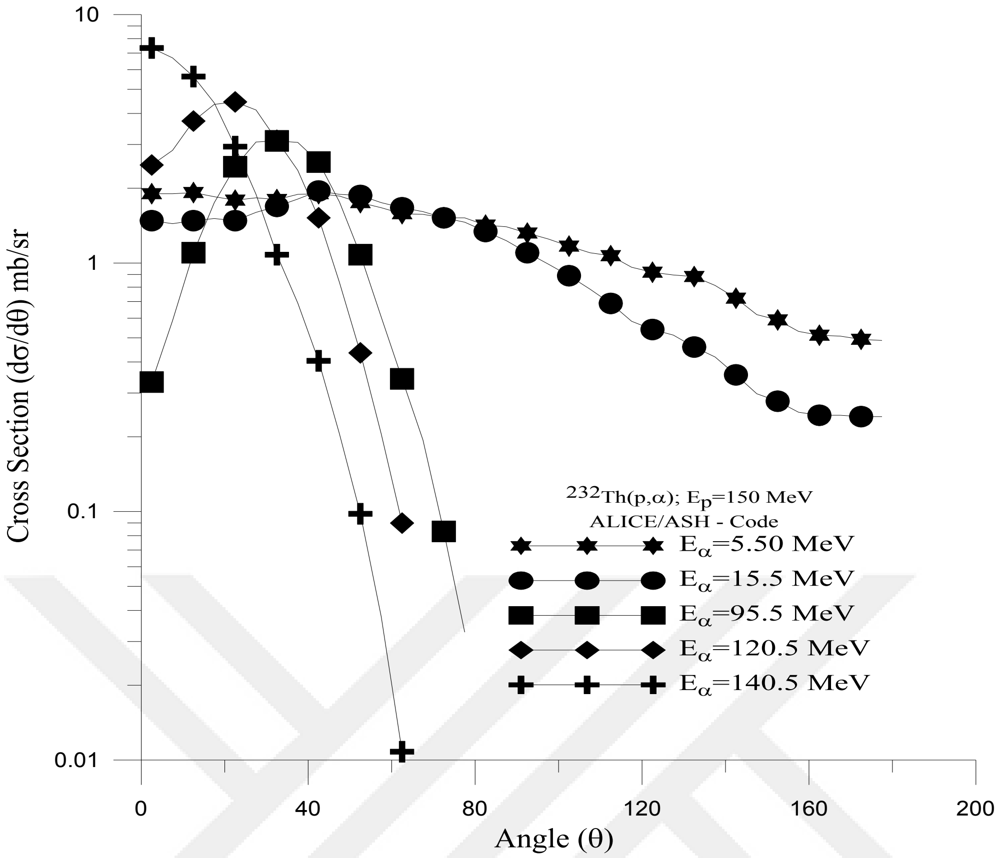

Figure 4.44. Angular Distributions (mb/sr) of the alpha generated as a result of bombardment of element $_{90}Th^{232}$ with 150 MeV energetic protons

4.4.4.15. α Angular Distribution for p + $_{90}Th^{232}$ Reaction at E_p = 180 MeV

The calculation for the angular distribution of ^{232}Th(p,α) reaction has been see in the Fig. 4.45. In this reaction α- particle emitted at angle (2.5°, 7.5°......... 177.5°). In this reaction, when E_α= 5.50 MeV the maximum point of reaction cross section equal to (1.34 mb), located at this angle (42.5°), and the minimum point of reaction cross section equal to (0.368 mb), located at this angle (177.5°). When E_α= 90.5 MeV the maximum point of reaction cross section equal to (2.32 mb) located at this angle (42.5°), and the minimum point of reaction cross section equal to (0.0544 mb), located at this angle (82.5°). When E_α= 100.5 MeV the maximum point of reaction cross section equal to (2.47 mb) located at this angle (37.5°), and the minimum point of reaction cross section equal to (0.0227 mb), located at this angle (82.5°). When E_α= 140.5 MeV the maximum point of reaction cross section equal to (3.52 mb) located at this angle (22.5°), and the minimum point of reaction cross section equal to (0.0169 mb), located at this angle (67.5°). When E_α=

170.5 MeV the maximum point of reaction cross section equal to (6.66 mb) located at this angle (2.5°), and the minimum point of reaction cross section equal to (0.0116 mb), located at this angle (47.5°). Figure (4.45) represents the evaluated results and angle-integrated emission Spectra measurements at E_p= 180 MeV.

Table 4.45. Alpha scattered angular distributions (mb/sr) for p + $_{90}Th^{232}$ reaction, E_p= 180 MeV energy. Calculations have been made by ALICE/ASH code program

^{232}Th(P, α); E_p=180 MeV ALICE/ASH – Code					
ANGLE/DEG.	E_α= 5.50 MeV	E_α= 90.5 MeV	E_α= 100.5 MeV	E_α= 140.5 MeV	E_α= 170.5 MeV
	Cross Section mb	Cross Section mb	Cross Section mb	Cross Section mb	Cross Section mb
2.5	1.31	0.0797	0.101	1.33	6.66
7.5	1.32	0.148	0.205	1.71	6.04
12.5	1.33	0.329	0.454	2.52	4.9
17.5	1.28	0.612	0.822	3.2	3.66
22.5	1.25	1.02	1.32	3.52	2.27
27.5	1.28	1.53	1.89	3.49	1.4
32.5	1.26	1.9	2.2	2.75	0.768
37.5	1.33	2.28	2.47	2.12	0.465
42.5	1.34	2.32	2.32	1.35	0.254
47.5	1.32	1.99	1.83	0.697	0.116
52.5	1.24	1.48	1.24	0.336	
57.5	1.19	0.964	0.745	0.146	
62.5	1.13	0.616	0.438	0.0574	
67.5	1.13	0.397	0.261	0.0169	
72.5	1.1	0.21	0.124		
77.5	1.1	0.114	0.0572		
82.5	1.03	0.0545	0.0227		
87.5	1.02				
142.5	0.543				
147.5	0.467				
152.5	0.445				
157.5	0.4				
162.5	0.386				
167.5	0.384				
172.5	0.372				
177.5	0.368				

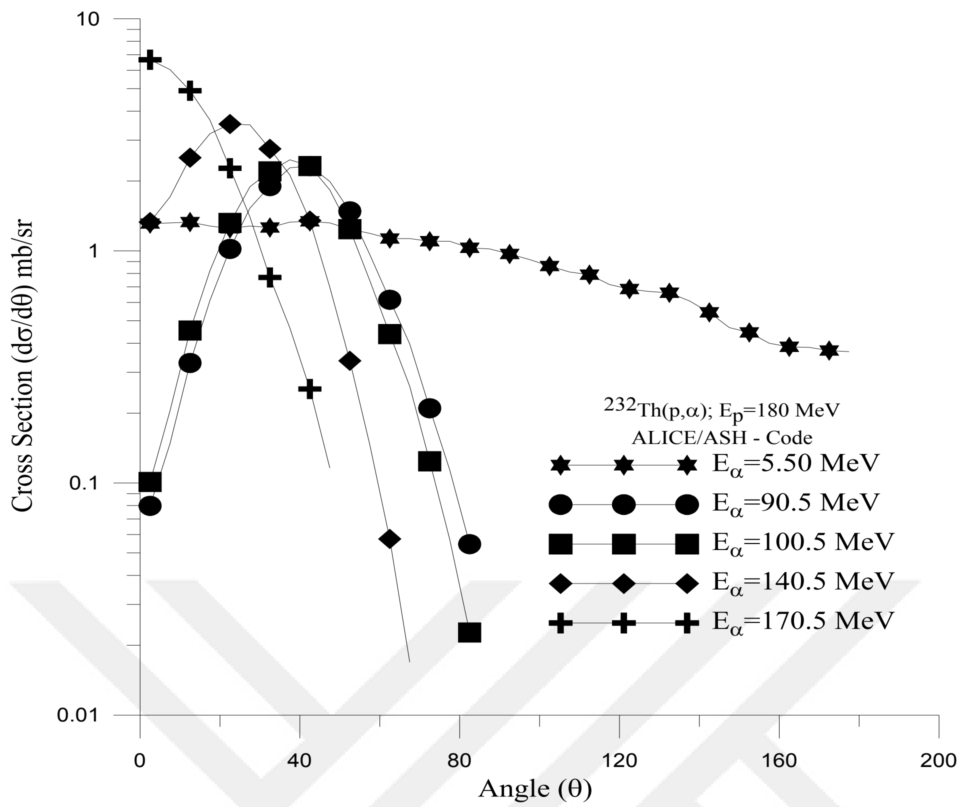

Figure 4.45. Angular Distributions (mb/sr) of the alpha generated as a result of bombardment of element $_{90}Th^{232}$ with 180 MeV energetic protons

4.4.4.16. α Angular Distribution for p + $_{90}Th^{232}$ Reaction at E_p = 210 MeV

The calculation for the angular distribution of $^{232}Th(p,\alpha)$ reaction has been see in the Fig. 4.46. In this reaction α- particle emitted at angle (2.5°, 7.5°......... 177.5°). In this reaction, when E_α= 5.50 MeV the maximum point of reaction cross section equal to (0.997 mb), located at this angle (42.5°), and the minimum point of reaction cross section equal to (0.29 mb), located at this angle (177.5°). When E_α= 90.5 MeV the maximum point of reaction cross section equal to (1.81 mb) located at this angle (42.5°), and the minimum point of reaction cross section equal to (0.0505 mb), located at this angle (87.5°). When E_α= 165.5 MeV the maximum point of reaction cross section equal to (2.93 mb) located at this angle (22.5°), and the minimum point of reaction cross section equal to (0.0871 mb), located at this angle (57.5°). When E_α= 180.5 MeV the maximum point of reaction cross section equal to (3.71 mb) located at this angle (17.5°), and the minimum point of reaction cross section equal to (0.0358 mb), located at this angle (57.5°). When E_α= 200.5 MeV the maximum point of reaction cross section equal to (6.57 mb) located at this angle (2.5°), and the minimum point of reaction cross section equal to (0.00025 mb), located at this angle (57.5°). Figure (4.46) represents the evaluated results and angle-integrated emission Spectra measurements at E_p= 210 MeV.

Table 4.46. Alpha scattered angular distributions (mb/sr) for p + $_{90}Th^{232}$ reaction, E_p= 210 MeV energy. Calculations have been made by ALICE/ASH code program

$^{232}Th(p, \alpha)$; E_p=210 MeV ALICE/ASH – Code					
ANGLE/DEG.	E_α= 5.50 MeV	E_α= 90.5 MeV	E_α= 165.5 MeV	E_α= 180.5 MeV	E_α= 200.5 MeV
	Cross Section mb	Cross Section mb	Cross Section mb	Cross Section mb	Cross Section mb
2.5	0.961	0.0744	1.04	2.85	6.57
7.5	0.976	0.0965	1.39	3.03	5.97
12.5	0.965	0.173	2.09	3.51	4.52
17.5	0.925	0.328	2.66	3.71	2.76
22.5	0.911	0.577	2.93	3.39	1.58
27.5	0.923	0.918	2.89	2.8	0.875
32.5	0.931	1.24	2.25	1.84	0.49
37.5	0.97	1.61	1.7	1.21	0.275
42.5	0.997	1.81	1.05	0.667	0.137
47.5	0.976	1.72	0.508	0.297	0.0407
52.5	0.927	1.42	0.226	0.116	0.0061
57.5	0.898	1.03	0.0871	0.0358	0.00025
62.5	0.833	0.723			
67.5	0.824	0.506			
72.5	0.822	0.289			
77.5	0.821	0.172			
82.5	0.777	0.0938			
87.5	0.775	0.0505			
92.5	0.741				
97.5	0.697				
102.5	0.651				
142.5	0.416				
147.5	0.365				
152.5	0.338				
157.5	0.312				
162.5	0.294				
167.5	0.296				
172.5	0.296				
177.5	0.29				

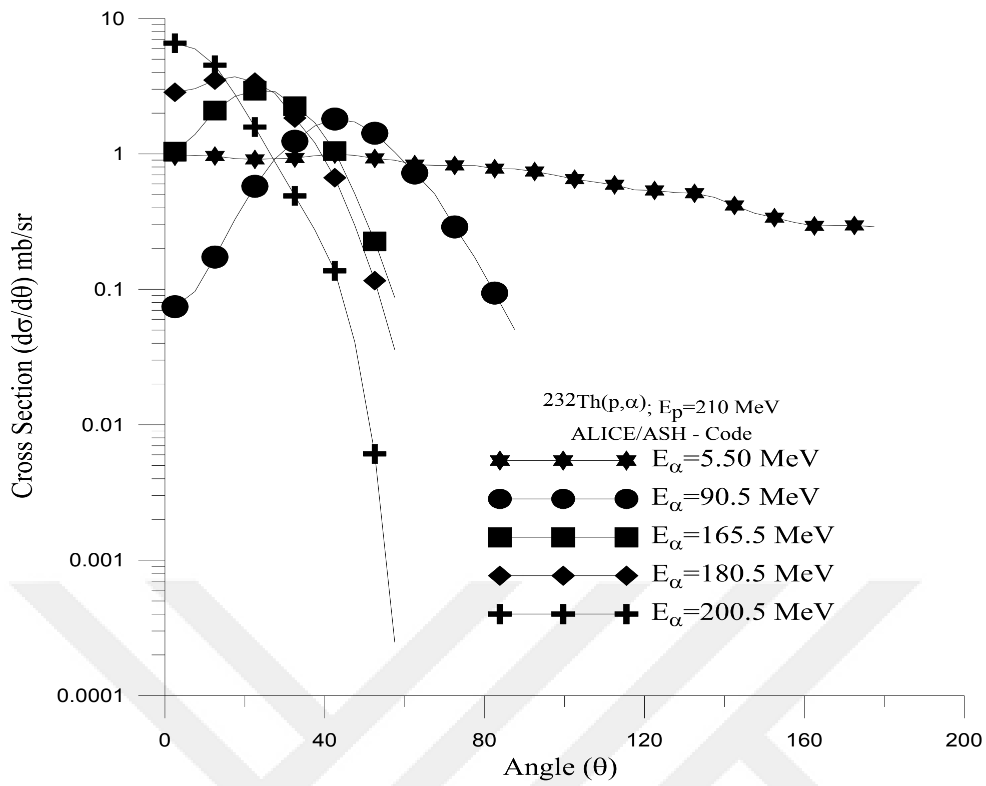

Figure 4.46. Angular Distributions (mb/sr) of the alpha generated as a result of bombardment of element ${}_{90}Th^{232}$ with 210 MeV energetic protons

4.4.4.17. α Angular Distribution for p + ${}_{90}Th^{232}$ Reaction at E_p = 240 MeV

The calculation for the angular distribution of $^{232}Th(p,\alpha)$ reaction has been see in the Fig. 4.47. In this reaction α- particle emitted at angle (2.5°, 7.5°......... 177.5°). In this reaction, when E_α= 5.50 MeV the maximum point of reaction cross section equal to (0.756 mb), located at this angle (42.5°), and the minimum point of reaction cross section equal to (0.231 mb), located at this angle (177.5°). When E_α= 80.5 MeV the maximum point of reaction cross section equal to (1.23 mb) located at this angle (42.5°), and the minimum point of reaction cross section equal to (0.144 mb), located at this angle (87.5°). When E_α= 155.5 MeV the maximum point of reaction cross section equal to (1.67 mb) located at this angle (27.5°), and the minimum point of reaction cross section equal to (0.082 mb), located at this angle (2.5°). When E_α= 205.5 MeV the maximum point of reaction cross section equal to (3.4 mb) located at this angle (17.5°), and the minimum point of reaction cross section equal to (0.145 mb), located at this angle (47.5°). When E_α= 230.5 MeV the maximum point of reaction cross section equal to (5.26 mb) located at this angle (2.5°), and the minimum point of reaction cross section equal to (0.0175 mb), located at this angle (47.5°). Figure (4.47) represents the evaluated results and angle-integrated emission Spectra measurements at E_p= 240 MeV.

Table 4.47. Alpha scattered angular distributions (mb/sr) for p + $_{90}Th^{232}$ reaction, E_p= 240 MeV energy. Calculations have been made by ALICE/ASH code program

$^{232}Th(p, \alpha)$; E_p=240 MeV ALICE/ASH – Code					
ANGLE/DEG.	E_α= 5.50 MeV	E_α=80.5 MeV	E_α = 155.5 MeV	E_α= 205.5 MeV	E_α= 230.5 MeV
	Cross Section mb	Cross Section mb	Cross Section mb	Cross Section mb	Cross Section mb
2.5	0.721	0.11	0.082	0.971	5.26
7.5	0.733	0.131	0.194	1.75	4.67
12.5	0.726	0.184	0.459	2.88	3.31
17.5	0.696	0.282	0.845	3.46	2.02
22.5	0.686	0.413	1.27	3.16	1.18
27.5	0.696	0.6	1.67	2.32	0.65
32.5	0.703	0.778	1.74	1.5	0.355
37.5	0.735	0.99	1.73	0.853	0.185
42.5	0.756	1.23	1.41	0.431	0.0808
47.5	0.743	1.21	0.94	0.145	0.0175
52.5	0.707	1.14	0.537		
57.5	0.686	0.985	0.262		
62.5	0.638	0.817	0.121		
67.5	0.633	0.656			
72.5	0.632	0.486			
77.5	0.632	0.34			
82.5	0.6	0.222			
87.5	0.6	0.144			
92.5	0.575				
97.5	0.542				
142.5	0.33				
147.5	0.291				
152.5	0.27				
157.5	0.249				
162.5	0.235				
167.5	0.237				
172.5	0.236				
177.5	0.231				

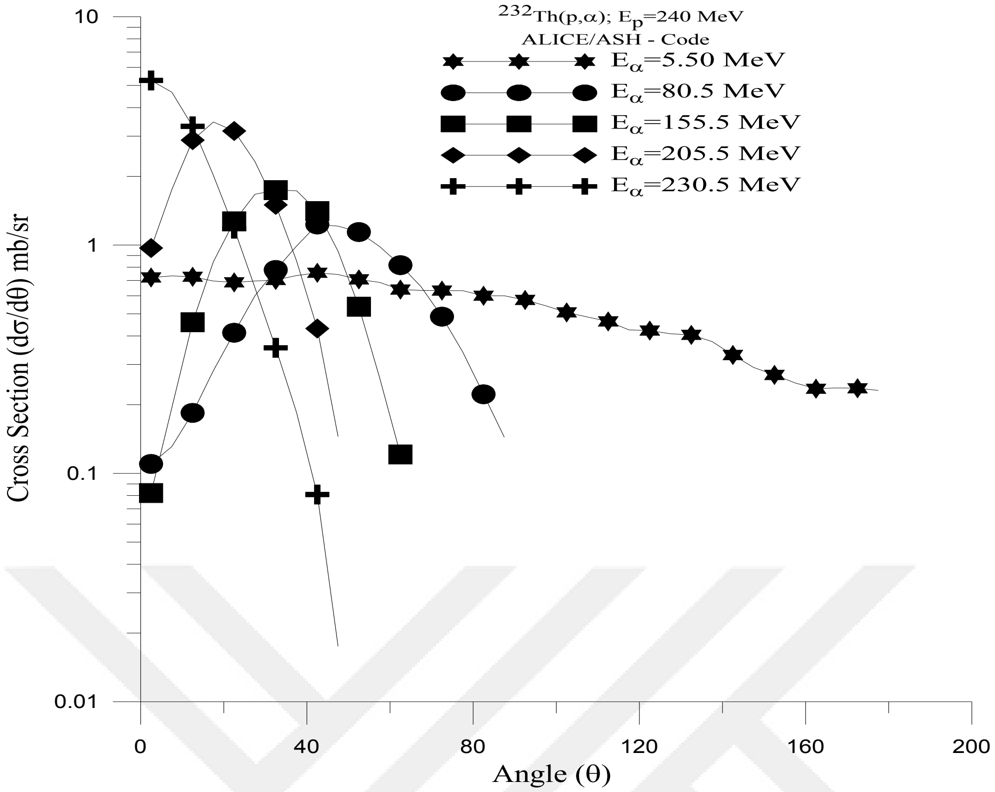

Figure 4.47. Angular Distributions (mb/sr) of the alpha generated as a result of bombardment of element $_{90}Th^{232}$ with 240 MeV energetic protons

4.4.4.18. α Angular Distribution for p + $_{90}Th^{232}$ Reaction at E_p = 270 MeV

The calculation for the angular distribution of $^{232}Th(p,\alpha)$ reaction has been see in the Fig. 4.48. In this reaction α- particle emitted at angle (2.5°, 7.5°......... 175°). In this reaction, when E_α= 5.50 MeV the maximum point of reaction cross section equal to (0.587 mb), located at this angle (42.5°), and the minimum point of reaction cross section equal to (0.188 mb), located at this angle (177.5°). When E_α= 105.5 MeV the maximum point of reaction cross section equal to (1.12 mb) located at this angle (42.5°), and the minimum point of reaction cross section equal to (0.061 mb), located at this angle (2.5°). When E_α= 195.5 MeV the maximum point of reaction cross section equal to (1.63 mb) located at this angle (27.5°), and the minimum point of reaction cross section equal to (0.0318 mb), located at this angle (62.5°). When E_α= 250.5 MeV the maximum point of reaction cross section equal to (3.47 mb) located at this angle (7.5°), and the minimum point of reaction cross section equal to (0.00163 mb), located at this angle (52.5°). When E_α= 265.5 MeV the maximum point of reaction cross section equal to (1.86 mb) located at this angle (2.5°), and the minimum point of reaction cross section equal to (0.0471 mb), located at this angle (37.5°). Figure (4.48) represents the evaluated results and angle-integrated emission Spectra measurements at (E_p= 270 MeV).

Table 4.48. Alpha scattered angular distributions (mb/sr) for p + $_{90}Th^{232}$ reaction, E_p= 270 MeV energy. Calculations have been made by ALICE/ASH code program

$^{232}Th(p, \alpha)$; E_p=270 MeV ALICE/ASH – Code					
ANGLE/DEG.	E_α= 5.50 MeV	E_α= 105.5 MeV	E_α= 195.5 MeV	E_α= 250.5 MeV	E_α= 265.5 MeV
	Cross Section mb	Cross Section mb	Cross Section mb	Cross Section mb	Cross Section mb
2.5	0.554	0.0611	0.173	3.34	1.86
7.5	0.564	0.0629	0.362	3.47	1.51
12.5	0.559	0.0769	0.72	3.4	0.728
17.5	0.536	0.145	1.1	2.59	0.471
22.5	0.529	0.281	1.42	1.77	0.298
27.5	0.537	0.488	1.63	1.11	0.17
32.5	0.544	0.701	1.47	0.642	0.0931
37.5	0.569	0.955	1.27	0.325	0.0471
42.5	0.587	1.12	0.902	0.13	
47.5	0.578	1.11	0.511	0.0224	
52.5	0.551	0.97	0.243	0.00163	
57.5	0.536	0.751	0.095		
62.5	0.499	0.566	0.0318		
67.5	0.496	0.428			
72.5	0.496	0.258			
77.5	0.497	0.154			
82.5	0.473				
87.5	0.474				
107.5	0.385				
137.5	0.304				
142.5	0.267				
147.5	0.235				
152.5	0.219				
157.5	0.202				
162.5	0.191				
167.5	0.193				
177.5	0.188				

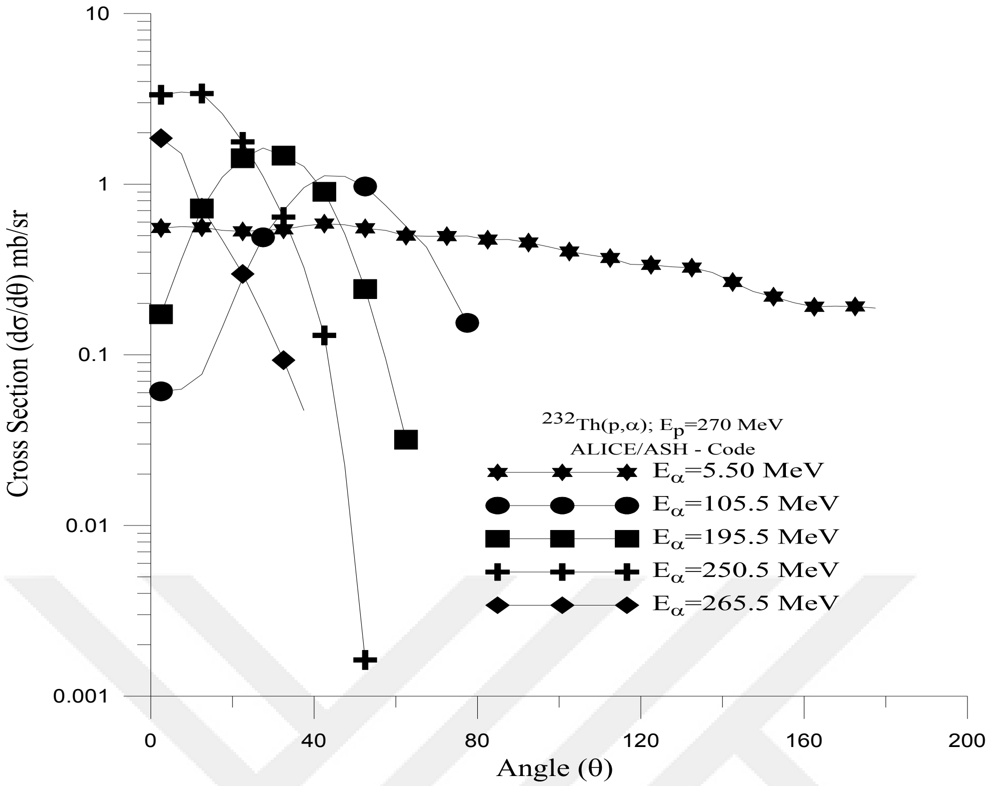

Figure 4.48. Angular Distributions (mb/sr) of the alpha generated as a result of bombardment of element $_{90}Th^{232}$ with 270 MeV energetic protons

5. CONCLUSION

In the our research, using equilibrium and pre-equilibrium reaction method, the (p, xn),(p,xp′), (p, xα) cross-section values for ^{232}Th and ^{206}Pb target nuclei has been calculated for 30–500 MeV incident energy ranges. The calculation results on the angular distribution and the optimum energy ranges for reaction process are given in Tables (1-48) and Figures (1-48). Generally the model calculations used for all reactions are in good contract with the measurement data. Also indicated in figures, the highest energy rate of the experimental excitation functions cannot measuring for by the equilibrium decay mechanism and the pre-equilibrium emission must be measured along with compound nucleus decay. However, the pre-equilibrium effects increase as the incident energy increases. Therefore, the proton induced nuclear reaction cross-section data are very important for several technical applications. In generally, the new evaluated hybrid and GDH model calculations (with ALICE/ASH) conforms the experimental data over the incident proton energy to 30-300 MeV in Figs. 31-48.

Over all the nuclear reaction models are frequently needed to provide estimates of the particle-induced reaction cross-sections, especially if the experimental data are not available or unable to measure the cross-sections due to the experimental difficulty. Therefore, nuclear reaction model calculations play an important role in the nuclear data evaluation.

As a result in CEM03 code for p + $_{90}Th^{232}$ at E_p=30 MeV in this reaction neutron emitted and produced has been made for four steps (Total, Cascade, Precompound, Total evaporation) at angle (5°, 15°……… 175°). As can be seen in Figure 4.1 cascade cross section and precompound cross section are not change, and there is no change at total cross section and total evaporation cross section, but when E_p= 450 MeV cascade cross section is decreasing when angular distributions are increasing and there is no change at precompound total cross section and total evaporation cross sectionas can be seen in Figure 4.13.

For p + $_{90}Pb^{206}$ in this reactions neutron emitted and produced has been make for four steps (Total, Cascade, Precompound, Total evaporation) at angle (5°,15°......... 175°). As can be seen in Figure 4.14 cascade cross section is decreasing when angular distributions are increasing. Similarly, Precompound slightly decreases while angular distribution increases and there is no change at total cross section and total evaporation cross section, but when E_p=450 MeV as can be seen in Figure 4.26 cascade cross section is decreasing when angular distributions are increasing and there is no change at Precompound, total cross section and total evaporation cross section.

As a result in ALICE/ASH code for p + $_{90}Pb^{206}$at E_p=30 MeV in this reaction α- particle emitted at these angles (2.5°,7.5°......... 177.5).In this reaction, maximum point of reaction cross section equal to 6.65 mb including in this energy range E_α= 5.50 MeV located at this angle 12.5° and the minimum point of reaction cross section equal to 0.00853 mb including in this energy range E_α= 15.5 MeV located at this angle 177.5°. Figure 4.31 represents the evaluated results and angle-integrated emission spectra at E_p =30 MeV. When E_p=270 MeV the maximum point of reaction cross section equal to 4.2 mb including in this energy range E_α= 255.5 MeV located at this angle 2.5° when E_α= 5.5 MeV the reaction cross section are not change. Figure 4.39 represents the evaluated results and angle-integrated emission Spectra measurements at E_p= 270 MeV.

α- particle emitted at angles (2.5°, 7.5°......... 177.5°)in reaction p + $_{90}Th^{232}$ at E_p=30 MeV. In this reaction, the maximum point of reaction cross section equal to10 mb including in energy range E_α= 5.50 MeV located at this angle 12.5° and the minimum point of reaction cross section equal to 0.0273 mb including in this energy range E_α= 15.5 MeV located at this angle 177.5°. Figure 4.40 represents the evaluated results and angle-integrated emission Spectra measurements at E_p= 30 MeV. When E_p=270 MeV the maximum point of reaction cross section equal to 3.47 mb including in this energy range E_α= 250.5 MeV located at this angle 7.5°, when E_α= 5.5 MeV the reaction cross section are not change. Figure 4.39 represents the evaluated results and angle-integrated emission Spectra measurements at E_p=270 MeV.

REFERENCES

Armbruster P, Benlliure J (2001) Basic Nuclear Data at High and Intermediate Energy for Accelerator-Driven Systems. NUPECC—Nuclear Science: Impact, Applications, Interactions

Asquith NL, Hashemi-Nezhad SR, Westmeier W, Zhuk I, Tyutyunnikov S, Adam J (2015) Study of 232Th(n,??) and 232Th(n,f) reaction rates in a graphite moderated spallation neutron field produced by 1.6 GeV deuterons on lead target. Nuclear Instruments and Methods in Physics Research, Section B: Beam Interactions with Materials and Atoms 344: 51–58

Atchison F (1980) Spallation and Fission in Heavy Metal Nuclei under Medium Energy Proton Bombardment. In Proc. Meeting on Targets for Neutron Beam Spallation Source, Julich,june 11-12, 1979, pp. 17-46, GS. Bauer,Ed, Jul-Conf-34, Kernforschungsanlage Julich GmbH, Germany

Aydin A, Şarer B, Tel E (2007) New calculation of excitation functions of proton-induced reactions in some medical isotopes of Cu, Zn and Ga. Applied radiation and isotopes 65(3): 365-370

Barashenkova VS, jinov AS, Sobolevskii NM, Toneev VD (1973) Interaction of particles and nuclei of High and ultrahigh energy with nuclei. Usp. Fiz. Nauk 109: 91—136

Barros GP, Pereira C, Veloso MAF, Costa AL, Reis PAL (2010) Neutron production evaluation from a ADS target utilizing the MCNPX 2.6.0 code. Brazilian Journal of Physics 40(4): 414–418

Bertini HW (1969) Intranuclear-cascade calculation of the secondary nucleon spectra from nucleon-nucleus interactions in the energy range 340 to 2900 MeV and comparisons with experiment. Physical Review 188(4): 1711

Bertrand FE, Peelle RW (1973) Complete hydrogen and helium particle spectra from 30- to 60-MeV proton bombardment of nuclei with A= 12 to 209 and comparison with the intranuclear cascade model. Physical Review C 8(3): 1045

Bethge KLAUS (1970) Alpha-Particle Transfer Reactions. Annual Review of Nuclear Science 20(1): 255-288

Blann M (1975) Preequilibrium Decay. Annual Review of Nuclear Science 25(1): 123–166

Blann M (1991) Recent progress and current status of preequilibrium reaction theories and computer code ALICE. LLNL, Report UCRL-JC-109052Adair RK (1954) Nuclear Potential Well Depth, Phys. Rev. 94: 737-8

Bodansky D (1962) Compound Statistical Features in Nuclear Reactions. Annual review of nuclear science 12(1): 79-122

Broeders CHM, Konobeyev YuA, Korovin AYu, Lunev VP, Blann M (2006) ALICE/ASH precompound and evaporation model code system for calculation of excitation functions, energy and angular distributions of emitted particles in nuclear reactions at intermediate energies 1–230

Bryant PJ (1994) A brief history and review of accelerators. Cern European Organization For Nuclear Research-Reports- Cern, 1-1Cambridge, Massachusetts 32

Cho C, Tak N, Choi J (2008) CFD analysis of the HYPER spallation target. Ann. Nucl. Energy 35: 1256–1263

Christofilos NC (1956) Unpublished report (1950) and U.S. Patent no. 2.736,799, filed March 10, 1950

Cockcroft JD, Walton ETS (1932) Experiments with high velocity positive ions. ii. The disintegration of elements by high velocity protons. In Proceedings of the Royal Society of London A, Mathematical, Physical and Engineering Sciences (Vol. 137, No. 831, pp. 229-242). The Royal Society

Courant ED, Livingston MS, Snyder HS (1952) The strong-focusing synchrotron – anew high-energy accelerator. Phys. Rev, 88: 1190-6, and Courant ED, Snyder HS (1958) Theory of the alternating-gradient synchrotron. Annals of Physics No. 3: 1–48

Cugnon J (1993) Cascade models and particle production: A comparison. In Particle Production in Highly Excited Matter (pp. 271-293). Springer US

David JC (2015) Spallation reactions, A successful interplay between modeling and applications. The European Physical Journal A 51(6): 1-57

Delalić Z, Todorović Ž (1988) Angular efficiency of detection of spallation products induced by 4 (GeV/c)/u deuterons in plastic detector material. Nuclear Instruments and Methods in Physics Research Section B: Beam Interactions with Materials and Atoms 35(1): 87-94

Demirkol I (2006) Analysis of Isotopic Yields of Primary Residues in 1 A GeV ^{208}Pb+ p Reactions. Chinese Journal of Physics 44(6): 418-431

Fermi E (1950) High energy nuclear events. Progress of theoretical physics, *5*(4): 570-583 Mashnik SG, Kerby LM, Gudima KK, Sierk AJ, Bull JS, James MR (2016) Production of Energetic Light Fragments in CEM, LAQGSM, and MCNP6. arXiv preprint arXiv:1607.02506

Finck JE, Crawley GM, Nolen Jr JA, Kouzes RT (1983*)* A study of ^{206}Pb by inelastic scattering of 35 MeV protons. Michigan State University, East Lansing, MI (USA), Nuclear Physics, SectionA , volume 407, page163

Fleury A, Alexander JM (1974) Reactions between medium and heavy nuclei and heavy ions of less than 15 MeV/amu. Annual Review of Nuclear Science 24(1): 279-340

Furihata S (2003) Development of a generalized evaporation model and study of residual nuclei production (Doctoral dissertation, Ph. D. thesis, Tohoku University)

Furihata S, Niita K, Meigo S, Ikeda Y, Maekawa F (2001) The Gem Code –a Simulatetion Program for the evaporation and fission process of an Excited Nucleus. JAERI- Data/Code 2001-015, JAERI, Tokai-mura, Naka-gam, Ibraaki-ken, Japan

Gaitanos T, Lenske H, Mosel U (2008) Fragment formation in proton induced reactions within a BUU transport model. Physics Letters B 663(3): 197-201

Gerstein G, Niederer J, Strauch K (1957) Elastic Scattering of 96-Mev Protons. Cyclotron, Harvard University, Cambridge, MA (USA), Physical Review, volume 108, page 427

Glendenning NK (1963) Nuclear stripping reactions. Annual review of nuclear science 13(1): 191-260

Goldberger ML (1948) The interaction of high energy neutrons and heavy nuclei. Physical Review 74(10): 1269

Goward FK, Barnes DE (1946) Experimental 8 MeV synchrotron for electron acceleration. Nature 158(4012): 413

Greider KR (1965) Reactions Between Complex Nuclei. Annual Review of Nuclear Science 15(1): 291-324

Griffin JJ (1966) Statistical model of intermediate structure. Physical review letters 17(9): 478

Gudima KK, Mashnik SG, Toneev VD (1983) Cascade-Exciton Model of Nuclear Reactions. Nuclear Physics A 401: 329–361

Gudima KK, Ososkov GA, Toneev VD (1975) Model of preequilibrium decay of excited nuclei. Joint Inst. for Nuclear Research, Dubna, USSR

Gupta D, Samanta C, Chatterjee A, Kailas S, Roy BJ (2001) Measurement of 42 MeV 7 Li projectile breakup on 208 Pb target near grazing incidence. Nuclear Physics A 683(1-4): 3-20

Hashemi-Nezhad SR, Zhuk I, Potapenko A, Westmeier W, Brandt R (2012) Registration of proton induced spallation products of U, Pb and Au in mica track detectors. Nuclear Instruments and Methods in Physics Research, Section A: Accelerators, Spectrometers, Detectors and Associated Equipment 679: 82–88

He M, Bai Y, Zhang Y, Song Y, Zhao Z (2016) Thermal-hydraulic analysis of an integrated spallation target module in ADS. Annals of Nuclear Energy 98: 12–18

Heikkinen A, Stepanov N, Wellisch JP (2003) Bertini intra-nuclear cascade implementation in Geant4. Computing in High Energy and Nuclear Physics 24–28

Holbrow CH, Barschall HH (1963) Neutron evaporation spectra. Nuclear Physics 42, 264-279

https://en.wikipedia.org/wiki/Thorium

https://en.wikipedia.org/wiki/Lead

Ignatyuk AV, Istekov KK, Smirenkin GN (1979) Role of collective effects in systematics of level density of nuclei (No. KFK-TR-632). Kernforschungszentrum Karlsruhe GmbH Germany

Iljinov AS, Mebel MV, Bianchi N, De Sanctis E, Guaraldo C, Lucherini V, Rossi P (1992) Phenomenological statistical analysis of level densities, decay widths and lifetimes of excited nuclei. Nuclear Physics A 543(3): 517-557

Ising G (1924) Prinzip einer methode zur herstellung von kanalstrahlen hoher voltzahl. Ark. Mat. Astron. Fys 18, 1-4

Janes GS, Levy RH, Bethe HA, Feld BT (1966) New type of accelerator for heavy ions. Physical Review 145(3): 925

Kalbach C (1978) Exciton number dependence of the Griffin model two-body matrix element. Zeitschrift für Physik A Hadrons and Nuclei 287(3): 319-322.

Kalbach C (1988) Systematics of continuum angular distributions: Extensions to higher energies. Physical Review C 37(6): 2350

Kowalczyk A. (2008) Proton induced spallation reactions in the energy range 0.1-10 GeV. arXiv preprint arXiv:0801.0700

Krása A, Rež AK (2010) Spallation Reaction Physics. Faculty of Nuclear Sciences and Physical Engineering at Czech Technical University, Prague

Krebs RE (2006) The history and use of our earth's chemical elements: a reference guide. Greenwood Publishing Group

Kumar V, Kumawat H, Goel U, Barashenkov VS (2003) Neutron spallation source and the Dubna Cascade Code. Pramana 60(3): 469-481

Livingston MS (1969) Particle accelerators: A brief history. Harvard University Press

Maiti M, Nandy M, Roy SN, Sarkar PK (2006) Angular distribution of neutrons from heavy ion induced reactions in thick targets. Nuclear Instruments and Methods in Physics Research Section A, Accelerators, Spectrometers, Detectors and Associated Equipment 556(2): 577-588

Malyshkin Y, Pshenichnov I, Mishustin I, Hughes T, Heid O, Greiner W (2012) Neutron production and energy deposition in fissile spallation targets studied with Geant4 toolkit. Nuclear Instruments and Methods in Physics Research, Section B: Beam Interactions with Materials and Atoms 289: 79–90

Manolopoulou M, Stoulos S, Fragopoulou M, Brandt R, Westmeier W (2006) Detection of spallation neutrons and protons using the nat Cd activation technique in transmutation experiments at Dubna. 64: 823–829

Mashnik S, Gudima K, Sierk A, Baznat M, Mokhov N (2005) CEM03.01 User Manual. Los Alamos National Laboratory Report LA-UR-05-7321

Matsumura H, Suzuki T, Miura T, Masumoto K, Ishihama S, Matsuda N, Aze T (2007) Spallation products of 197Au induced by secondary particles from 12-GeV proton bombardment of a thick aluminum target. Nuclear Instruments and Methods in Physics Research, Section B: Beam Interactions with Materials and Atoms 256(2): 591–598

McMillan EM (1945) The synchrotron—a proposed high energy particle accelerator. Physical Review 68(5-6): 143

Meot F, Tahar MH, Tsoupas N (2015) High Power from Fixed-field Rings in the Accelerator-driven Sub-critical Reactor Application. Physics Procedia 66: 129–139

Metropolis N, Bivins R, Storm M, Turkevich A, Miller JM, Friedlander G (1958) Monte Carlo calculations on intranuclear cascades. I. Low-energy studies. Physical Review 110(1): 185

Meulders JP, Beijers H, Benlliure J, Bersillon O, Cugnon J, Eudes P, Michel11 R (2000) High and Intermediate Energy Nuclear Data for Accelerator Driven Systems–The HINDAS Project. In Proc. Sixth Information Exchange Meeting on Actinide and Fission Product Partitioning and Transmutation, Madrid, Spain

Michel R, Peiffer F, Stück R (1985) Measurement and hybrid model analysis of integral excitation functions for proton-induced reactions on vanadium, manganese and cobalt up to 200 MeV. Nuclear Physics A 441(4): 617-639

Oliphant ML, Gooden JS, Hide GS (1947) The acceleration of charged particles to very high energies. Proceedings of the Physical Society 59(4): 666

Parel RE, Lichtenstein H (1989) User guide to LCS: The LAHET Code system. LANL Report No. LA-UR-89-3014, Los Alamos

Quanzhi Y, Youlian L, Zhiliang H, Bin Z, Wen Y, Tianjiao L (2015) Nuclear Instruments and Methods in Physics Research B Decay heat calculations for a 500 kW W – Ta spallation target. Nuclear Instruments and Methods in Physics 351: 41–45

Ribanský I, Obložinský P, Běták E (1973) Pre-equilibrium decay and the exciton model. Nuclear Physics A 205(3): 545-560

Ricciardi MV, Armbruster P, Benlliure J, Bernas M, Boudard A, Czajkowski S, Yordanov O (2006) Light nuclides produced in the proton-induced spallation of U238 at 1 GeV. Physical Review C - Nuclear Physics 73(1): 1–25

Ridikas D, Mittig W (1998) Neutron production and energy generation by energetic projectiles, protons or deuterons?. Nuclear Instruments and Methods in Physics Research Section A, Accelerators, Spectrometers, Detectors and Associated Equipment 418(2): 449-457

Russell GJ (1990) Spallation Physics - An Overview. International Collaboration on Advanced Neutron Sources KEK. Tsukuba 291–299

Sandberg JV (1982) Angular and energy distribution measurements of secondary hadron fluxes with multireaction spallation detectors at CERN SPS. Nuclear Instruments and Methods in Physics Research 200(2-3): 211-218

Santos BM, Pinheiro ARC, Gonçalves M, Duarte SB, Cabral RG (2016) On the nucleon effective mass role to the high energy proton spallation reactions. Nuclear Physics A 948: 78–92

Sathik NPM, Ansari MA, Singh BP, Ismail M, Rashid MH (2002) Preequilibrium emission in α induced reactions on bromine and thallium. Physical Review C 66(1): 014602

Serber R (1947) Nuclear reactions at high energies. Physical Review 72(11): 1114

Shen WQ, Wang B, Feng J, Zhan WL, Zhu YT, Feng EP (1989) Total reaction cross section for heavy-ion collisions and its relation to the neutron excess degree of freedom. Nuclear Physics A 491(1):130-146

Shetty NV (2013) Study of particle transport in a high power spallation target for an accelerator-driven transmutation system (Doctoral dissertation, university library)

Sidorov VA (1962) Evaporation neutron spectra. Nuclear Physics 35: 253-259

Stepan M, Arnold S (2012) CEM03.03 User Manual. Los Alamos National Laboratory, Report LA-UR-12-01364

Takeuchi Y, Sakaguchi H, Nakamura M, Ichihara T, Yosoi M, Ieiri M, Kobayashi S (1986) Quadrupole and hexadecapole moments of ^{232}Th and ^{238}U from inelastic scattering of 65 MeV polarized protons. Kyoto Univ, Kyoto (JPN) Department of Physics, Physical Review, Part C, Nuclear Physics, volume 34, issue 2, page 493,08

Tamura T (1969) Coupled-channel approach to nuclear reactions. Annual review of nuclear science 19(1): 99-138

Tel E, Aydin A, Kaplan A, Ugur FA, Sahan H, Sahan M (2011) The newly calculations of production cross sections for some positron emitting and single photon emitting radioisotopes in proton cyclotrons. INTECH Open Access Publisher

Thomas TD (1968) Compound Nuclear Reactions Induced by Heavy Ions. Annual review of nuclear science 18(1): 343-406

Tsujimoto K, Sasa T, Nishihara K, Takizuka T, Takano H (2000) Accelorator-driven system for transmutation of high-level waste. Prog. Nucl. Energ 37(1): 339–344

Van der Meer S (1972) Stochastic damping of betatron oscillations in the ISR. CERN/ISR-PO/ 72–31

Veksler VI (1945) A new method of acceleration of relativistic particles. J. Phys 9: 153-158

Wagner V. et al. (1996) Neutron Production in Spallation Reactions. Report UJF-EXP-96/03 of NPI AS CR PRI in _ Rez (in Czech)

Wang H, Otsu H, Sakurai H, Ahn DS, Aikawa M, Doornenbal P, Yoshida K (2016) Spallation reaction study for fission products in nuclear waste: Cross section measurements for 137Cs and 90Sr on proton and deuteron. Physics Letters, Section B: Nuclear, Elementary Particle and High-Energy Physics 754: 104–108

Weisskopf V (1937) Statistics and nuclear reactions. Physical Review 52(4): 295

Weisskopf VF, Ewing, DH (1940) On the yield of nuclear reactions with heavy elements. Physical Review 57(6): 472

Wlazło W, Enqvist T, Armbruster P, Benlliure J, Bernas M, Boudard A, Volant C (2000) Cross sections of spallation residues produced in 1A GeV 208Pb on proton reactions. Physical Review Letters 84(25): 5736–9

Wood RM, Borchers RR, Barschall HH (1965) Neutrons from protons on isotopes of tin. Nuclear Physics 71(3): 529-545

Yu Quanzhi (2016) Energy deposition calculated by PHITS code in Pb spallation target. Nuclear Instruments and Methods in Physics Research Section B, Beam Interactions with Materials and Atoms 367: 8-13

Zamani M, Stoulos S, Fragopoulou M, Manolopoulou M, Krivopustov M (2010) Annals of Nuclear Energy Indirect measurement of inelastic cross section of relativistic protons in Pb target. Annals of Nuclear Energy 37(7): 923–926

Zenihiro J, Sakaguchi H, Murakami T, Yosoi M, Yasuda Y, Terashima S, Iwao Y, Takeda H, Itoh M, Yoshida HP, Uchida M (2010) Neutron density distributions of ^{204,206,208}Pb deduced via proton elastic scattering at E_p=295MeV. Kyoto Univ, Kyoto (JPN) Department of Physics, Physical Review, Part C, Nuclear Physics, volume 82, page 044611

CURRICULUM VITAE

Fulname	: Bilal Othman HAMARASHID
Gender	: Male
Martial	: Single
Date of birth	: 16.10.1991
Birth place	: Sulaimani
Nationality	: IRAQ
Present address	: Sulaimani
Telephon No	: 009647503079273 _00905522053979

I was born in 1991. I was graduated from the University of sulaimani Faculty of Science Department of Physic production in 2013. I enrolled at the Postgraduate Programme in Bingol University Institute of Science Department of Physics in 2015, and completed my research in 2017.